ISOLATION, PURIFICATION AND CHARACTERIZATION OF A 'FACTOR' FROM *FUSARIUM OXYSPORUM* RESPONSIBLE FOR PLATINUM NANOPARTICLE FORMATION

A thesis submitted in the fulfilment of the requirement for the degree of

MASTER OF SCIENCE
OF
RHODES UNIVERSITY

in the

Department of Biochemistry, Microbiology and Biotechnology
Faculty of Science

by

Yageshni Govender

ABSTRACT

Nanoparticles are microscopic particles in the nanometre range of between 1-100 nm. A wide variety of metal nanoparticles have been found to be produced by prokaryotic and eukaryotic organisms including several fungal species, when exposed to solutions containing metal salts. Previous studies have suggested that this bioreduction of metal particles may occur *via* an active reductase/hydrogenase enzyme process where H_2 is the electron donor and positively charged platinum species act as the electron acceptors becoming reduced to a neutral metal nanoparticle. In view of this on going research, the current study investigated the "factors" in the fungus *Fusarium oxysporum* which were responsible for platinum nanoparticle formation.

The fungus *F.oxysporum* was used in this study as it has been previously shown to produce a variety of nanoparticles including gold and silver. During exposure of the biomass to H_2PtCl_6 the initial response to the platinum salts was metal internalisation and subsequent reduction of H_2PtCI_6 to produce platinum nanoparticles. The observed localization and distribution of platinum precipitates provided some evidence for a hydrogenase mediated bioreduction of platinum salts to produce nanoparticles. Factors secreted by the fungus into the extracellular fluids, were shown to be responsible for platinum nanoparticle formation. From the identification, purification and characterisation studies it was concluded that a hydrogenase and other "factors" were responsible for platinum nanoparticle formation in *F.oxysporum.* Purification of the hydrogenase by freeze-drying and Sephacryl S_{200} size exclusion- ion exchange chromatography revealed the enzyme to be a dimer with a 29.4 and 44.5 kDa when analysed by a 10 % SDS-PAGE. Characterisation of the enzyme revealed optimal activity at a pH of 7.5 and temperature of 38 °C while it exhibited a poor thermal stability with a half life of 36 minutes. The kinetic parameters V_{max} and K_m were 3.16 U ml^{-1} and 3.64 mM respectively. The purified hydrogenase was used in subsequent experiments for the reduction of platinum salts, H_2PtCl_6 and $PtCl_2$. the results indicated an over 90 % reduction of the platinum salts and TEM micrographs indicated the production of platinum nanoparticles under the various experimental conditions.

Keywords: *Fusarium oxysporum*, platinum nanoparticles, hydrogenase

TABLE OF CONTENTS

INVESTIGATION OF THE "FACTORS" RESPONSIBLE FOR PLATINUM NANOPARTICLE FORMATION.....57

LIST OF FIGURES

LIST OF TABLES

LIST OF ABBREVIATIONS

µl	Microlitre
Å	Angstrom
atm	Atmosphere
AFM	Atomic Force Microscopy
BSA	Bovine Serum Albumin
e.g.	For example
EDX	Energy Dispersive X-ray Microanalysis
FD	Freeze Drying
g	Gram
x g	x G- force
H_2PtCl_6	Hexachloroplatinic (IV) Acid
hr	Hour
hrs	Hours
IEC	Ion Exchange Chromatography
kDa	Kilo dalton
keV	Kilo Electron Volt
MGYP	Malt Extract-Glucose-Yeast Extract-Peptone
min	Minute
mins	Minutes
ml	Millilitre
mM	Millimolar
NADH	Nicotinamide Adenine Dinucleotide (reduced)
nm	Nanometre
PDA	Potato Dextrose Agar
PGMs	Platinum Group Metals
$PtCl_2$	Platinum (II) Chloride
PVP	Polyvinylpyrrolidone
s	Seconds
SDS -PAGE	Sodium Dodecyl Sulphate – Polyacrylamide Gel Electrophoresis
SDS	Sodium Dodecyl Sulphate
SEC	Size Exclusion Chromatography

SEM	Scanning Electron Microscopy
STEM	Scanning Transmission Electron Microscopy
TEM	Transmission Electron Microscopy
UV	Ultraviolet
XEDS	X-ray Energy Dispersive Spectroscopy

ACKNOWLEDGEMENTS

I would like to extend my sincere appreciation to the following people for their contribution towards this thesis:

- God almighty, for the life and strength He gave throughout the course of this project.
- My supervisor Prof Chris G. Whiteley who supported me through the wonderful and difficult times I encountered during my research.
- Ms. M. Gericke (Mintek) for her constant help and support.
- Mintek ADM Researchers: Dr C. Claasens for help with the AFM, Dr A. Douglas and Dr. D. Compton for help with the TEM- XEDS.
- Prof J. Neethling and Dr N. Hashe from Nelson Mandela Metropolitan University for help with the TEM- EDX microanalysis.
- Lab 309 members Dr C.Togo, Taurai Mutanda, Aluwani Nemakula and Tamsyn Riddin for their support during my studies.
- A very special thank you to Nasheen Ragubeer for his constant support throughout all the difficult and happy times I have encountered during this period.
- To Sabashni Raman, thank you for the weekly calls, encouragement and support throughout my studies.
- This thesis is dedicated to my parents who prayed and supported me constantly. Thank you for believing in me and giving me the strength to prevail.
- A debt of gratitude to Mintek for the funding.

INTRODUCTION AND LITERATURE REVIEW

1. Introduction

Developments during the past decade in the scientific and engineering communities have resulted in a tremendous upsurge of interest in the properties of small particles in the field of nanoscience and nanotechnology. The unit nanometre derives its prefix *nano-* from the Greek word meaning "dwarf" (Vo-Dinh, 2005), therefore nanotechnology is the study of small structures and materials with structured features, in between those of atoms and bulk materials (Rao and Cheetham, 2001; Bhattacharya and Gupta, 2005), with at least one dimension in the nanometre range 1-100 nm.

Nanostructures are similar in size to many biological species, which comprise a variety of basic structures (Table 1.1). To give a better idea of the length of a nanometre, the hydrogen atom is about 0.1 nm, while a virus may be approximately 100 nm and an erythrocyte 2 500 nm in diameter, however it is living cells that are the best examples of machinery that operate at nanoscale, and currently there is no engineered mechanical, biological or chemical technology that matches the ability to perform at perfection levels seen in living cells.

1.1 What is nanoscience and nanotechnology

'Nanoscience' is the study of phenomena exhibited by materials at atomic, molecular and macromolecular levels, of dimensions ranging from a few nanometres to less than a hundred nanometres. In chemistry, this size range has been associated with colloids, micelles, polymer molecules and similar structures. In physical and electrical engineering, nanoscience is often associated with quantum behaviour, and electron behaviour in nanoscale structures. The fields of biology and biochemistry are also associated with nanoscience as cellular components (Table 1.1), such as DNA and RNA are considered to be nanostructures (Dowling, 2004). Whilst nanoscience is described as the study of the properties exhibited by nanomaterials, nanotechnology is the application of science to control matter at the molecular level. At the molecular level, the properties differ significantly from that of bulk materials.

Nanotechnology is thus referred to as the term for designing, characterization, production and application of structures, devices and systems by controlling shape and size at nanometre scale (Cao, 2004). Rao *et al*. (2004) described nanoscience and nanotechnology as a field which focuses on (i) the development of synthetic methods and surface analytical tools for building structures and materials, (ii) to understand the change in chemical and physical properties due to miniaturization, and (iii) the use of such properties in the development of novel and functional materials and devices.

Table 1. 1 Typical biological and atomic structures in the nanometre size range (Adapted from Rao *et al*., 2004)

Structure	Diameter (nm)
Hydrogen atom	0.1
5 silicon atoms	1
10 hydrogen atoms	1
DNA	2-12
Small proteins e.g. Chymotrypsin	4
Large proteins e.g. Aspartate transcarbamylase	7
Ribosome	20
Virus	100
Red blood corpuscle	2 500
Single strand of human hair	60-120 000

Nanoscience therefore offers exciting possibilities to study a state of matter, which is an intermediary between bulk and isolated atoms or molecules, and the effect of spatial confinement on electron behaviour, providing an opportunity to explore the problems related to surface or interface because of their interfacial nature (Zhang *et al*., 1994).The area of research in the field of nanotechnology is as diverse as physics, chemistry, material science, microbiology, biochemistry and also molecular biology. The interface of nanotechnology in combination with biotechnology and biomedical engineering has emerged by the use of nanoscale structures in diagnosis, gene sequencing, and drug delivery.

1.1.1 Emergence of nanotechnology

The "first" scientific study of nanoparticles took place in 1831, when Michael Faraday investigated the red ruby colloids of gold and made public that the colour was due to the small size of metal particles. For over 2000 years gold and silver have been used in glassware usually as nanoparticles, where they have been frequently used as colourants for church windows (Erhardt, 2003). It was only in 1959 that Nobel laureate physicist Richard Feynman thought of using atoms and molecules for fabricating devices, though it was only later in 1974 that the term nanotechnology was derived. Norio Taniguchi, a researcher at the University of Tokyo, used the term nanotechnology while engineering the materials precisely at the nanometre level (Bhat, 2003).

The primary driving force for miniaturization at that time came from the electronics industry, which aimed to develop tools to create smaller electronic devices on silicon chips of 40–70 nm dimensions. The use of the term, nanotechnology has since grown to include a diverse range of tiny technologies, such as material sciences (designing of new materials for wide-ranging applications), electronics (memories, computers, components and semiconductors) and biotechnology (diagnostics and new drug delivery systems) (Bhat, 2003).

1.1.2 Miniaturization and it's role in nanotechnology

Every substance, irrespective of composition, exhibits different properties when their size is reduced to less than 100 nm. The electron structure of a nanocrystal critically depends on its size, since for small particles the electronic energy levels are discrete and non- continuous as in bulk materials. This arises primarily due to the confinement of electrons within particles of dimension smaller than the bulk electron delocalisation length, a process termed as quantum confinement (Henglein, 1993). The special significance of nanotechnology is that the behaviour of matter is very different from what is familiar, generally understood or commonly accepted. Laws relating to physical, chemical, biological, electrical, magnetic and other properties at the nano-scale are different from those applicable to macro matter; as it is the laws of quantum mechanics that apply at this scale (Bhat, 2003).

The properties of nanomaterials which are dictated by the laws of quantum physics results in one or more of the following changes as described by Bhat (2003):

i. Miniaturization which is accompanied by a change in the physical properties.
ii. The bulk material behaviour is dominated by surface behaviour.
iii. Metals become harder, whilst ceramics become softer.
iv. Thin polymers become less permeable.
v. The production of stronger, more heat resistant, transparent materials.
vi. An increased chemical resistance corresponding with reduced weight.
vii. The development of new electrical properties.
viii. Emergence of new biological properties.

The properties of traditional materials change at nano level due to this quantum effect, and the behaviour of surfaces start to dominate the behaviour of bulk materials. The optical, mechanical, electrical, magnetic and chemical properties can therefore be systematically manipulated by adjusting the size, shape and composition of nanoscale materials. Quantum effects play an important role, as a reduction in size significantly changes the materials optical, magnetic and/or electrical properties. The extensive range of applications (Figure 1.1) shown by nanomaterials is as a result of the quantum effect (Bhat, 2003; Royal Society, 2003). Therefore analytical tools and synthetic methods allow for the control, composition and design of this nanometre range, yielding important advances in almost all fields of science.

Living organisms are built of cells (~10 µm in diameter) but the cell components are much smaller (usually in the sub-micron size domain). Proteins present in these cells have a typical size of 5 nm (Salata, 2004), which can be compared to the smallest man made nanoparticle. This size comparison has led to the possible use of nanoparticles as probes, which would afford scientists the ability to identify and understand cellular machinery (Taton, 2002).

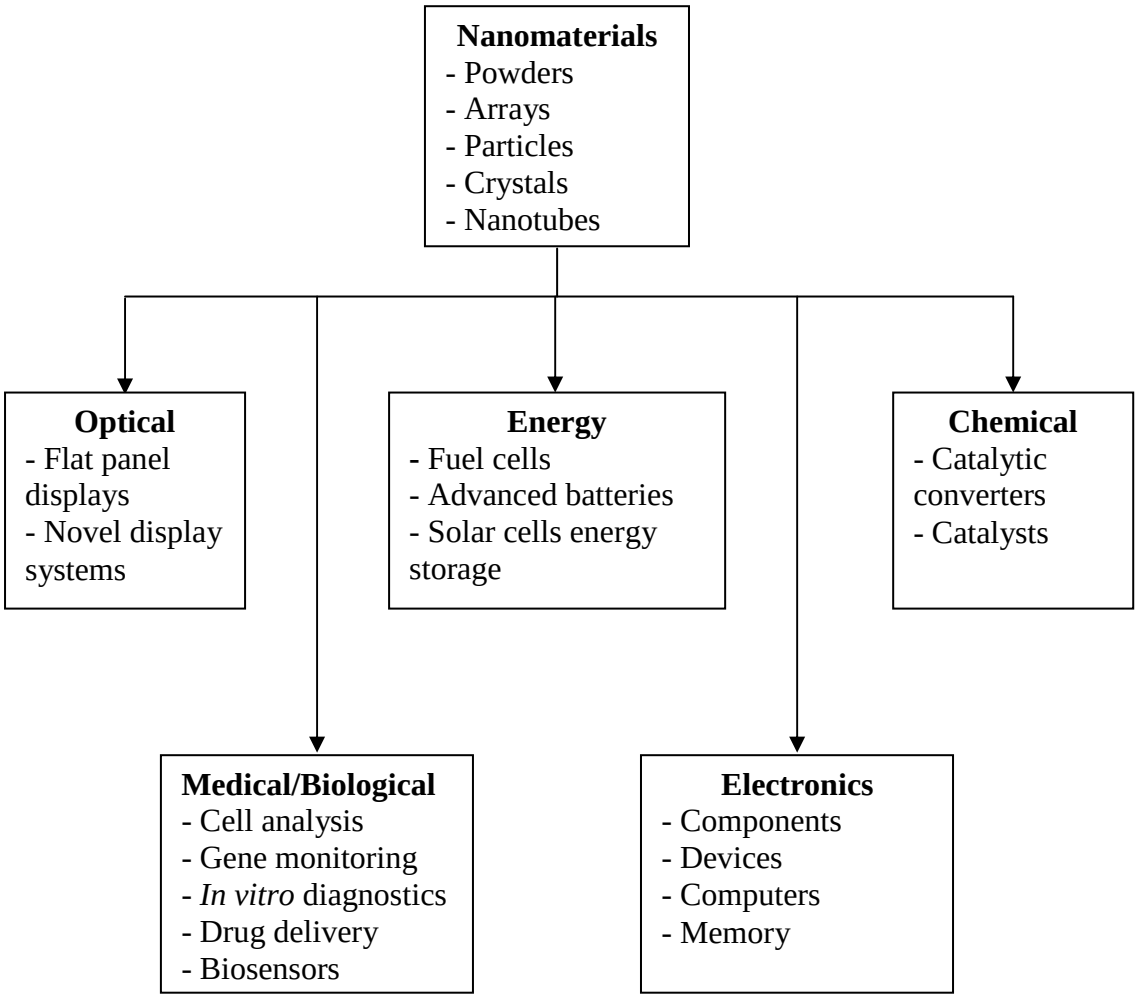

Figure 1. 1 Applications of nanomaterials adapted from Bhat (2003)

As aforementioned, the fact that nanoparticles exist in the same area as proteins makes nanomaterials suitable for bio-labelling or bio-tagging. Commercially, there has been major advancement in the use of nanomaterials for pharmaceutical applications, mainly for drug delivery (Salata, 2004). Numerous companies have exploited the quantum size effects in semiconductor nanocrystals, which are used for various industrial applications such as tagging of biomolecules for the use of bio-conjugated gold nanoparticles for cellular labelling (Bhat, 2003). Colloidal silver nanoparticles are currently being used in anti-microbial formulations and dressings (Mazzola, 2003), whilst titanium nanoparticles have been used in filters for bactericidal purposes (Salata, 2004). Nanomaterials have various applications and not surprisingly there are various techniques currently used to produce nanoparticles.

1.2 Methods for nanoparticle formation

Nanomaterials are abundant in nature as living organisms operate basically at a nanoscale level. Nanotechnologists seek to produce and utilize both novel and natural nanomaterials in larger quantities and within a more consistent size range (Doyle, 2006). Nanoparticles are viewed as fundamental building blocks of nanotechnology, and are the starting point for the preparation of various nanostructured materials and devices (Senapati *et al.,* 2005).

Nanoparticles can be produced using two techniques, (i) the top down approach or (ii) the bottom up approach. The top down approach refers to the breakdown of larger structures by use of ultra fine grinders, lasers and vaporisation followed by cooling (Senapati *et al.,* 2005; Doyle, 2006). The bottom up approach allows the rearrangement of these molecules to form complex structures with new and useful properties (Doyle, 2006). Both of these approaches play important roles in the nanotechnology industry however, both have their advantages and weaknesses.

For the top down approach the main challenge is the creation of increasingly small structures with sufficient accuracy, as compared to bottom up approach, where the main challenge lies in making the structure large enough and of adequate quality to be useful as materials (Fendler, 1998). The bottom up approach supports a better opportunity to obtain nanostructures with fewer defects, more homogenetic chemical composition with better short and long range ordering. The bottom up process is mainly driven by the reduction of Gibbs free energy; therefore the nano-structured materials are in a state closer to thermodynamic equilibrium (Doyle, 2006). This approach is contrary to the top down approach, which introduces internal stress in addition to surface defects (Senapati *et al.,* 2005).

Nanotechnologists however prefer to use the bottom up approach which involves the synthesis of nanostructures from the bottom, atom by atom, molecule by molecule or cluster by cluster (Senapati *et al.,* 2005). The various methods for the synthesis of nanoparticles by this ‘bottom up’ method are described as follows:

1.2.1 The Sol Process

In this approach, the reagents (metal ion solutions) are rapidly added into a reaction vessel containing a hot co-ordinating solvent such as alkyl phosphate, pyridine and alkylamine furan (Qu *et al*., 2001). This quick addition of reagents to the reaction vessel increases the precursor concentration, with the solution becoming supersaturated due to the high chemical reaction temperatures (Murray *et al*., 1993). As a result a short nucleation burst occurs and the concentration of the metal species in solution drops below the critical point of nucleation (Peng and Peng, 2001). This method produces a nano-cluster growth of metal species, and if this period of growth during the nucleation time is short enough, nano-clusters maybe uniform and mono-dispersed (Qu *et al*, 2001). There are a number of reports in the literature on nanoparticle synthesis utilizing this method, with a wide range of nanoparticles been successfully synthesised such as CdSe (Qu *et al*., 2001), CdS (Qu *et al*., 2004), ZnO (Shim and Guyot-Sionnest, 1998), bimetallic clusters such as CdSe/ZnS (Talapin *et al.*, 2001), CdSe/CdS (Chen *et al*., 2003) and CdSe nanorods (Peng *et al*., 2002).

1.2.2 Chemical Precipitation

During this process organic molecules are utilised to control the release of the reagents and metal ions in solution during the precipitation process (Senapati *et al.*, 2005). The particle size is influenced by the reactant concentration, pH and temperature. By engineering these factors, CdTe (Gao *et al*., 1998) and HgTe (Rogach *et al*., 1999) nanoparticles have been produced by this approach. Although the method of using precipitation to produce nanoparticles is considered to be straightforward and simple, very complicated nano-structures such as CdS/ HgS/ CdS (Braun *et al*., 2001) and CdS/ $(HgS)_2$ / CdS (Harrison *et al*., 2000) have been produced.

1.2.3 Synthesis of nanoparticles using pyrolysis

Pyrolysis is a chemical process in which chemical precursors decompose into solid compounds and the unwanted waste evaporates away (Senapati *et al.*, 2005). It has been used to prepare various kinds of nanoparticles including metals, metal oxides, semiconductors, and composite materials. Generally the pyrolytic synthesis of compounds leads to powders with a size distribution in the micrometer range, though to get uniform nano-sized material, revisions of the procedure need to be changed

such as slowing of the reaction or decomposition in an inert solution (Senapati *et al.*, 2005).

1.2.4 Use of micelles

The use of reversed micelles in the synthesis of metal nanoparticles has been well documented in the literature, with reducing agents such as $NaBH_4$, N_2H_4 and H_2 being used (Ingelsten *et al*., 2001). A variety of nanoparticles such as Pt, Rh, Pd and Ir have been synthesised using this process (Sangregorio *et al*., 1996). The water content of the micelles seems to greatly affect the shape of nanoparticles and thus nano-wires such as $BaCO_3$ and $BaSO_4$ have been synthesised (Qi *et al*., 1997).

1.2.5 Synthesis of nanoparticles using bio-based protocols

Tremendous growth in the nanotechnology field is due to the availability of new methods for nanomaterials synthesis as well as improved tools for characterization and manipulation. Various methods for the synthesis of nanomaterials, nanotubes and their assemblies are available including various organic, inorganic and biological systems (Bhattacharya and Gupta, 2005). Although solution based chemical methods have been the building blocks for nanoparticle synthesis, there has been an increase in focus to develop green chemistry, or eco-friendly methods for nanomaterials synthesis (Sastry *et al*., 2004, Bhattacharya and Gupta, 2005). Novel methods have emerged from biomimetics, an interdisciplinary approach which is defined as the "materials science and engineering through biology" (Klaus-Joerger *et al*., 2001).

Nanobiotechnology is the term currently used to describe the production of nanomaterials using biological means (Sastry *et al*., 2004). Both biomimetics and nanobiotechnology embrace the study of biology as one of the central features of biological systems is their capacity to integrate molecular synthesis within higher levels of structural and dynamical organisation (Mann, 1995). It is known that biological systems provide a variety of metal or metal containing particles in the nanometre range (Klaus-Joerger *et al*., 2001). Many multicellular organisms use inorganic materials such as calcium carbonate or silica in combination with organic matrices (proteins, lipids or polysaccharides) (Mann, 1995), to produce materials such as skeletal units, bones and teeth (Mann, 1995; Klaus-Joerger *et al*., 2001).

1.2.5.1 Role of bacteria in nanomaterials synthesis

It is only in relatively recent years that scientists have turned towards bacteria as possible eco-friendly nanofactories (Bhattacharya and Gupta, 2005). Beveridge and co-workers showed that gold nanoparticles of nanoscale dimensions can be readily precipitated within bacterial cells during incubation with Au^{3+} (Southam and Beveridge, 1996; Bhattacharya and Gupta, 2005). Klaus-Joerger and colleagues demonstrated that the metal resistant bacterium *Pseudomonas stutzeri* AG259, (isolated from a silver mine) produced Ag^{+} ions when challenged with concentrated $AgNO_3$, forming silver nanoparticles with well defined size (ranging from a 3-200nm) and distinct morphology (Klaus-Joerger *et al*., 1999). Most of the nanoparticles formed were found to be composed of elemental silver, with the occasional formation of Ag_2S observed.

Biofilms of metal nanoparticles embedded in a biological matrix may have important applications in the synthesis of eco-friendly and economically viable cement materials for optically functional thin film coating (Senapati *et al.,* 2005). Joerger *et al.* (2000) showed that heat treatment of the Ag nano-bacteria biomass yielded hard coatings of a cement, which was resistant to mechanical scratching with a knife and whose optical properties could be tailored by varying the silver loading factor. The cement material was composed primarily of graphite carbon and up to 5 % by weight (of the dry biomass) of silver.

Nair and Pradeep (2002) demonstrated that exposure of large concentrations of metal ions to bacteria could also be used to produce nanoparticles. These authors showed that *Lactobacillus*, present in buttermilk, produced nanoparticles when exposed to gold and silver ions, resulting in the production of nanoparticles within the bacterial cell. They also concluded that the nucleation of the gold and silver nanoparticles occurs on the cell surface through sugars and enzymes in the cell wall, following which the metal nuclei are transported into the cell where they aggregate and grow to larger-sized particles. Holmes and co-workers (1995) demonstrated that exposure of *Klebsiella aerogenes* to Cd^{2+} ions resulted in the formation of CdS nanoparticles in the nanometre range 20-200 nm.

In an extension of the bacteria based methodology for the growth of nanoparticles the thermophilic iron-reducing *Thermoanaerobacter ethanolicus* was shown to substitute metals (Co, Cr, Ni) into magnetic octahedral-shaped nanoparticles (Roh *et al*., 2001). Until recently a vast range of prokaryotes were used as prospective nanoparticle synthesisers, though the use of eukaryotes could offer exciting possibilities in nanobiotechnology.

1.2.5.2 Potential of eukaryotes in nanoparticle synthesis

Dameron and co-workers (1989) were the first to demonstrate that the yeasts such as *Schizosaccharomyces pombe* and *Candida glabrata* were capable of intracellular production of CdS nanoparticles when challenged with cadmium salt in solution. Yeast cells exposed to Cd^{2+} ions produce metal-chelating peptides (glutathiones), accompanied by an increase in the intracellular sulphide concentration and the formation of nanocrystalline CdS. The use of fungi in the synthesis of nanoparticles is a relatively recent addition to the list of microbes described in section 1.2.5.1. One of the novel works defining the use of fungi for nanoparticle synthesis was carried out by Mukherjee and colleagues for production of silver nanoparticles using *Verticillium* (Mukherjee *et al*., 2001). The novel use of fungi to produce nanoparticles continued and nanoparticles of gold (Mukherjee *et al*., 2002) and platinum (Riddin *et al*., 2006) were synthesised using the fungus *Fusarium oxysporum*. With increasing success of bio-organisms in the formation of nanomaterials, the potential of nanotechnology is also increasing in the spectrum of science.

1.3 Fusarium oxysporum

The genus *Fusarium* contains many plant pathogenic fungi, with members inciting diseases in plants, humans and domestic animals (Leslie and Summerell, 2006). *Fusarium oxysporum*, a member of this genus, is a cosmopolitan soil saprophyte, responsible for an enormous range of plant diseases, usually involving vascular wilt syndrome, damping off problems (Nelson *et al.*, 1981), crown and root rots (Jarvis and Shoemaker, 1978).

1.3.1 Taxonomy, Pathology and Ecology

F.oxysporum is the most widely distributed of all *Fusarium* species and can be isolated from most soils, the Arctic, tropical and deserts (Summerell and Rugg, 1992). It is one of the most economically important species in the *Fusarium* genus, as a result of its numerous hosts, and the level of loss resulting from infection. *F.oxysporum* has also been associated with various human infections including corneal infections (Rosa *et al*., 1994), dermatitis (Guarro and Gene, 1995), local and systemic infections (Leslie and Summerell, 2006).

1.3.2 Commercial and Industrial Applications of F.oxysporum

Various strains of *F.oxysporum* have the ability to metabolise, usually during catabolism, numerous sugars and a variety of other compounds including aromatics, glycerol and penicillin V (Leslie and Summerell, 2006). This fungus has also shown the ability to accumulate significant levels of arsenic (Granchinho *et al*., 2002) and to reduce the toxicity of asbestos by chelation of the iron from the asbestos fibres (Martino *et al*., 2004). A phospholipase produced by *F.oxysporum* is now commercially available, and is currently utilised during an oil-degumming step in the refining of vegetable oils (Clausen, 2001).

1.4 Platinum

Members of the Platinum Group Metals (PGMs) include platinum, palladium, rhodium, ruthenium, iridium and osmium, forming an essential group of elements of increasing usage in the technology developing world (Rao and Reddi, 2000).

1.4.1 Sources of platinum

Platinum can be found occurring naturally, accompanied by small quantities of iridium, ruthenium, palladium, osmium and rhodium. Although platinum is found in the earths crust, it is characteristically similar to other PGMs with reference to low crystal abundance, only 1-10 ngg^{-1} (Matthey, 2006). The main sources of alluvial deposits are in the Ural Mountains of Siberia and in certain West American States. Sperrylite (platinum arsenide) can be found in nickel-bearing sulphide ore deposits at Sudbury, Ontario. In South Africa a large suite of platinum containing chalcogenide minerals are found associated with sulphide mineralisation.

South Africa is however the leading country with 85 % of the world population PGM and has 78 % of the worlds economic resources (Rao and Reddi, 2000).

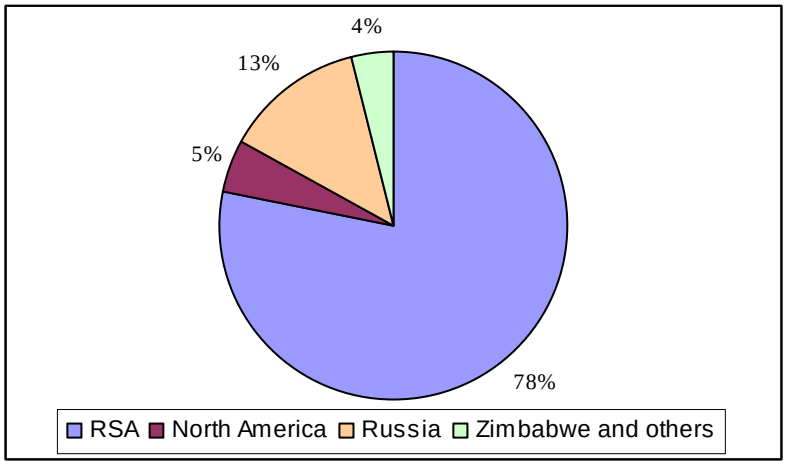

Figure 1. 2 Major suppliers of platinum adapted from Rao and Reddi (2000).

1.4.2 Demands and applications of platinum

PGMs have varied applications in diverse fields. Although gold is the traditional metal for jewellery, platinum has benefited from its new fashion awareness. It has a co-efficient of expansion almost equal to that of soda-lime-silica-glass, and has therefore been used in the manufacturing of sealed-in electrodes in glass apparatus. Platinum does not oxidise in air at any temperature; however it is corroded by halogens, cyanides, sulphur, and caustic alkalis. Although platinum is extensively used in the jewellery industry, it is used extensively as wire (for electrochemical cells), vessels for laboratory uses and many industrial products (such as thermocouples). Platinum resistance wires are used for constructing high temperature electric furnaces. It is also used for coating missile nose cones, jet engine fuel nozzles, gas turbine blades, which have to perform reliably for long periods under stressful conditions (high temperatures under oxidizing conditions).

Platinum is an excellent catalyst in its finely divided state, and has been used during the contact process for sulphuric acid production. This has resulted in the increased interest in the use of platinum as a catalyst in fuel cells and antipollution devices for automobiles, for the purpose of reducing levels of carbon monoxide, unburnt hydrocarbons and nitrogen oxides in the exhaust gases (Rao and Reddi, 2000).

A fuel cell is described as an electrochemical mechanism that combines hydrogen and oxygen to produce heat, electricity and water. The electrodes used are platinum-coated; these pollution free technologies have become a major player in the automobile industry and hence boost platinum demand (Rao and Reddi, 2000).

This new pollution free technology has resulted in an increase in platinum consumption in the auto-catalyst industry, using 71 % of the total world platinum supply. The demand for platinum in electrical and electronic applications is expected to grow by 18 % as a result of high levels of platinum usage in computer hard drives. The chemical platinum requirements are expected to rise with the increase in demand for platinum gauze during nitric acid production.

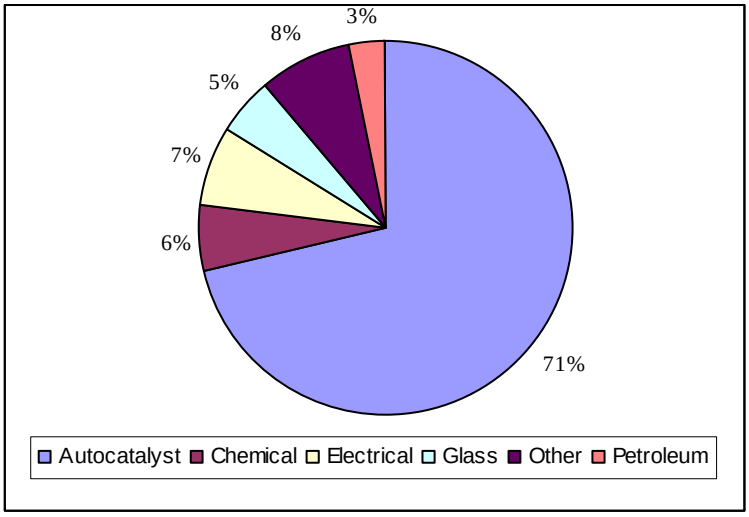

Figure 1. 3 Industrial demand of platinum by application, adapted from Rao and Reddi (2000).

1.4.3 Physical-Chemical Properties

Platinum belongs to group 10 in the periodic table, has an atomic number of 78 and a molecular weight of 195.084. It is a silvery white metal when pure and is malleable and ductile. Some of the useful physical and chemical properties of platinum are listed in Table 1.2. Platinum is insoluble in almost all acids, however, it dissolves in aqua regia (a mixture of hydrochloric and nitric acids) to form chloroplatinic acid, an important compound, used in platinum nanoparticle synthesis (Matthey, 2006; Riddin *et al.*, 2006).

Table 1. 2 Physical and chemical properties of platinum, adapted from Matthey (2006).

Platinum Properties	
1. Density (kg/m^3) at 20°C	2.154 x 10^{-4}
2. Melting point range (°C)	2041-2045
3. Boiling point range (°C)	3800- 4530
4. First ionisation potential (eV)	8.9 – 9
5. Resistivity (μohm.cm at 20 °C)	10.3
6. Electrochemical oxidation potential (v)	-1.2

1.4.4 Platinum nanoparticle applications

Platinum nanoparticles possess an unusual property which may be useful for manufacturing new substances and for the development of new materials. Researchers at the Japan Fine Ceramics Centre, Nagoya, Japan, discovered that platinum nanoparticles when heated to high temperatures fuse together with the material they coat, and using microscopy discovered that the platinum molecules actually "burrow" into the surface of zeolite they cover (Kato *et al* ., 2004). These scientists suggested that this phenomenon could be used to produce tailored porous materials, thereby providing a number of applications in the ceramics industry. Other practical applications of platinum nanoparticles include their use in semiconductor chips, hydrogen storage in fuel cells and particle chemotherapy targeted against cancer cells (Salata, 2004). The latest application of platinum nanoparticles is the advent of a new digital memory device, created by the incorporation of platinum nanoparticles into the tobacco mosaic virus to make a novel electronic memory element (Knez and Gösele, 2006).

1.5 Mechanisms of PGM metal reduction using microorganisms

Biological systems at room temperature and near neutral pH involve low energy consumption and are environmentally safe (Konishi *et al.*, 2007) providing an attractive, environmentally friendly "green chemistry" method for nanoparticle synthesis and recovery. Noble metals such as silver (I) and gold (III) have been biologically reduced and deposited using microorganisms (Klaus *et al.*, 1999; Kashefi *et al.*, 2001; Lloyd 2003; Lloyd *et al.*, 2003; Sastry *et al.*, 2003; Konishi *et al.*, 2006), plants (Gardea-Torresdey *et al.*, 2002) and plant extracts (Shankar *et al.*, 2004), however much less is known about the bioreductive deposition of PGM.

Sulphate-reducing bacterium *Shewanella oneidensis* is capable of reducing soluble Pd (II) into insoluble Pd (0) using formate, lactate, pyruvate or hydrogen as the electron donor (De Windt *et al*., 2005). Yong *et al.* (2002) demonstrated that the bioreductive deposition of Pt (IV) and rhodium (III) could not be achieved using *Desulfovibrio desulfuricans*, despite other studies reporting to the contrary (Ngwenya and Whiteley, 2006; Rashamuse and Whiteley, 2007). Recent studies demonstrated that cells of the metal ion reducing bacterium *Shewanella algae* (Konishi *et al.*, 2007) and fungus *F.oxysporum* (Riddin *et al*., 2006) were capable of depositing Pt nanoparticles by the bioreduction of $PtCI_6^{2-}$ ions. The various physio-chemical and biological processes in microorganisms result in metal transformation. There are currently six established mechanisms in which microorganisms interact with metals: exclusion by a permeability barrier, intra- and extracellular sequestration, active transport efflux pumps, enzyme detoxification and the reduction in the sensitivity of cellular targets to ions (Bruins *et al*., 2000). The type of resistance mechanism that microorganisms exhibit in response to the presence of metal ions depends on the concentration of available metals e.g. *E.coli* can tolerate metal concentrations up to the 100 µM (Val's and de Lorenzo, 2000).

1.5.1 Metal exclusion by permeability barrier

Alterations in the cell wall, membrane or envelope of microorganisms are an example of metal exclusion by permeability barrier. This mechanism is thought to be an attempt by the microorganism to protect metal-sensitive, essential cellular components. One of the prominent examples of this is in *E.coli*, where the exclusion of Cu (II) resulted from altered production of the membrane channel protein porin (Rouch *et al*., 1995). This is thought to occur as a result of a single gene mutation, which decreases the permeability of the membrane to metal ions (Ji and Silver, 1995).

1.5.2 Intracellular sequestration of metals by protein binding

Intracellular sequestration is the accumulation of metals within the cytoplasm to prevent exposure to essential cellular components. Two examples for this form of metal resistance: metallothionein production in *Synechococcus* sp. and cystein–rich proteins in *Pseudomonas* sp (Silver and Phung, 1996).

Metallothioneins are low weight (6-7 kDa), cysteine rich residues, found in higher plants, eukaryotic microorganisms and prokaryotes, and in eukaryotes they are responsible for detoxification of metals by the formations of complexes (Mejare and Bellow, 2001). The biosynthesis of metallothioneins is regulated at the transcriptional level and is induced by several factors e.g. hormones, cytotoxic agents and metals including Cd, Zn, Hg, Cu, Au, Ag, Co, Ni and Bi (Kagi and Schäffer, 1988; Mejare and Bellow, 2001). The non essential metal ions such as Cd, Hg, Pb, Bi, Ag, Au and Pt are sequestered by metallothioneins (Kagi, 1991; Mejare and Bellow, 2001).

1.5.3 Extracellular sequestration

Metal resistance based on extracellular sequestration has been hypothesised in bacteria, several yeast species and fungi (Joho *et al*., 1995). The yeast *Saccharomyces cervisiae*, carries a methylglyoxal resistance gene which has the ability to form extracellular metal-glutathione complexes in metal rich media (Murata *et al*, 1985). A similar mechanism exists in Cu (II) resistant fungi (Murphy and Levy, 1983) and these fungi secrete oxalate to form a metal-oxalate complex.

1.5.4 Active transport of metal ions away from the microorganism

Efflux systems or active transport represents the largest category of metal resistance systems. Microorganism use active transport/efflux systems to export toxic metals from the cytoplasm. These mechanisms are considered to be chromosomal or plasmid –coded. Non-essential metal ions enter the cell through the nutrient transport systems; however, they are rapidly exported. These active transport systems can be ATPase or non ATPase–linked, and is thought to be highly specific for cation or anion export (Nies, 1995).

1.5.5 Enzymatic detoxification of a metal to a less toxic form

An example of a model for enzymatic detoxification response in microorganisms is mercury resistance. Mercury is toxic as it binds to and inactivates essential thiols which are a part of enzymes and proteins. Bacteria contain a set of genes that forms Hg (II) resistance operons which detoxifies and removes Hg (II) (Ji and Silver, 1995, Ehrlich, 1997). This set of genes also encodes the production of a periplasmic binding protein and membrane associated transport system, which collects Hg (II) from the surrounding environment and transports it to the cytoplasm for detoxification (Misra, 1992).

1.5.6 Reduction in metal sensitivity of cellular targets

Some microorganisms adapt to the presence of toxic metals by altering the sensitivity of essential cellular components, providing natural protection (Rouch *et al*, 1995). This protection is achieved by mutations that decrease sensitivity but do not alter basic function, or by increasing production of a particular cellular component in order to keep ahead of metal inactivation (Valls and de Lorenzo, 2000). Several applications exist for a metal resistance mechanism: metal recovery by bacterial sequestration/precipitation in wastes, bioaccumulation of valuable metals (Ag, Au, and Pt), bioleaching, and recently the ability to produce nanoparticles (Sastry *et al*., 2004)

1.6 Hydrogenases

Hydrogen plays an important role in the metabolism of microorganisms, where the reaction

$$2H^+ + 2e^- \leftrightarrow H_2 \ldots\ldots (1)$$

is catalysed by metalloenzymes known as hydrogenases (Armstrong, 2004). These hydrogenase enzymes are found in a variety of organisms ranging from aerobes to anaerobes, autotrophs to heterotrophs, prokaryotes to eukaryotes, fermentative organisms and sulphate reducers (Stallings, 2004). The various hydrogenases found in different microbial species differ in molecular weight, quaternary structure, active site orientation, and specificity with respect to the type of electron carriers (Zadvorny *et al*., 2004). The first hydrogenase was described in 1931, as a bacterial enzyme that catalysed the reversible oxidation of hydrogen to protons and electrons according to reaction 1 (Stephenson and Strickland, 1931).

The catalytic processes of hydrogenases involve the following steps:

(i) activation or production of hydrogen at the active centre,

(ii) transfer of two electrons between the active site and the redox partner of the hydrogenase and

(iii) transfer of two hydrogen atoms between the active centre and the medium solvent (De Lacey *et al*., 2000).

Most, if not all, hydrogenases can catalyse the reaction in either direction *in vitro*; they are usually committed to catalyse either hydrogen uptake or evolution *in vivo*, depending on the demands of the host organism (Vignais *et al*., 2001).

1.6.1 Classification of hydrogenases

Until 2004, hydrogenases were classified according to the metals believed to be found at their active sites. Only three classes were recognised (i) iron only (Fe-only), (ii) nickel-iron (NiFe), and (iii) "metal free". In 2004, Lyon *et al*. showed that "metal free" hydrogenases in fact did contain iron, therefore those enzymes previously called "metal free" were renamed Fe-S free, as this protein, unlike the Fe-only enzymes, contained no inorganic sulphide group (Lyon *et al*., 2004). The vast majority of known hydrogenases belong to the first two classes, with over 100 of these enzymes been genetically and/or biochemically characterised.

1.6.1.1 The NiFe hydrogenase

In some NiFe hydrogenases, one of the Ni-bound cysteine residues is replaced by selenocysteine. On this basis of sequence similarity, the NiFe and Ni-Fe-Se hydrogenases are considered to be a superfamily. The Ni-Fe hydrogenases are heterodimeric proteins consisting of small (S) and large (L) subunits. The small subunit contains three iron-sulfur clusters while the large subunit contains a nickel-iron centre (Figure 1.4). Periplasmic, cytoplasmic, and cytoplasmic membrane-bound hydrogenases have been found (Nicolet *et al.*, 2000).

The Ni-Fe hydrogenases, when isolated, are found to catalyse both H_2 evolution and uptake, with low-potential multihaem cytochromes such as cytochrome c_3 acting as either electron donors or acceptors, depending on their oxidation state. Ni-Fe hydrogenases have low specific activities and have been shown to function in the oxidation of hydrogen. This class of hydrogenases are found predominantly in all *Desulfovibrio sp* therefore a great deal of research has been done on this type of enzyme from *D. gigas* (Albrecht, 1994). They are periplasmic proteins consisting of two subunits of molecular masses 60 and 28 kDa, however other subunits may be present allowing the hydrogenase to interact with dedicated electron carriers (e.g. NAD^+, F_{420}, and cytochrome *b* (Albrecht, 1994). According to De Lacey *et al*. (2000), this metallo-protein contains 12 Fe atoms, 12 acid labile sulphides and one Ni atom per molecule. X-ray structure studies revealed that the active site is located in the large subunit near the interface with the small subunit.

The active site consists of a binuclear NiFe centre and accessibility of hydrogen to the active site of this protein seems quite clear. X-ray crystallographic and molecular dynamic studies have shown the existence of hydrophobic channels that connect the molecular surface of the enzyme with the active site. However, there is still some great controversy on whether the splitting of the hydrogen occurs on the nickel or iron atom (De Lacey *et al*., 2000).

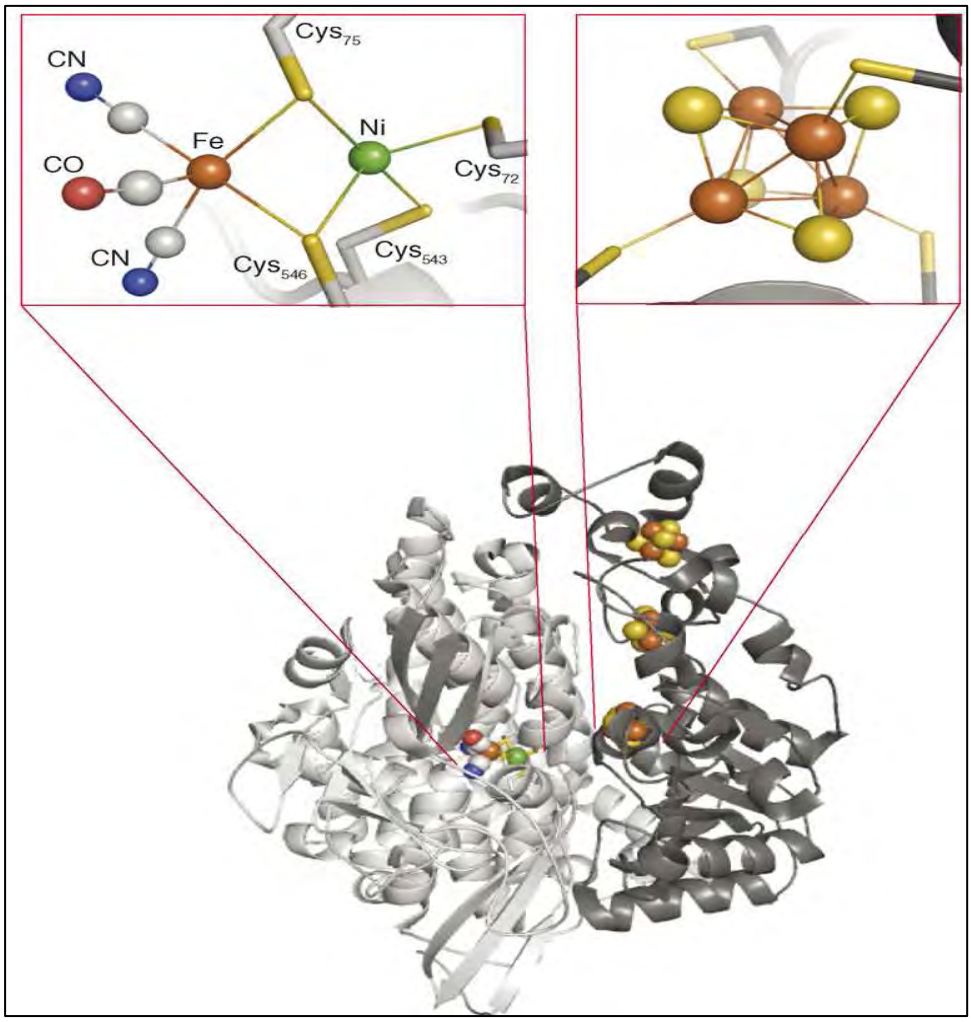

Figure 1. 4 The structures of the ready oxidized form of the [NiFe] hydrogenase from *Desulfovibrio fructosovorans* (pdb 1YRQ), the dinuclear cluster of the active site in the large subunit, and one of the Fe–S clusters in the small subunit are shown. The large subunits are depicted as light grey ribbons and the small subunits are dark grey ribbons. The colour scheme is: iron, orange; nickel, green; sulphur, yellow; oxygen, red; and nitrogen, blue. Figure adapted from Leach and Zamble (2007).

1.6.1.2 Fe-only hydrogenases

The hydrogenases containing Fe-S clusters and no other metals than iron are referred to as either Fe hydrogenases (Fe-Hases) or Fe-only hydrogenases (Figure 1.5). There are currently three recognized families of Fe-only hydrogenases:

(i) The cytoplasmic, soluble, monomeric Fe-Hases. These are found in strict anaerobes such as *Clostridium pasteurianum* and *Megaspaera elsdenii*. This family is extremely sensitive to inactivation by O_2 and catalyses both H_2 evolution and uptake. They are also found in the chloroplast of green alga *Scenedesmus obliquus*, and they catalyse H_2 evolution. The $[Fe_2S_2]$ ferredoxin functions as a natural electron donor linking the enzyme to the photosynthetic electron transport change.

(ii) The periplasmic, heterodimeric Fe-Hases from *Desulfovibrio sp.* These Fe-Hases can be purified aerobically and catalyse mainly H_2 oxidation.

Although the Ni-Fe and Fe-only hydrogenases belong to different classes they share common features in their structures.

(i) Each enzyme has an active site and a few Fe-S clusters which are buried in the protein.

(ii) The active site, which is believed to be the place where catalysis takes place, is also a metallo-cluster with each metal being coordinated by carbon monoxide (CO) and cyanide ligands (CN^-) (Lyon *et al*., 2004).

Fe-only hydrogenases have high specific activities and function to evolve hydrogen. Studies have demonstrated that Fe – only hydrogenases generally contain two [4Fe – 4S] clusters (the F-clusters) in a ferredoxin-like domain. Studies on the *Desulfovibrio desulfuricans* Fe hydrogenase have shown that it is a periplasmic protein made of two different subunits of molecular masses 43 and 10 kDa. It has been demonstrated that the location of hydrogenases in bacterial cells is representative of its function.

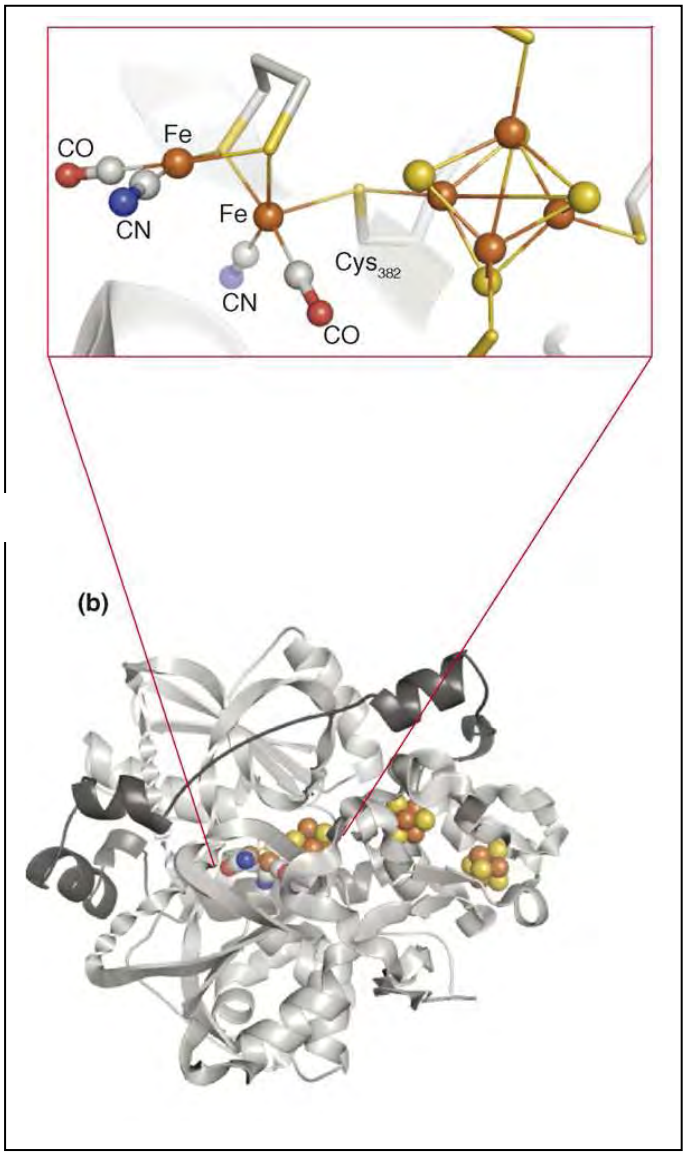

Figure 1. 5 The structure of the [Fe-only] hydrogenase from *Desulfovibrio desulfuricans* (pdb 1HFE) is shown as well as the H cluster. The large subunits are depicted as light grey ribbons and the small subunits are dark grey ribbons. The colour scheme is: iron, orange; nickel, green; sulphur, yellow; oxygen, red; and nitrogen, blue. Figure adapted from Leach and Zamble (2007).

1.6.2 Role of hydrogenases in nanoparticle formation

Fungi like other microorganisms can produce chemical transformations of metals by oxidation, reduction, methylamine and dealkylation (Gadd, 1993), although information is not widely available as compared to bacteria. Enzymatic metal transformations are suggested to be involved as part of the survival mechanism, as the transformed metal species could be less toxic than their original species.

A copper reducing enzyme, copper reductase catalyses Cu (II) reduction to Cu (I) with NADH or NADPH as the electron donor (Wakatsuki *et al*., 1991; Gadd, 1993). That study showed the location of Cu reductase to be in the cell wall and the process to have a role in the regulation of Cu uptake (Wakatsuki *et al*., 1991). Other fungal reductions of metals include the reduction of tellurite to elemental tellurium (Smith, 1974; Gadd, 1993), selenate to selenium, with site of deposition on the fungal cell walls and membranes (Konetzka, 1977). Literature illustrates that enzymes are known to play a role in metal transformations; however the role of enzymes in nanoparticle formation is a relatively new and developing field of study.

The mechanism of formation of nanoparticles in microorganisms is unknown, though there are hypotheses which suggest that different biosynthetic products such as α-hydroxy carboxylic acids or reduced co-factors play an important role in the reduction of metal salts to nanoparticles (Willner *et al*., 2006). Bacterial hydrogenases have been harnessed for the removal of heavy metals from solution by reduction to less soluble metal species (Macaskie *et al*., 2005). A study conducted on the exposure of *F.oxysporum* to $AuCl_4$ (aq) and $CdSO_4$ (aq), yielded Au and CdS nanoparticles, and initial results from that study indicated the presence of four protein bands. Reaction with the protein mixture following dialysis did not yield nanoparticles, however with the addition of NADH to the dialysate, Au and CdS nanoparticle formation was restored. The authors believe that it is a NADH dependent enzyme which is responsible for nanoparticle formation in *F.oxysporum* (Ahmad *et al*., 2002a; Mukherjee *et al*., 2002).

A mechanism for the involvement of hydrogenases in metal reduction has been proposed in *F.oxysporum* (Figure 1.6). Under the ideal conditions *F.oxysporum* can reduce the platinum salt back to a base metal via hydrogenase activities to produce platinum nanoparticles. The protons generated from the oxidation of molecular hydrogen by hydrogenases are utilised for the metabolic activities of the cell, whilst the electrons released are channelled away to electron acceptors through the electron transport chain. Ordinarily this electron acceptor would be another ion, but if *F. oxysporum* comes into contact with certain metal ions, it would use these as the electron dump/sink.

During this process positively charged platinum particles act as electron acceptors, whereby they become reduced to a neutral metal species after two cycles, thus leading to the reduction of the platinum salt, resulting in subsequent nanoparticle formation.

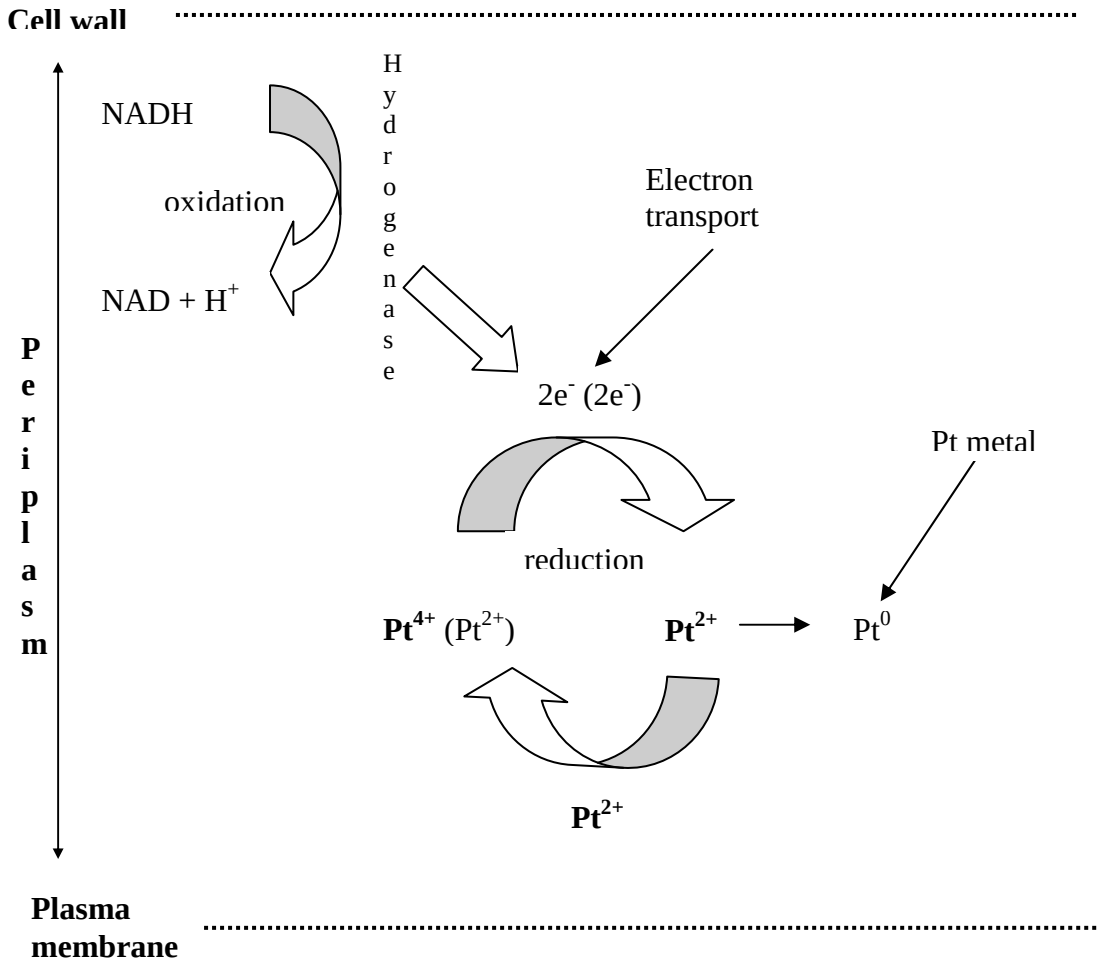

Figure 1. 6 Proposed schematic representation of platinum (IV) reduction by a hydrogenase in *F.oxysporum* (Mintek and Whiteley, 2006).

1.7 Hypothesis, Aims and Objectives

Hypothesis

The bioreduction of platinum ions into nanoparticles by metal peptides /reductase/hydrogenase enzymes, in the fungus *Fusarium oxysporum*, under varying conditions of temperature, pH and metal chloride concentration forms nanoparticles of a predefined shape and size.

Aim

On the basis of broad metal reductase activity *via* hydrogenase, *F.oxysporum* can reduce platinum salts enzymatically to produce platinum nanoparticles.

Objectives

1. Produce nanoparticles both inter- and extracellulary.

2. Identify, isolate and purify those factors (enzymes/proteins) involved in Pt nanoparticle formation.

3. Test the purified 'factor(s)' ability to produce platinum nanoparticles.

INTERCELLULAR BIOSYNTHESIS OF PLATINUM NANOPARTICLES USING *FUSARIUM OXYSPORUM*

2. Introduction

In the field of nanotechnology, the controlled synthesis of nanoparticle size, shape and monodispersity is essential in order to explore their unique chemical and physical properties. Currently there are various chemical and physical synthetic methods (Murray *et al*., 1993; Motte *et al*., 1997; Fendler and Meldrum, 2004) aimed at controlling the size and distribution of nanoparticles. Most of these methods, however, utilise toxic and expensive chemicals, and problems are often experienced with nanoparticle stability, agglomeration of particles and the inability to control crystal growth (Brust and Kiely, 2002; Kowshik *et al*., 2003; Huang and Yang, 2005). Consequently there is a growing need for the development of non-toxic, clean, eco-friendly and inexpensive synthetic protocols, thereby shifting the focus from conventional chemical methods to 'green' processes.

In recent years the utilization of biological systems has emerged as a novel technology for the synthesis of various nanoparticles in an attempt to control nanoparticle shape, composition, size and monodispersity (Southam and Beveridge, 1996; Klaus *et al*., 1999; Joerger *et al*., 2000; Klaus-Joerger *et al*., 2001; Nair and Pradeep, 2002;). Beveridge and colleagues (Beveridge and Murray, 1980; Southam and Beveridge, 1996) demonstrated that gold nanoparticles could be readily precipitated within bacterial cells by the incubation of the cells with Au^{3+} ions. Klaus-Joerger and co-workers (Klaus *et al*., 1999; Klaus-Joerger *et al*., 2001) demonstrated that the bacterium *Pseudomonas stutzeri* AG259, isolated from a silver mine, exhibited the ability to reduce $AgNO_3$ to form silver nanoparticles within the periplasm of the bacterium. Nair and Pradeep (2002) showed that nanoparticles of gold, silver and their respective alloys could be synthesised within the cells of *Lactobacillus sp.* following cell exposure to the corresponding metal salts. Strategies are currently being employed to widen the scope of microorganisms that until recently, has relied on the use of prokaryotes, specifically bacteria, for intercellular synthesis of nanoparticles.

A number of different genera of fungi have been investigated in the synthesis of gold (Mukherjee *et al*., 2001b; 2002; Ahmad *et al*., 2003b; He *et al*., 2007), silver (Mukherjee *et al*., 2001a, Ahmad *et al*., 2003a; Duran *et al*., 2005; Vigneshwaran *et al*., 2006; Vigneshwaran *et al*., 2007), silica and titanium (Bansal *et al*., 2005) and zirconia nanoparticles (Bansal *et al*., 2004).

2.1 Biosynthesis of platinum nanoparticles

Transition metal nanomaterials have attracted attention due to their greater catalytic properties than their bulk materials (Yang *et al*., 2007). The properties of the transition metal platinum, include a high melting point of 1769 °C, and resistance to corrosion as well as chemical attack (Rao and Reddi, 2000; Yang *et al*., 2007). To maximise the industrial applications and catalytic affectivity of platinum nanoparticles, the shape and size of platinum must be controlled. Various platinum nanoparticle synthetic methods ranging from one to hundreds of nanometres in size, with shapes ranging from tetrahedral, cubic, hexagonal, polyhedral, irregular prismatic, and spherical, have utilised different stabilising protective agents such as octadecylamine (Kumar *et al*., 2004; Huang *et al*., 2005) and polyvinylpyrrolidone (Tang *et al*., 2005; He *et al*., 2007;), with nearly all of these methods using organic solvents and other highly reactive chemical agents (Yang *et al*., 2007).

The traditional method of platinum nanoparticle formation involved the reduction of a platinum salt in solution usually by a citrate salt, hydrogen, or sodium borohydride (Lengke *et al*., 2006). Though many studies have synthesised platinum nanoparticles using chemical methods (Roach *et al*., 1999; Peng and Peng, 2001; Qu *et a*l., 2001; Liu *et al*., 2007; Shukla *et al*., 2007), the formation of nanoparticles by biological methods has not been fully investigated. In 2006, Lengke and colleagues, synthesised spherical nanoparticles within bacterial cells of the filamentous cyanobacterium *Plectonema boryanum* UTEX 485 (Lengke *et al*., 2006) and Konishi *et al*. (2007) synthesised biogenic platinum nanoparticles using the bacterium *Shewanella algae*.

2.2 Quantitative analysis of platinum nanoparticles

Most or all molecules absorb ultraviolet or visible light. Absorbance is directly proportional to the path length, *b*, and the concentration, *c*, of the absorbing species. Beer-Lambert law states that $A = \varepsilon bc$, where ε is a constant of proportionality, called the absorbtivity. Ultraviolet and visible (UV-Vis) absorption spectroscopy is the measurement of the reduction of a beam of light as it passes through a sample surface, therefore the absorption measurements can be made at a single wavelength or over an extended spectral range. Ultraviolet and visible light are energetic enough to promote outer electrons to higher energy levels, therefore UV-Vis spectroscopy is applied to molecules or organic solvents in solution. The UV-Vis spectra have broad features that are of limited use for sample identification but are very useful for quantitative measurements. The concentration of an analyte in solution can be determined by measuring the absorbance at a specific wavelength and by applying the Bee-Lambert law.

UV-Vis absorption spectroscopy is one of the important tools which has been routinely utilised in nanomaterial characterisation. Colour transitions arise during the bioreduction of metal salts to metals, thus leading to corresponding changes in the ability to absorb light in the UV or visible region of the electromagnetic spectrum. The appearance of colour arises from the property of the coloured material to absorb selectively within either the UV or visible region of the spectrum. This absorption energy consequently leads to a transition of electrons from ground to an excited state. Colloidal solutions of platinum nanoparticles exhibit a dark brown to black colour due to the well known surface plasmon absorption. Typically an aqueous solution of hexachloroplatinic acid absorbs in the UV at 201 nm and 261 nm, whilst the platinum absorption band appears at 215 nm (Ingelsten *et al*., 2001). This surface plasmon resonance is caused by the coherent oscillation of the free conduction electrons induced by light.

2.3 Qualitative analysis of platinum nanoparticles

The introduction of the electron microscope has contributed immensely to the field of biology, bringing about complete reappraisal of the micro-anatomy of biological tissues, organisms and cells. As scientists have been able to view any specimen at magnifications up to (and including) 350 000 times (Bozzola and Russell, 1999).

The most recent developments in electron microscopy have come from biotechnologists, who have used the electron microscope to obtain an understanding of metal-microbe interactions resulting in metal reduction, and now nanoparticle formation.

In order to understand the metal uptake and reduction mechanism, changes in the intracellular organisation and morphology of *F.oxysporum* cells, and nanoparticle formation, following exposure to high metal concentrations, electron microscopy techniques – scanning electron microscopy (SEM), transmission electron microscopy (TEM) and scanning transmission electron microscopy (STEM) can be used. The former is used to monitor for any morphological changes of *F.oxysporum* cells whilst TEM can be used to establish the distribution and localisation of platinum nanoparticles within the cells, and platinum nanoparticles released by the biomass. STEM coupled with energy dispersive X-ray (EDX) microanalysis can be used to identify for platinum precipitates and platinum nanoparticles within the cells. The sections which follow cover the basic principles of SEM, TEM and EDX.

2.3.1 Scanning electron microscope

The scanning electron microscope is one which is capable of producing high resolution images of a sample surface. As SEM images have a 3-dimensional quality, they are advantageous in providing information on the shape, size and arrangement of the particles/structures which lie on the sample surface. SEM imagery, however, can not be used to visualise internal contents of the sample cells. In a typical scanning electron microscope, electrons are thermionically emitted from a tungsten or LaB_6 cathode filament towards the anode. The electric beam (with energy ranging from a few keV- 50 keV) is focused by two successive condenser lenses into a beam with a fine spot size. This beam then passes through the objective lens, where pairs of scanning coils deflect the beam either linearly or in a certain manner over a rectangular area of the sample surface. When the primary electrons strike the surface they are inelastically scattered by atoms in the sample. As a result of these scattering events, the primary beam effectively spreads and fills a teardrop shaped volume extending about 1µm into the surface. It is these interactions that lead to the subsequent emission of electrons and x-rays that are then detected to form the image (Bozzola and Russell, 1999).

To minimise surface tension, samples are prepared by chemical fixation with glutaraldehyde and dehydrated in ethanol prior to drying. Once the sample is dried, the sample surface is coated with an electrically conductive layer of gold. As the electrons are generated from the tungsten wire into the gun of the microscope, electrical currents are passed through the wire and focused by magnets onto the sample surface. Once the electrons strike the gold surface coating, they are reflected back onto a detector that is transmitted to a computer screen and photographed to produce an SEM image.

2.3.2 Transmission electron microscope

The transmission electron microscope is useful for understanding and visualising of arrangement and workings within a cell. TEM replaces visible light (λ 500 nm) with a focused beam of electrons (λ 0.005 nm), providing the microscope with a better optimal resolution of images. This is how TEM can reveal the finest details of internal structure even at an atomic level. During specimen viewing, the specimen must be free from water and/or other volatile compounds, as the sample has to be stable during exposure to the electron beam and high vacuum conditions. The transmission electron microscope has three basic components: (i) illumination (electron gun), (ii) imaging (condenser, objective, intermediate and projector lenses) and (iii) viewing (fluorescent screen). The condenser lens converge the electron beam from the gun into the specimen that then penetrates the sample thereby producing an image which is magnified by the objective lens. The projector lens, then projects the image onto the viewing plane (either photographic, fluorescent or the eye). The energy of the electrons in the TEM determines the degree of penetration of electrons in a specific sample (Bazzola and Russell, 1999).

2.3.3 Energy Dispersive X-ray (EDX) microanalysis

EDX microanalysis is sometimes referred to also as EDS or EDAX analysis. It is a technique used for identifying the elemental composition of the specimen, or an area of interest. The EDX microanalysis system works as an integrated feature of a scanning transmission electron microscope and can not operate on its own without the latter. During EDX microanalysis, the specimen is bombarded with an electron beam inside the microscope. The bombarding electrons collide with the specimen atoms own electrons, knocking some of them off in the process (Bazzola and Russell,

1999). A position vacated by an ejected inner shell electron is eventually occupied by a higher-energy electron from an outer shell. To be able to do so, however, the transferring outer electron must give up some of its energy by emitting an X-ray. The amount of energy released by the transferring electron depends on which shell it is transferring from, as well as which shell it is transferring to. Furthermore, the atom of every element releases X-rays with unique amounts of energy during the transferring process. During the measure of the amounts of energy present in the X-rays being released by a specimen during electron beam bombardment, the identity of the atom from which the X-ray was emitted can be established (Titchmarsh, 1993). The output of an EDX microanalysis is an EDX spectrum and is a plot of how frequently an X-ray is received for each energy level (Bazzola and Russell, 1999). An EDX spectrum normally displays peaks corresponding to the energy levels for which the most X-rays had been received (Titchmarsh, 1993). Each peak is unique to an atom, and therefore corresponds to a single element. The higher a peak in a spectrum, the more concentrated the element is in the specimen. An EDX spectrum plot not only identifies the element corresponding to each of its peaks, but the type of X-ray to which it corresponds as well (Titchmarsh, 1993). For example, a peak corresponding to the amount of energy possessed by X-rays emitted by an electron in the L-shell going down to the K-shell is identified as a K-α peak. The peak corresponding to X-rays emitted by M-shell electrons going to the K-shell is identified as a K-β peak (Figure 2.1).

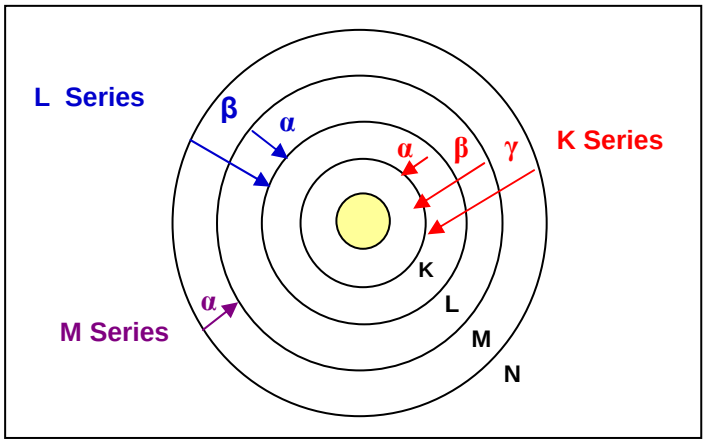

Figure 2. 1 Elements in an EDX spectrum are identified based on the energy content of the X-rays emitted by their electrons as these electrons transfer from a higher-energy shell to a lower-energy one. Figure adapted from Titchmarsh (1993).

The intercellular method of biosynthesis of metal nanoparticles and semiconductors, have been reported mainly for gold and silver (Klaus-Joerger *et al.,* 2001; Konishi *et al.,* 2006; Mukherjee *et al.,* 2001). Thus the purpose of this study was to screen and evaluate the ability of *Fusarium oxysporum*, to produce platinum nanoparticles intercellulary, and to follow platinum nanoparticle formation using electron microscopy and UV spectroscopy.

2.4 Materials and Methods

2.4.1 Materials

Hydrogen hexachloroplatinic acid (IV) (H_2PtCl_6), yeast extract, malt extract and potato dextrose agar (PDA) were obtained from Sigma- Aldrich, anhydrous sodium carbonate and D (+) glucose from Merck (South Africa) Pvt Ltd, and peptone from Fluka-BioChemika. All ddH_2O used in these experiments was obtained from a Millipore Milli-Q system. UV spectroscopy measurements were recorded on a PowerWave microplate spectrophotometer (Bio-Tek Instruments) with 96 well plates, operated at 1nm using the KC Junior software programme. A TESCAN Vega Electron Microscope was used for SEM. Thin sections were viewed using a JEOL 1210 transmission electron microscope at an acceleration voltage of 100 kV. The Analysis Soft Imaging System was used to determine platinum nanoparticle size and distribution. A scanning transmission electron microscope EM 420 coupled to an EDAX-DX-4 energy dispersive X-ray system operating at 120 kV was used for analysis of the platinum nanoparticles.

2.4.2 Fungal strain, growth media and culture conditions

The fungus *Fusarium oxysporum* PPRI 6377 and PPRI 5456 were obtained from the Agricultural Research Institute (ARC), Pretoria, South Africa, with the former originally arising from a Thrips on *Allium cepa* host in the Caledon region, Western Cape, South Africa, and the latter from a *Lycoperscium* host (garden tomato), in the Muldersvlei region, Stellenbosch, South Africa. The isolates were maintained on PDA plates at 28 °C, with stock cultures being maintained by subculturing at monthly intervals. The fungus was grown at pH 7.0 and 28 °C for 7-9 days, and the PDA plates were stored at 4 °C.

From actively growing stock culture, subcultures were made on fresh plates and after 7-9 days were used as starting material for the synthesis of nanoparticles. For the biosynthesis of nanoparticles, the fungal isolates were grown in 500 ml Erlenmeyer flasks each containing 100 ml malt extract-glucose-yeast-peptone (MGYP) broth, composed of malt extract (0.3 %), glucose (1 %), yeast extract (0.3 %) and peptone (0.5 %) at 28 °C under shaking at 180 rpm for 96 hours. The mycelial mass was then separated from the MGYP broth by centrifugation (10 000 x g, 4 °C, 25 min) and the settled mycelia were washed thrice with sterile ddH_2O and utilised for the synthesis of platinum nanoparticles.

2.4.3 Biosynthesis of platinum nanoparticles

During the biosynthesis of platinum nanoparticles, *F. oxysporum* wet biomass (1.0 g) was exposed to an aqueous solution hydrogen hexachloroplatinic acid (IV) (H_2PtCl_6) (10 ml, 20 mM) in Erlenmeyer flasks. According to Riddin *et al.* (2006), optimal conditions for platinum nanoparticle formation were pH 9 at 75 °C. The temperature was lowered to 65 °C, to minimize enzyme denaturation, and the flasks were equilibrated by adjusting the pH with anhydrous Na_2CO_3 to pH 9. The flasks were placed in an incubator shaker (65 °C; 180 rpm) and the reduction of platinum routinely monitored by removing aliquots (1.5 ml) every 60 min over a 24 h period. In a control experiment, the same amount of biomass was suspended in 10 ml ddH_20 and colour change as well as reduction of metal ions was monitored in an identical manner. The procedure described above was carried out for both isolates 5456 and 6377.

2.4.4 Quantitative analysis using UV spectroscopy

The reduction of H_2PtCl_6 was routinely monitored by measuring the UV spectra of the solution at 285 nm. Literature suggests that H_2PtCl_6 peaks in the UV region at 201/261 nm (Duff *et al*., 1995; Ingelsten *et al*., 2001) and in the visible region at 456 nm, while metallic platinum absorbs in the UV at 215 nm (Rivadulla *et al*., 1997). Consequently when particles are formed the peaks at 261 and 456 should disappear with a concomitant appearance of a peak at 215 nm. In the present study, however, this was not found to be the case; instead a spectral scan of H_2PtCl_6 showed that it has its absorbance peak in the UV region at 285 nm.

Hence the concentration of H_2PtCl_6 before, and after reaction, can be established from a standard curve at this wavelength (Appendix A). To reduce interference of the fungal cells with the measurements, the aliquot samples were centrifuged in Eppendorf Microtubes, in a microcentrifuge (12 000 x g, 5 min). The supernatant was then used for readings in the UV spectrophotometer and analyses with the TEM, whilst the pellet was used for SEM, TEM and EDX thin section analyses.

2.4.5 Qualitative analysis of platinum nanoparticles

2.4.5.1 Morphological characterization using SEM

F.oxysporum cells previously incubated with H_2PtCl_6 were collected during routine monitoring (as described in 2.4.3), centrifuged and used for the SEM analyses. The platinum loaded cells were first fixed overnight in 2.5 % glutaraldehyde in phosphate buffer (0.1 M, pH 7.0, 1.0 ml) solution. The fixative was decanted and the fungal cells were then washed (twice) in phosphate buffer (0.1 M, pH 7.0, 1.0 ml, 10 min). The cells were thereafter dehydrated in a series of ethanol solutions (30 %, 50 %, 70 %, 80 %, 90 %, and twice in absolute ethanol) with each step lasting 15 min. The fungal samples were dried in liquid CO_2 at critical point (120 min, 32°C, 80 bar pressure), then mounted onto stubs with double side sticky tapes, and coated with gold for 30 min in a Large Desk II Cold Sputter Etch Coater. *F.oxysporum* cells not exposed to H_2PtCl_6 were treated in exactly the same way and served as a control.

2.4.5.2 Distribution and localisation of platinum and/or platinum nanoparticles within F.oxysporum cells using TEM

Pellets obtained from the periodic monitoring (as described in 2.4.3) were placed in labelled Eppendorf tubes containing 2.5 % glutaraldehyde in phosphate buffer (0.1 M, pH 7, 1.0 ml) and allowed to fix overnight. The glutaraldehyde was decanted and the samples washed twice with cold phosphate buffer (0.1 M, pH 7, 1.0 ml) for 10 min during each step. The buffer was decanted and the pellet was fixed in 1 % osmium tetroxide (OsO_4) in phosphate buffer (0.1 M, pH 7, 1.0 ml) for 90 min. The OsO_4 was removed by washing twice in cold phosphate buffer (0.1 M, pH 7, 1.0 ml) with each step lasting 10 min. The pellets were then dehydrated using a series of ethanol solutions (30 %, 50 %, 70 %, 80 %, 90 % and rinsed twice in absolute ethanol) with each step lasting 10 min, then immersed in propylene oxide (twice, 15 min each).

Propylene oxide was decanted and the tubes were filled with 75:25 propylene oxide: resin, left overnight, then a 50:50 propylene oxide: resin (90 min), a 25:75 propylene oxide: resin (90 min) and lastly pure resin which was left for 36 hrs at 60 °C to polymerise. Sections (100-150 nm thick) were cut from the polymerised resin blocks using a microtome and placed onto a carbon coated copper grid. They were then stained with 5 % uranyl acetate for 30 min, washed twice in ddH_20 and blot dried on filter paper and further stained in lead citrate for 5 min. *F.oxysporum* cells not exposed to H_2PtCl_6 were treated in an identical manner to the exposed sample, and served as a control.

2.4.5.3 Energy dispersive x-ray (EDX) microanalysis of platinum precipitate and within the cells

The concentration ratios of the metals in the cells were obtained by using the technique of energy dispersive X-ray (EDX) microanalysis. Quantification was achieved using the standard less thin foil model that includes the absorption correction and with a theoretical k factor calculated according to Zaluzec (Williams and Carter, 1996). All elements present in the spectrum were used in the quantification and the atomic percentages obtained were then used to calculate the concentration ratios of the various elements present in the *F.oxysporum* cells. The samples were prepared as described in section 2.4.5.2, however due to the higher acceleration voltage used for EDX microanalysis, thicker sections were required. As a result, 250 nm thick sections were cut and collected on copper grids. The sites of the metal ion deposition and localisation observed were confirmed from the EDX spectra obtained from the EDAX-DX-4 energy dispersive X-ray system. Analysis of the cells was obtained by focusing the electron beam on the area of interest (e.g. the periplasm or the cell wall).

2.4.5.4 TEM identification of platinum nanoparticles released by the biomass

The supernatant samples obtained (as described in 2.4.4) were analysed for platinum nanoparticles. A carbon coated copper grid was prepared by dissolving the formvar coating in chloroform for 2-5 s. For TEM analysis, the nanoparticle films were formed by placing a droplet of the supernatant onto the copper grids and allowed to air dry for a 2 hr period prior to analysis. *F.oxysporum* cells not exposed to H_2PtCl_6 were also treated as above, and served as a control.

2.5 Results and Discussion

2.5.1 Quantitative analysis using UV spectroscopy

Incubation of *F.oxysporum* cells (5456) with H_2PtCl_6 showed a drop of concentration of the platinum chloride from an initial 20 mM to 11.1 mM after 1 hr then a further drop to 3.4 mM after 3 hr stabilising to approximately 2.3 mM after 7 hr (Figure 2.2). Isolate 6377, on the other hand, showed a decrease in the platinum chloride concentration from the initial 20 mM to 12.7 mM after the first hour then a further drop to 5.1 mM after 3 hr, thereafter an unexpected increase in the H_2PtCl_6 concentration to 10.1 mM at 24 hr, was observed.

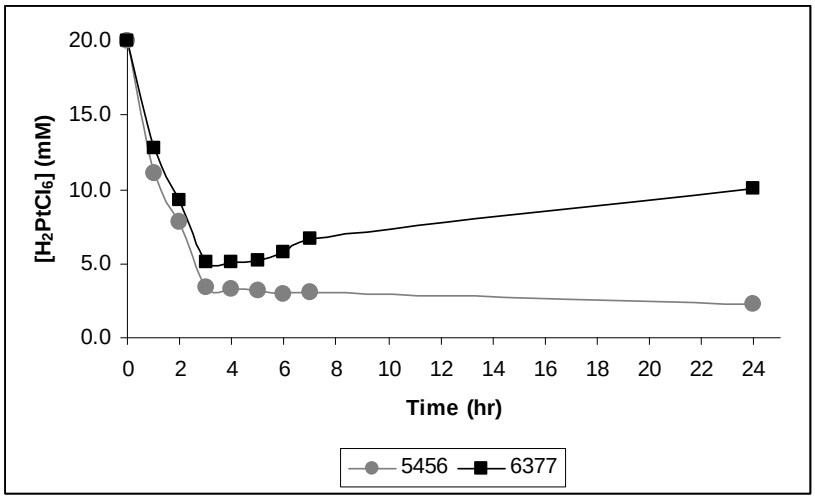

Figure 2. 2 Bioreduction of H_2PtCl_6 in an unbuffered reaction solution with fungal isolates 5456 and 6377.

The sudden increase could have been as a result of the subsequent bioreduction of H_2PtCl_6 to produce platinum with the release of HCl ions. Duff *et al*. (1995) studied the reduction of H_2PtCl_6 in the presence of polyvinylpyrrolidone (PVP) as a stabiliser, in aqueous solution and those authors proposed a two stage reaction:

$$H_2PtCl_6^{2-} \rightarrow PtCl_4^{2-} + 2Cl^- + 2H^+ \qquad (1)$$

$$PtCl_4^{2-} \leftrightarrow Pt + 4Cl^- \qquad (2)$$

These authors also suggested that addition of HCl was found to slow down the reaction. This could mean that a high concentration of chloride ions could retard the reduction of platinum complex to form metallic platinum nanoparticles (Duff *et al*., 1995; Ingelsten *et al*., 2001).

The sudden increase could have been as a result of the possible reversal of reaction 2, and the *in situ* formation of $PtCl_4^-$. This can be seen with isolate 6377 (Figure 2.2) where H_2PtCl_6 is initially reduced, however there was a subsequent increase in H_2PtCl_6 levels. The answer to this would be to carry out the reaction in a buffered medium and consequently subsequent reductions were carried out in a sodium carbonate buffer (0.05 M, pH 9). With the addition of the carbonate buffer to the reaction medium, the bioreduction of H_2PtCl_6 improved (Figure 2.3). Incubation of *F.oxysporum* cells (5456) with H_2PtCl_6 showed a drop of concentration of the platinum chloride from an initial 20 mM to 6.2 mM after 1 hr then a further drop to 1.0 mM after 3 hr stabilising to approximately 0.8 mM after 7 hr. Isolate 6377 showed a decrease in the platinum chloride concentration from the initial 20 mM to 6.8 mM after the first hour then a further drop to 3.2 mM after 3 hr and stabilised to approximately 1.94 after 7 hr.

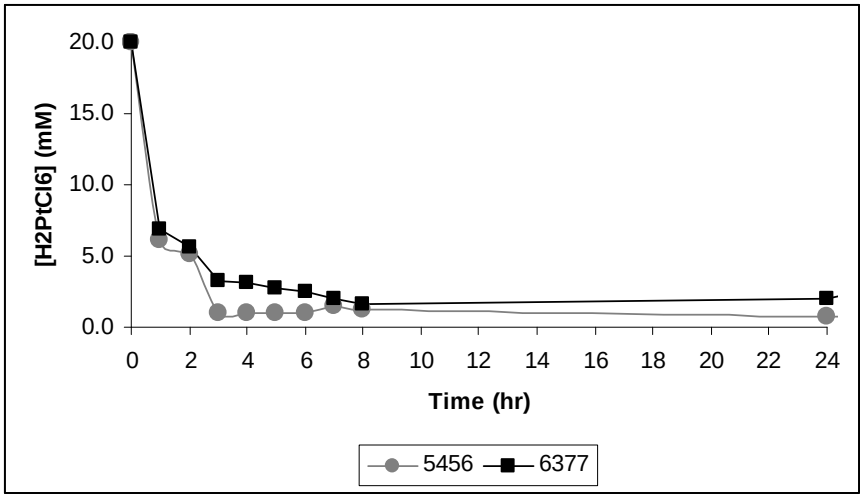

Figure 2. 3 Bioreduction of H_2PtCl_6 bioreduction in a buffered solution (Na_2CO_3 buffer, 0.05 M, pH 9)

2.5.2 Qualitative analysis of platinum nanoparticles

2.5.2.1 Visual confirmation of platinum nanoparticle formation

Two isolates of *F.oxysporum* were used in this study. The bright yellow colour of the biomass before exposure with H_2PtCl_6 ions that changes to dark brown to black on completion of the reaction can be observed for both isolates (Figure 2.4). The controls that contain only H_2PtCl_6, and *F.oxysporum* isolates in ddH_2O did not exhibit any colour change.

The appearance of the dark brown to black colour change suggests that *F. oxysporum* bioreduced H_2PtCl_6, resulting in the production of platinum nanoparticles. Although literature (Liu *et al.*, 2004; Huang *et al.*, 2004) suggests that this subsequent colour change is an indicator of platinum nanoparticle formation, it is not adequate confirmation of nanoparticle formation; however, the quantitative results confirmed that the H_2PtCl_6 was bioreduced by *F.oxysporum*.

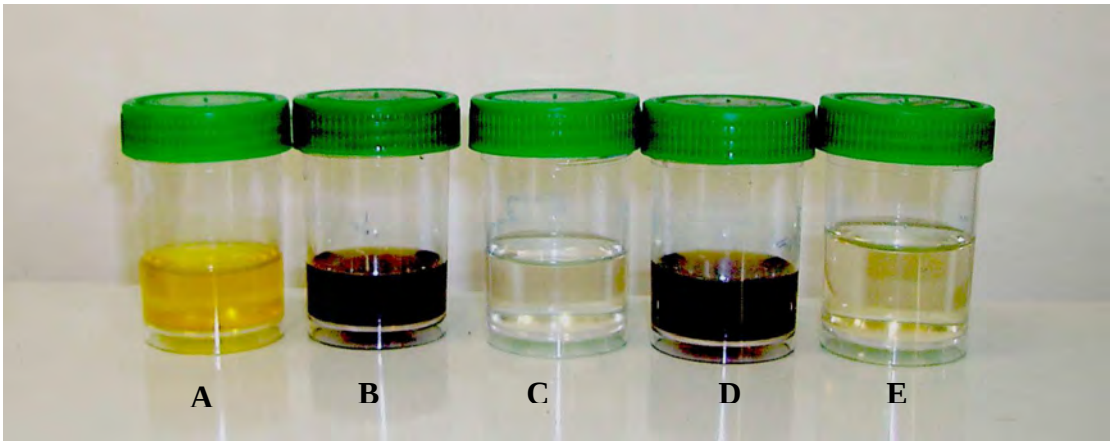

Figure 2. 4 (A) Control 1 containing only H_2PtCl_6 (20 mM), (B and D) fungal isolates 5456 and 6377 respectively exposed to H_2PtCl_6, (C and E) Controls 2 and 3 respectively containing only fungal extracts of isolate 5456 and 6377 in ddH_20

2.5.2.2 Morphological characterization using SEM

Results obtained showed that native *F.oxysporum* cells occurred in highly branched networks, and the filaments appeared as thin filaments approximately 1.5 – 2.6 µm wide and 3.7 – 5.2 µm in length (Figure 2.5 A, C). Exposure of isolates to the H_2PtCl_6 solution for 24 hrs (Figures 2.5 B, D), resulted in breaking and shortening of the filaments, with filaments between 1.3 – 2.2 µm in length. The cells elongated in the presence of the salt with the diameter changing to 2.5 - 4.0 µm in isolate 5456 and to 2.1 – 2.8 µm in isolate 6377. The cell surface appeared more irregular and very uneven in comparison to the control in which the cell surface was much smoother. Furthermore the cell surfaces appeared darker due to the uptake of H_2PtCl_6. A similar shortening of cell length, increase in cell width and darkening of cells was observed in sulphur-reducing bacterial cells exposed to platinum (Rashamuse and Whiteley, 2007), palladium (Lloyd *et al.*, 1998), uranium (Lovely and Phillips, 1992) and rhodium (Ngwenya and Whiteley, 2006).

In other studies, metal uptake had been shown to have detrimental effects such as broken cells of *Citrobacter sp* strains during the excessive accumulation of uranium on cell surfaces (Jeong *et al.,* 1997; Macaksie *et al.,* 2000).

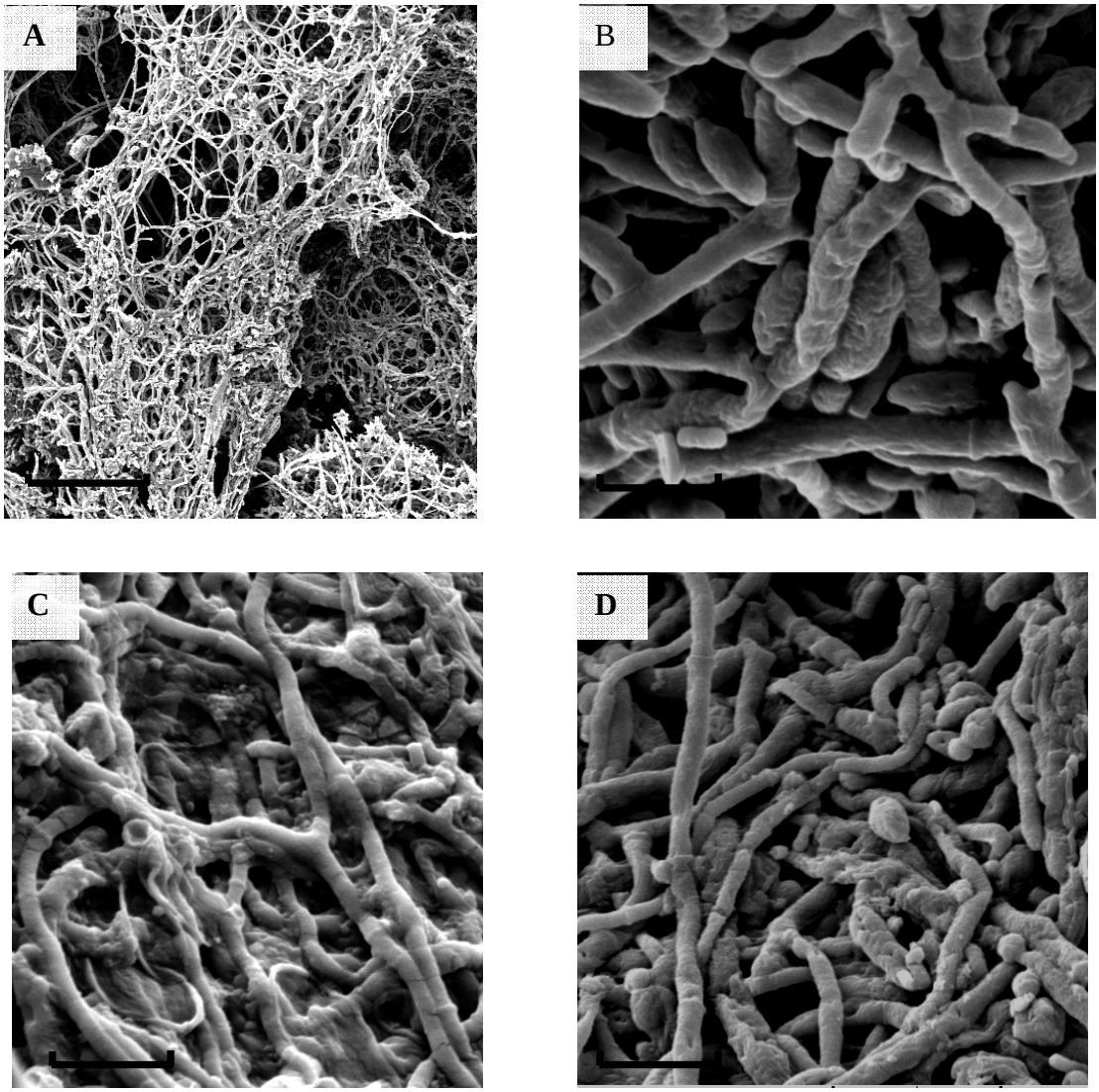

Figure 2. 5 SEM micrograph of *F.oxysporum* isolates before exposure (A) 5456 and (C) 6377 and after exposure to H_2PtCl_6 (B) 5456 and (D) 6377. Bar = 100 µm. Magnifications = 10 000 x (A) and 30 000 x (B, C and D)

From the SEM images there was no visible evidence that the *F.oxysporum* cells that had been lysed. This can be attributed to the ability of the cells to maintain an osmotic balance through a response mechanism during exposure to high metal concentration (Valls and Lorenzo, 2002). Information on the location of the platinum nanoparticles relative to the fungal cells would be important in elucidating the mechanism of their formation and thus may be obtained from TEM analysis of thin sections of the fungal cells.

2.5.2.3 Distribution and localisation of platinum and/or platinum nanoparticles within F.oxysporum cells using TEM

The TEM micrographs indicated that the cells of both *F.oxysporum* isolates when exposed to H_2PtCl_6 (20 mM) for 1 (Figure 2.6 B, 2.7 B) and 3 hr (Figure 2.6 C, 2.7 C), formed dark precipitates of what appears to be platinum rich areas throughout the cytoplasm was observe with minimal deposits in the periplasmic region. With isolate 5456 following 24 hr of exposure to the platinum salt, the cytoplasm containing the platinum precipitates starts to clear and the precipitate is diffused from the cytoplasm and deposited into the periplasm forming a dark band (Figure 2.6 D). In contrast the cytoplasm of isolate 6337, at 24 hours of exposure to the platinum salt remains dark and dense with platinum precipitate though some of the Pt accumulates on the cell membrane (Figure 2.7 D).

The numerous air spaces (vacuoles) observed in the cell interiors has been suggested to occur as a result of an energy dependant efflux system of metal ions due to their presence in high concentration (Alm, 2003). Studies have shown that *E.coli* resistance to high concentrations of zinc and copper as a result of this efflux mechanism during which the metal is transported away from the cell and subsequently accumulated on cells surfaces (Beard *et al*., 1997). A similar resistance mechanism was observed in *E.coli* when exposed to PGMs with platinum and palladium found to be toxic as compared to rhodium and the other PGMs (Alm, 2003). In other studies with microorganisms, cells have been shown to possess a specific degree of metal tolerance, and thus metal uptake continues until equilibrium is reached. Once inside the cells the metal is subject to enzymatic reduction (Hughes and Poole, 1989). In studies with platinum (Rashamuse and Whiteley, 2007) and palladium (Lloyd *et al*., 1998) metal dense areas were observed in the periplasm, strongly suggesting the involvement of an enzymatic reduction process mediated by a periplasmic hydrogenase (Lloyd, 2003). Nucleation of silver and gold nanoparticles were shown to occur on the cell surface possibly through interaction with sugars or enzymes in the cell wall, thereafter the metal nuclei were transported into the cell where they were seen to aggregate and grow producing larger sized nanoparticles (Nair and Pradeep, 2002).

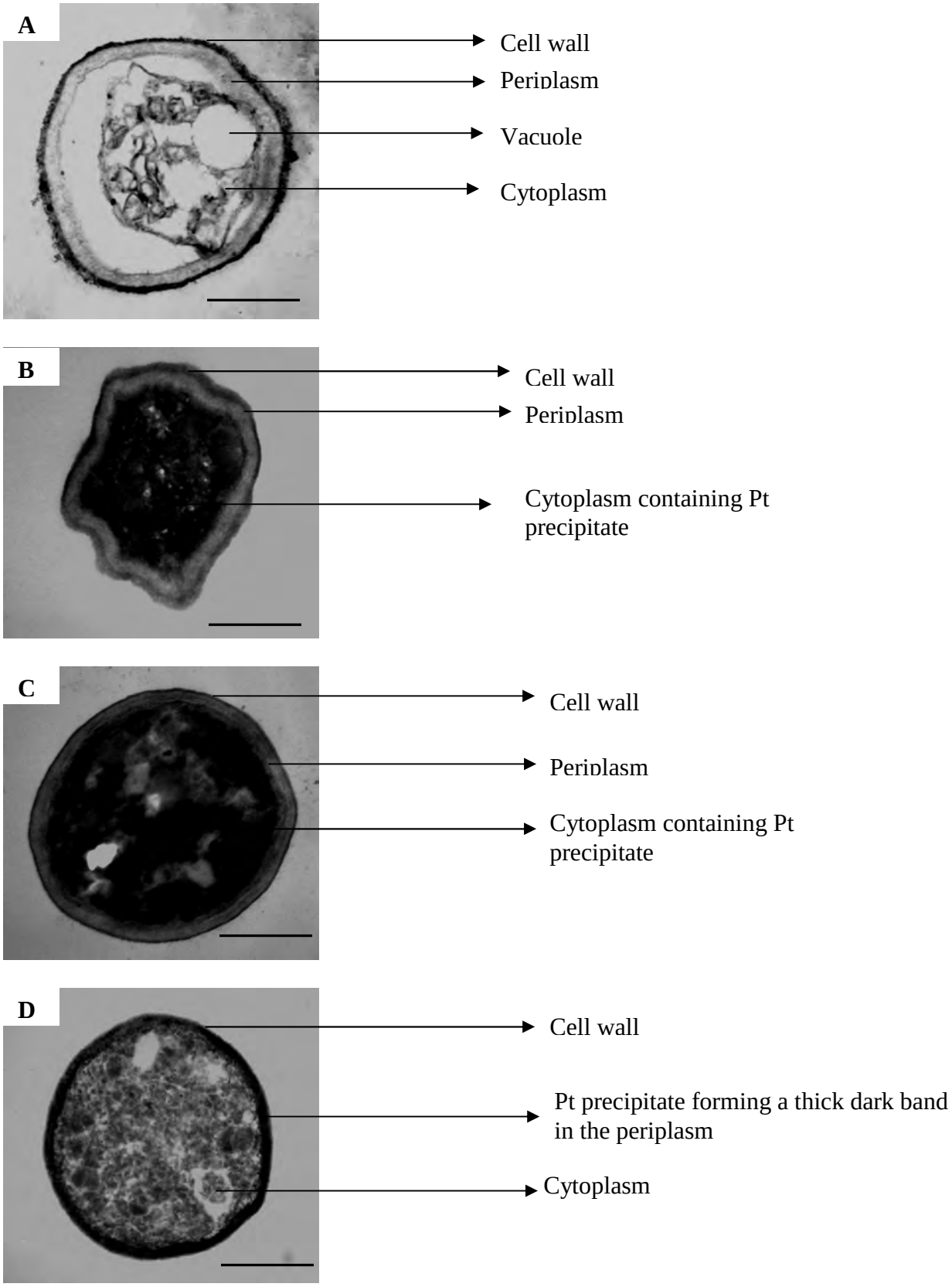

Figure 2. 6 TEM Micrographs of isolate 5456 before (A) and after exposure for (B) 1 hour, (C) 3 hours and (D) 24 hours to H_2PtCl_6. Magnification = 30 000x. Bar = 1000 nm

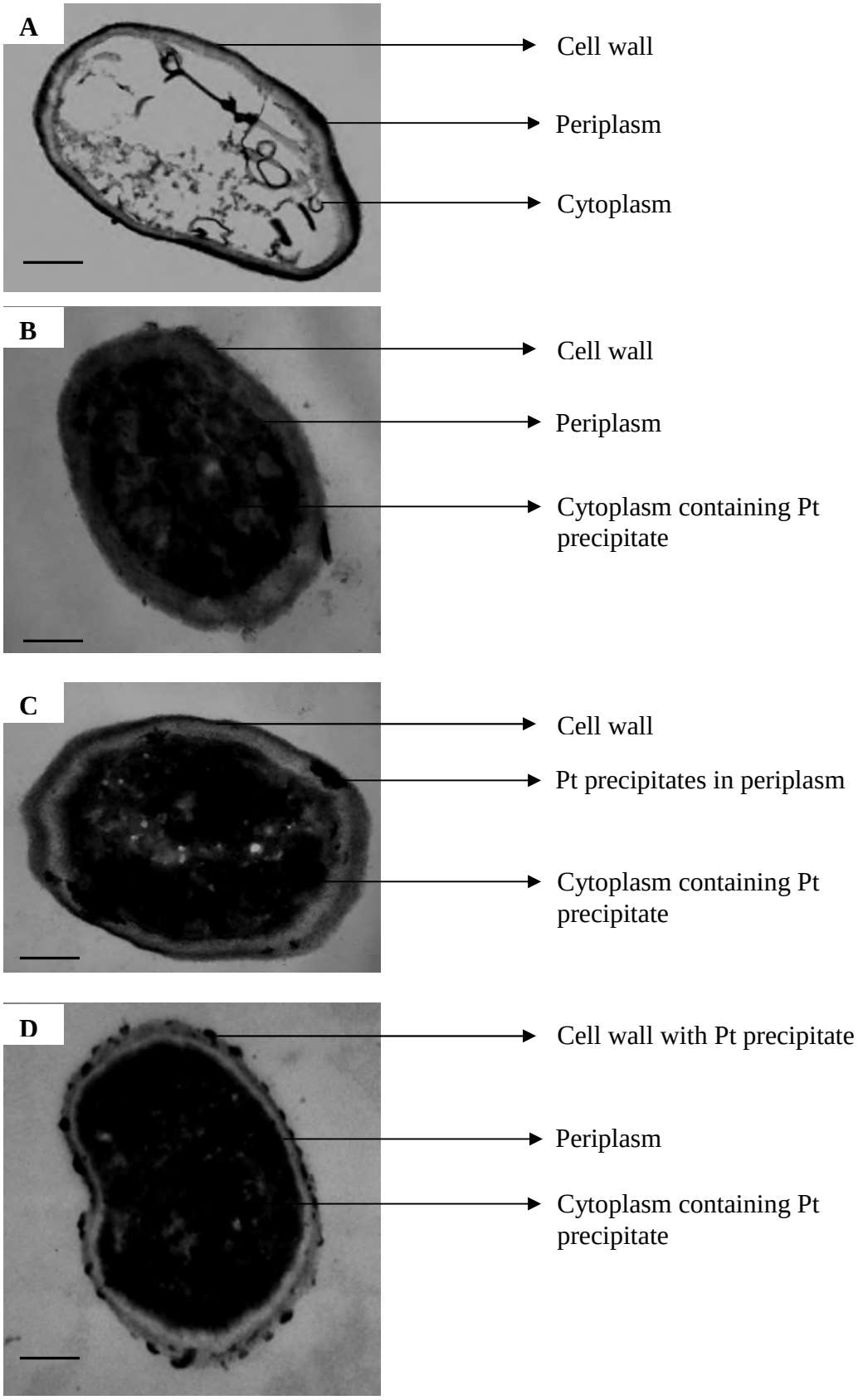

Figure 2. 7 TEM micrographs of isolate 6377 before (A) and after exposure for (B) 1 hour, (C) 3 hours and (D) 24 hours to H_2PtCl_6. Magnification = 30 000x. Bar = 1000 nm

Konishi *et al*. (2007) identified that platinum nanoparticles were bioreduced from H_2PtCl_6 and deposited in the periplasm, suggesting that an enzymatic process was responsible for the bioreduction of H_2PtCl_6. These authors suggested that the platinum deposition process occurred in two steps: (1) the uptake of H_2PtCl_6 into the periplasmic space and (2) the enzymatic reduction of H_2PtCl_6 ions into elemental platinum. In the present study results indicate that *F.oxysporum* cells incorporate more platinum, as exposure of fungal cells for prolonged periods increased the overall metal uptake. *F.oxysporum* cells were exposed to H_2PtCl_6, platinum precipitates appeared in the periplasm and cell membrane, indicating an enzymatic reduction of platinum chloride mediated by a periplasmic of membrane bound hydrogenase enzyme.

2.5.2.4 EDX microanalysis of the platinum precipitates

In order to confirm the electron dense precipitates observed (Figures 2.6 and 2.7) contained platinum, *F.oxysporum* sections were analysed by EDX. A prerequisite for the detection of elements by EDX microanalysis was the minimum composition of 1 % of the area under analysis. Restrictive criteria (e.g. biological variables) prevented quantitative analysis of the metal concentration within the cells, forcing qualitative interpretation of the results. Analysis of the 24 hr samples by EDX confirmed that platinum was located in the periplasmic area for isolate 5456 (Figure 2.8 B), and on the cell wall for isolate 6377 (Figure 2.9 B). Cells not challenged with platinum did not show any platinum peaks in the EDX spectra (Figures 2.8 A, 2.9 A). Some elements observed in the spectra originated from external sources e.g. Ca as we were working with a biological source, Os as a result of secondary staining and Cl from the reduction of H_2PtCl_6.

The SEM, TEM and EDX results indicate that *F.oxysporum* can bioaccumulate platinum precipitates within the cells, it does not confirm the existence of platinum nanoparticles and therefore the solution surrounding the fungal biomass was analysed using TEM to determine the presence of platinum nanoparticles.

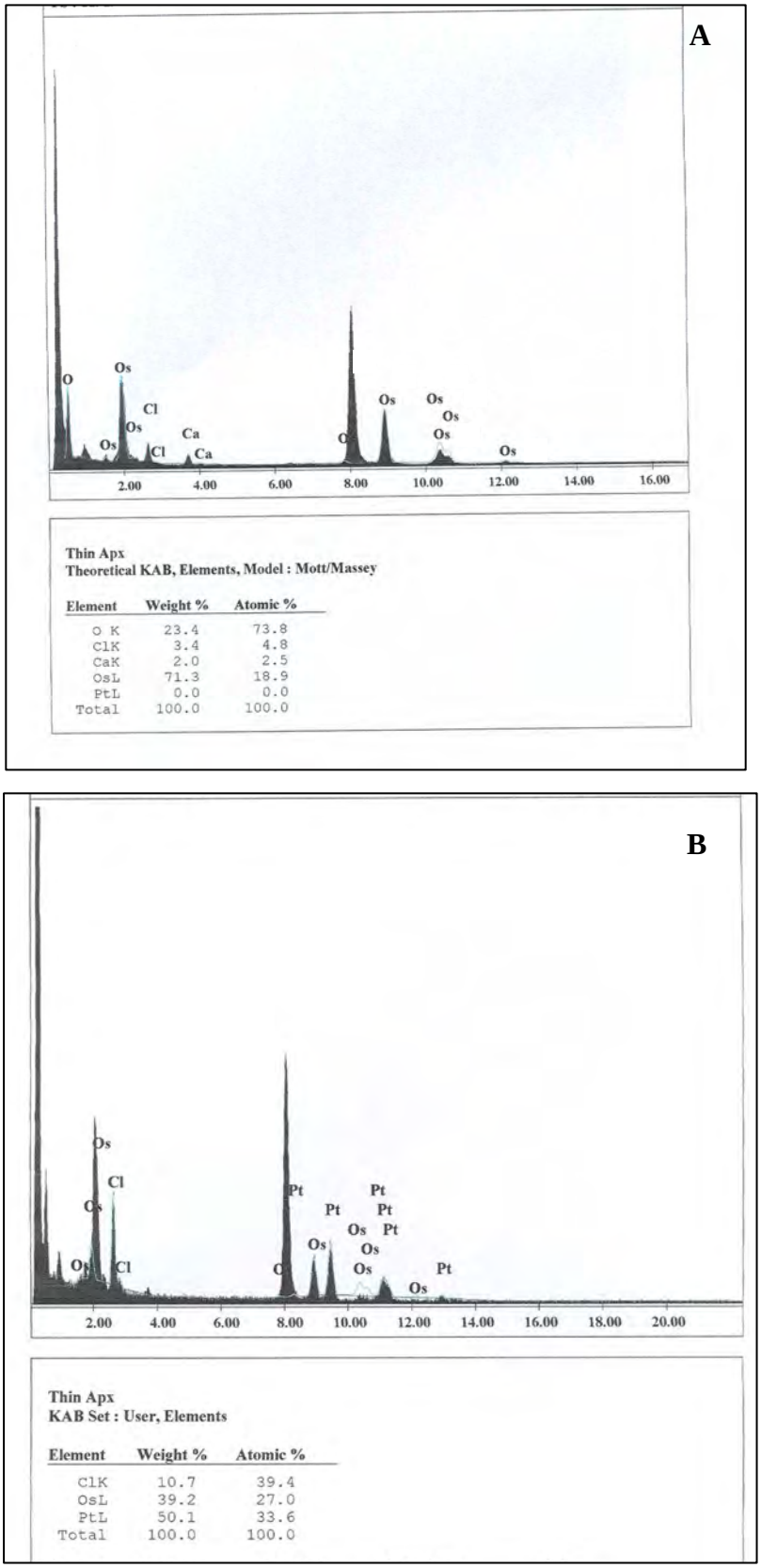

Figure 2. 8 EDX diffraction analysis spectra of the thin sections of isolate 5456 before (A) and after (B) 24 hour exposure to H_2PtCl_6.

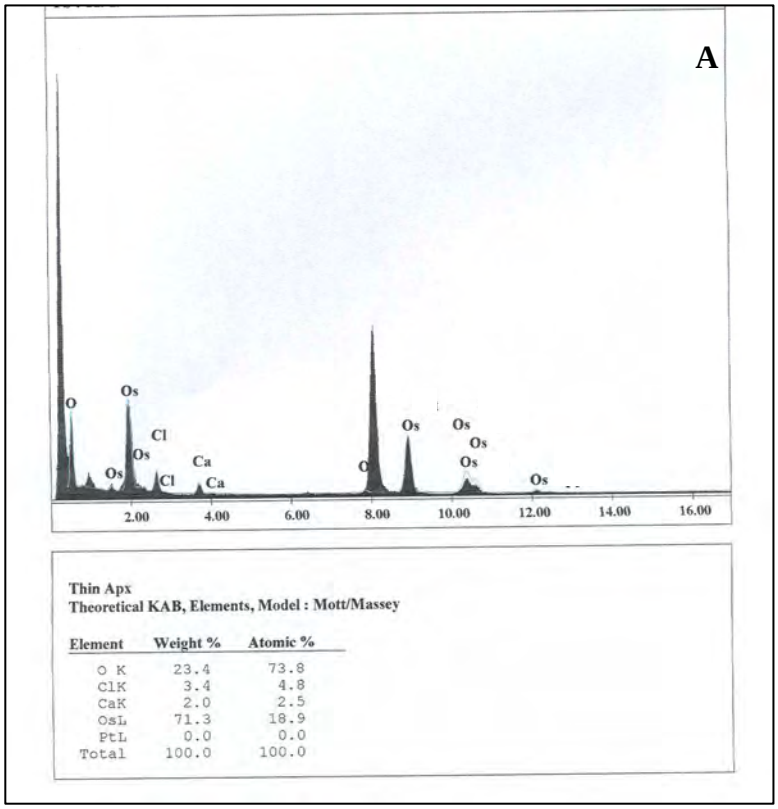

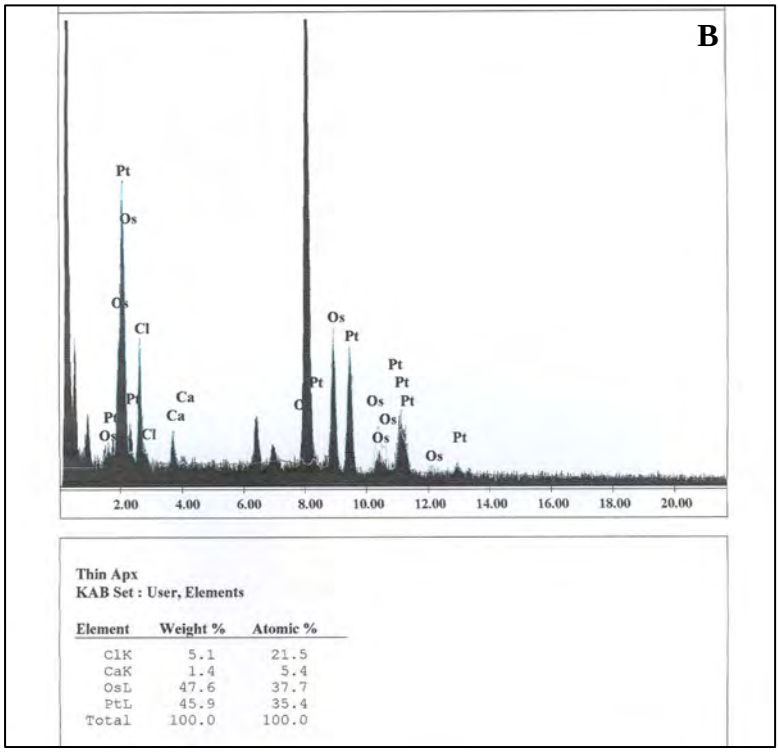

Figure 2. 9 EDX diffraction analysis spectra of the thin sections of isolate 6377 before (A) and (B) after 24 hour exposure to H_2PtCl_6

2.5.2.5 Identification of platinum nanoparticles released by the biomass using TEM

Transmission electron micrographs indicated that isolate 5456 produced platinum nanoparticles which were irregular in shape (Figure 2.10 A, B). The nanoparticles shown in those images and other similar images show that the particle sizes differ from 1-120 nm (Figure 2.10 C). Whilst the distribution of size is varied a vast majority of nanoparticles are between 10-60 nm in size with the mean particle size between 30-40 nm, unlike isolate 6377 that produced nanoparticles particles more uniform in size (Figure 2.11 A, B). The particle size histogram (Figure 2.11 C) of isolate 6377 shows that the range of nanoparticle size was from 1-65 nm. The size distribution range is much smaller with the majority of nanoparticles between 10- 30 nm in size though the mean particle size is 10-20 nm, at least twice as small than the mean particle range produced by isolate 5456.

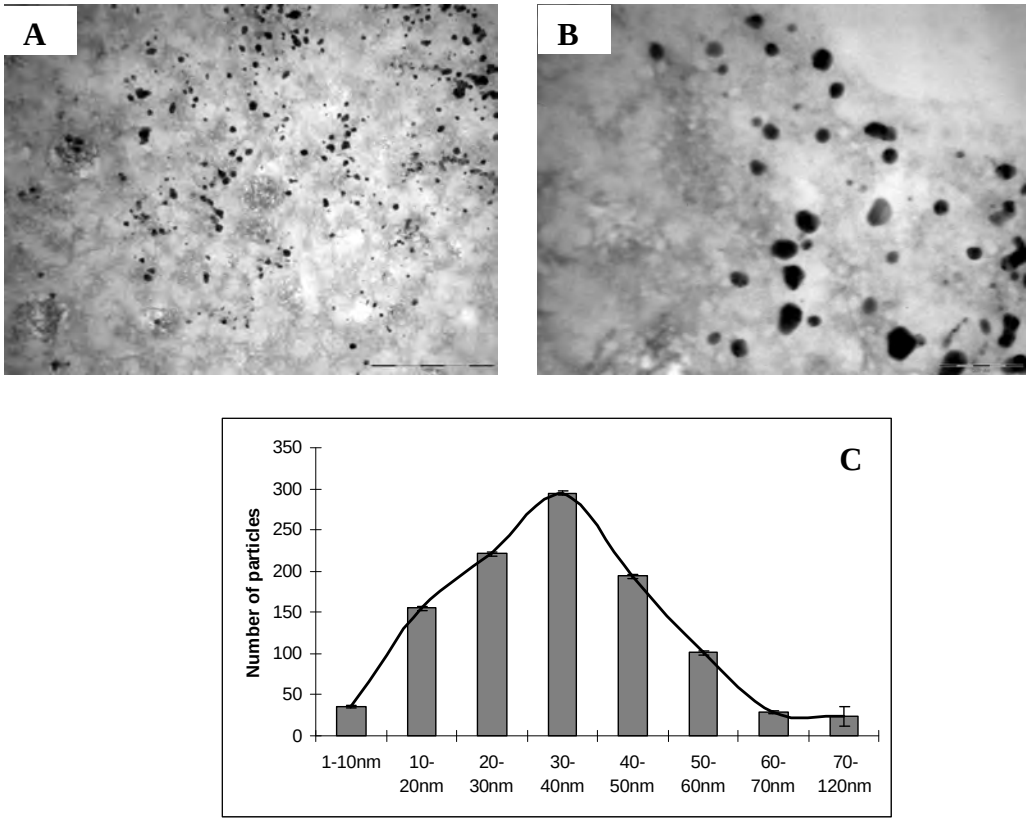

Figure 2. 10 (A and B) TEM micrographs from drop-cast films of the platinum nanoparticle solution during the bioreduction of H_2PtCl_6 with isolate 5456 biomass for 24 hours at different magnifications (A) 30 000x and (B) 60 000x. (C) Particle size distribution histogram determined from the TEM micrographs A and B. All error bars represent SE.

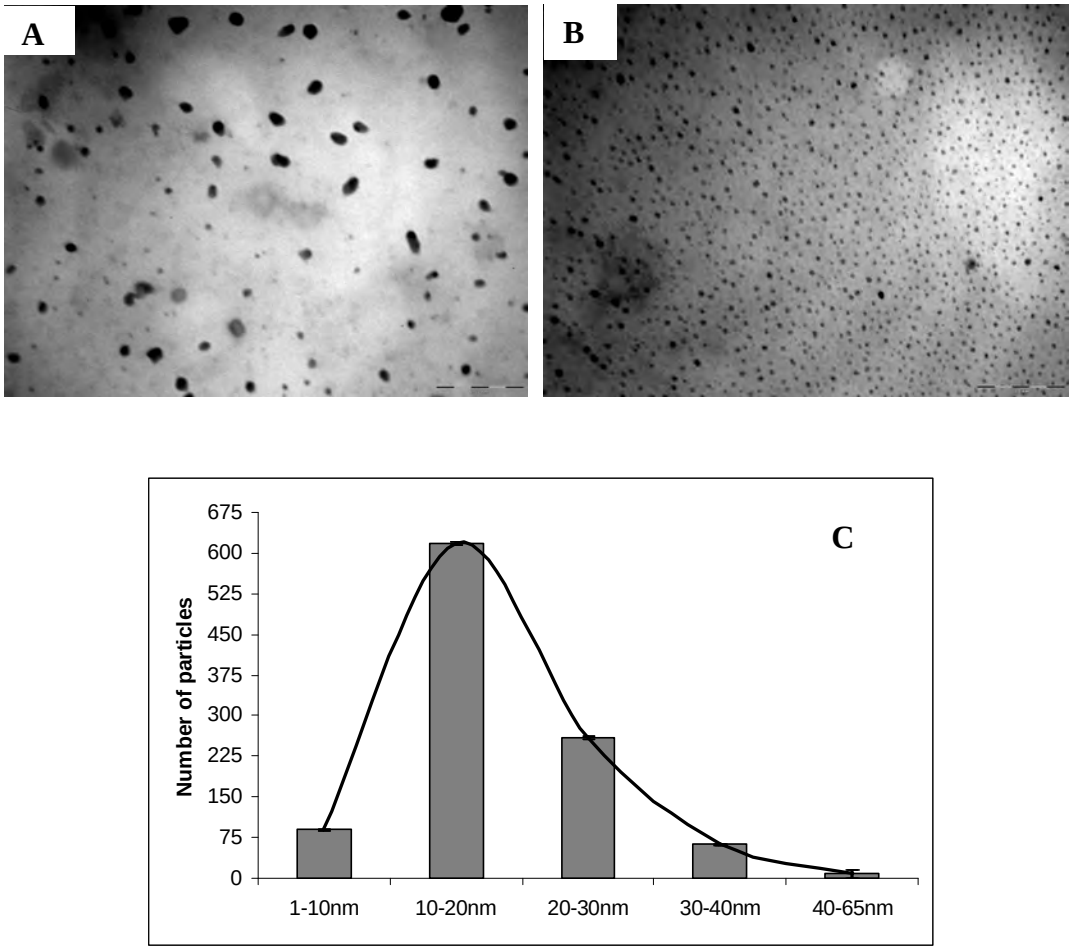

Figure 2. 11 (A and B) TEM micrographs from drop-cast films of the platinum nanoparticle solution formed during the bioreduction of H_2PtCl_6 with isolate 6377 biomass for 24 hours at different magnifications (A) 100 000 x and (B) 80 000 X. (C) Particle size distribution histogram determined from the TEM micrographs A and B. All error bars represent SE.

2.6 Summary

In this chapter it has been shown that *Fusarium oxysporum*:

i. Can be used to produce platinum nanoparticles.
ii. The initial response to the platinum salts was metal internalisation and subsequent reduction of H_2PtCI_6 to produce platinum nanoparticles.
iii. Changes in the morphology of the fungal cells were observed as a result of platinum chloride uptake.

iv. The observed localisation and distribution of platinum precipitates seems to provide some evidence for a hydrogenase mediated bioreduction (Rashamuse and Whiteley, 2007) of platinum salts to produce nanoparticles.

From an application point of view, it is essential that these nanoparticles are harvested from within the fungal biomass, which is possible by ultrasound treatments of the Pt nano-*F.oxysporum* biomass or by reactions with suitable detergents. However it would be more practical if the metal ions exposed to the fungus could be produced outside the fungal biomass thus leading to the formation of platinum nanoparticles in solution. The possibility of producing platinum nanoparticles extracellulary will be investigated in Chapter 3.

EXTRACELLULAR SYNTHESIS OF PLATINUM NANOPARTICLES USING *FUSARIUM OXYSPORUM*

3. Introduction

Metallic nanoparticles have been extensively researched because of their unique properties and potential applications in catalysis (Lewis, 1993; Toshima *et al*., 1997); electronics (Kamat, 2002); biological sensors (Bruchez Jr *et al*., 1998; Chan and Nie, 1998; Emory and Nie, 1998) and controlled drug delivery (Rao and Cheetham, 2001). Nanoparticles derived from PGMs are currently used as automobile and industrial catalysts because they possess high corrosion resistance and at high temperatures are stable to oxidation (Lloyd *et al*., 2005). Platinum nanoparticles are synthesised in a variety of different sizes and shapes, including cubic, hexagonal, polyhedral, irregular prismatic, spherical, and icosahedral in aqueous solution (Sarathy *et al*., 1997; Chen and Kimura, 2001). The traditional route of platinum nanoparticle synthesis includes the reduction of platinum salts in solution by citrate salts, hydrogen or sodium borohydride (Lengke *et al*., 2006), however synthesis of platinum nanoparticles using biological methods is a relatively recent addition to the field of nanobiotechnology. The development of biologically inspired experimental processes for the biosynthesis of metallic nanoparticles is evolving into an important branch of nanotechnology (Shahverdi *et al*., 2007). The intercellular method of platinum nanoparticle formation was demonstrated using *F.oxysporum* (Chapter 2), however this makes the job of down stream processing difficult, and thus avoids the purpose of developing a simple and cheap process.

From an application point of view, it would be important to harvest the platinum nanoparticles formed in the periplasm of the *F.oxysporum* fungal cells. Techniques used to release the intercellular platinum nanoparticles from the *F.oxysporum* biomass include ultrasound treatments, or by chemical reactions with suitable reagents. However if the platinum salt exposed to the fungus could be reduced outside the biomass, leading to the formation of platinum nanoparticles, it is believed that this would improve the availability.

Studies have shown that other fungal species, when exposed to metal salts, produced nanoparticles extracellulary. *Thermospora* sp. (Ahmad *et al*., 2003b), and *Tricothecium* sp. (Ahmad *et al*., 2005) reduced $AuCl_4$ producing Au nanoparticles extracellulary, and *Aspergillus fumigatus* reduced $AgNO_3$ to Ag nanoparticles (Bhainsa and D'Souza, 2006). The fungus used in this present study, *F.oxysporum*, has also been shown to reduce metal ions producing CdS and Ag (Ahmad *et al.*, 2002) and Au (Mukherjee *et al*., 2002) nanoparticles extracellulary.

3.1 Materials and Methods

3.1.1 Materials

Hydrogen hexachloroplatinic acid (IV) (H_2PtCl_6), yeast extract, malt extract and potato dextrose agar (PDA) were obtained from Sigma-Aldrich, anhydrous sodium carbonate and D (+) glucose from Merck (South Africa) Pvt Ltd., and peptone from Fluka-BioChemika. All ddH_2O used in these experiments was obtained from a Millipore Milli-Q system. UV spectroscopy measurements were recorded on a PowerWave microplate spectrophotometer (Bio-Tek Instruments) with 96 well plates, operated at 1 nm using the KC Junior software programme. Platinum nanoparticles were viewed using a JEOL 1210 transmission electron microscope operating at 100 kV. The Analysis Soft Imaging System was used to determine platinum nanoparticle size and distribution.

3.1.2 Fungal strain, growth media and culture conditions

The method as described in section 2.4.2 was followed. The mycelial mass was separated from the MGYP broth by centrifugation (10 000 x g, 4 °C, 25 min) and the settled mycelia were washed three times with sterile ddH_2O. The fungal biomass (1 g biomass/10 ml ddH_2O) was incubated in Erlenmeyer flasks, covered in aluminium foil in a constant environment room (28 °C, 96 hrs). Following the end of the incubation period, the fungal mycelial mass was removed from the extracellular solution by centrifugation (10 000 x g, 4 °C, 25 min). The fungal mycelial mass was discarded and the extracellular fluid was used for the synthesis of platinum nanoparticles.

3.1.3 Synthesis of platinum nanoparticles

During the synthesis of platinum nanoparticles, 10 ml of the extracellular fluid was exposed to an aqueous solution of H_2PtCl_6 (10 ml, final concentration of 20 mM) in Erlenmeyer flasks. Optimal conditions for platinum nanoparticle formation were at pH 9 and 75 °C (Riddin *et al*., 2006). Though in the present study, the temperature was lowered to 65 °C, minimising enzyme denaturation and the flasks were equilibrated by adjusting the pH with anhydrous Na_2CO_3 to pH 9. The flasks were placed in an incubator shaker (65 °C, 180 rpm) and the reduction of platinum routinely monitored by visual inspection and UV spectroscopy by removing aliquots (1.5 ml) ever 60 min over a 24 hr period. In a control experiment, the same amount of H_2PtCI_6 was maintained at the same reaction conditions, with colour change and metal reduction monitored in exactly the same way. The procedure described above was carried out for both isolates 5456 and 6377.

3.1.4 Analysis of platinum nanoparticles

3.1.4.1 Quantitative analysis using UV spectroscopy

The same procedure as described in section 2.4.4 was followed.

3.1.4.2 Qualitative analysis using TEM

A carbon coated copper grid was prepared by dissolving the formvar coating in chloroform for 2-5 s. For TEM analysis, the nanoparticle films were formed by placing a droplet of the extracellular fluid onto the copper grids, which were allowed to air dry for a 2 hr period prior to analysis.

3.2 Results and Discussion

3.2.1 Quantitative analysis using UV spectroscopy

Sample aliquots periodically removed during the 24 hr incubation period were analysed for H_2PtCl_6. The results (Figure 3.1) indicate that over an extended incubation time, the H_2PtCl_6 concentration decreased from an initial value of 20 mM however when extracellular fluid from isolate 5456 was incubated with H_2PtCI_6 the concentration decreased to 10.2 mM after an hour incubation, and continued to decrease until the concentration of H_2PtCl_6 stabilised at 24 hr (3.9 mM).

When extracellular fluid (10 ml) extracted from isolate 6377 was exposed to H_2PtCl_6 (20 mM) the concentration decreased to 6.7 mM (within an hour), and continued to decrease until the 24 hr incubation time period, where the concentration stabilised at 2.6 mM. The decrease in H_2PtCl_6 levels during the first hr indicates a rapid conversion of the salt to platinum nanoparticles, furthermore isolate 6377 appears to reduce H_2PtCl_6 more rapidly than isolate 5456. The experiment was continued for 30 hrs to ensure that the H_2PtCl_6 did not increase (as observed in section 2.5.1) and the results indicated that after 24 hr the platinum chloride levels start to increase for both isolates, in a similar fashion to intercellular synthesis of platinum nanoparticles (Chapter 2). The fluctuations in changes in H_2PtCl_6 levels, could be attributed to the release of chloride ions (produced during the reduction of H_2PtCl_6) reacting with the platinum nanoparticles to produce a platinum chloride salt. Studies have indicated that the presence of HCl can slow down the reduction of H_2PtCl_6 (Duff *et al*., 1995; Ingelsten *et al*., 2001). This is evident (Figure 3.1) as following 24 hours of incubation, the concentration of H_2PtCl_6 decreased at a slower rate as compared to the first 6 hours. To counter the effect of the released chloride ions, a sodium carbonate buffer (0.05 M, pH 9) was included in the reaction medium.

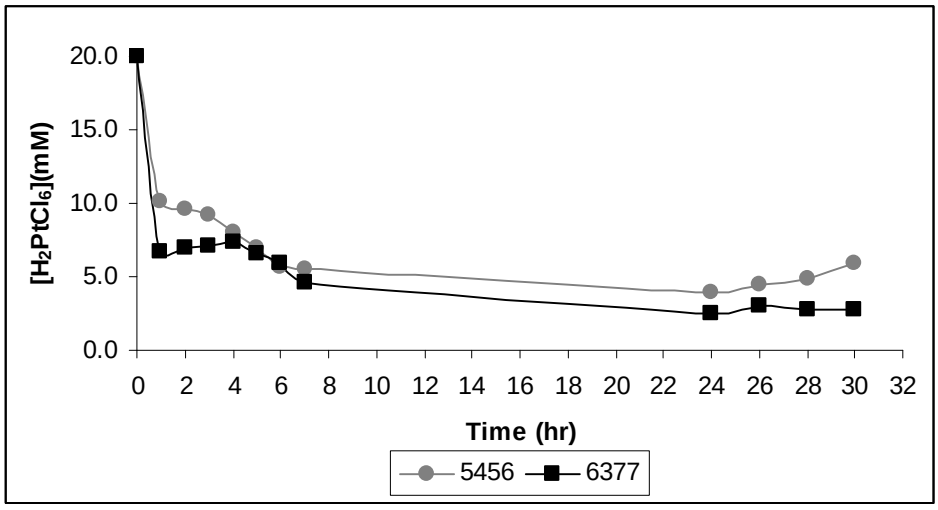

Figure 3. 1 Bioreduction of H_2PtCI_6 in an unbuffered reaction solution with extracellular fluids extracted from the fungal isolates 5456 and 6377.

With the addition of the carbonate buffer to the reaction medium, the bioreduction of H_2PtCI_6 improved considerably. With isolate 5456 following 24 hr incubation, the H_2PtCI_6 levels had decreased from 20 mM to 1.6 mM in a buffered medium (Figure 3.2) compared to the unbuffered reaction (24 hours; 3.9 mM).

Similar results were seen for isolate 6377 (Figure 3.2) where the bioreduction had improved with 2.6 mM (unbuffered) to 1.4 mM (buffered). The inclusion of the buffer improved the efficiency of the reduction of H_2PtCI_6 by the extracellular fluids enabling the reaction to occur at a faster rate. The buffer increased the stability of the reaction mixtures as it neutralised the released HCI, thus preventing any reaction with the platinum nanoparticles.

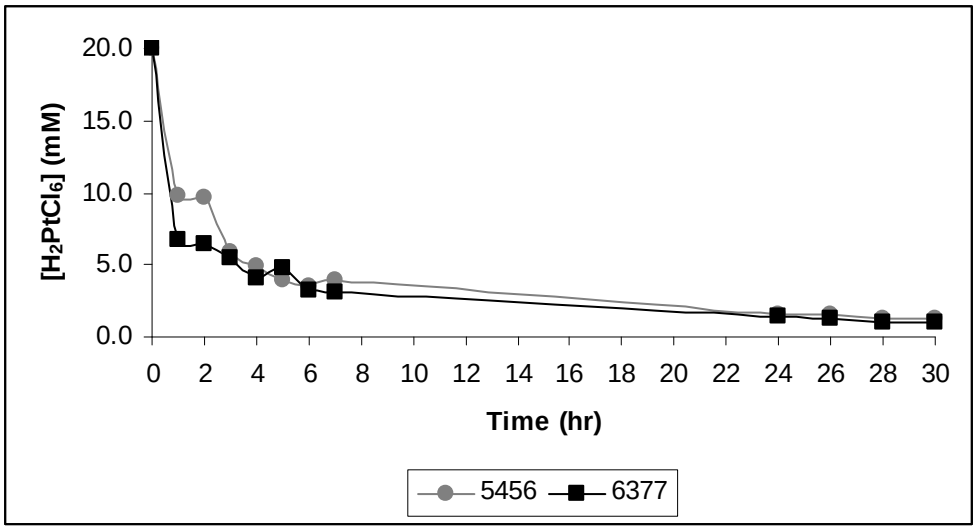

Figure 3. 2 Bioreduction of H_2PtCI_6 in a buffered solution (Na_2CO_3, 0.05 M, pH 9) during incubation with extracellular fluid extracted from isolates 5456 and 6377.

3.2.2 Qualitative analysis of platinum nanoparticles

3.2.2.1 Visual confirmation

The bright yellow colour of H_2PtCl_6 ions before exposure to the fungal extracellular fluid and the distinct colour change to dark brown or black on completion of the bioreduction from both *F.oxysporum* isolates can be clearly seen (Figure 3.3).The control, containing just H_2PtCl_6 (20 mM), did not exhibit any colour change during the reaction. The appearance of the dark brown to black colour change suggests that the *F. oxysporum* extracellular fluid reduced H_2PtCl_6 resulting in the production of platinum nanoparticles. Observations indicate that the colour change of both isolates is different. Whilst both changed from yellow, isolate 5456 produced a darker brown to black solution, yet isolate 6377 produced a lighter brown colour (Figure 3.3). Literature (Huang *et al.*, 2004; Liu *et al.*, 2004) suggests that the observed colour changes can be used as an indicator of platinum nanoparticle formation.

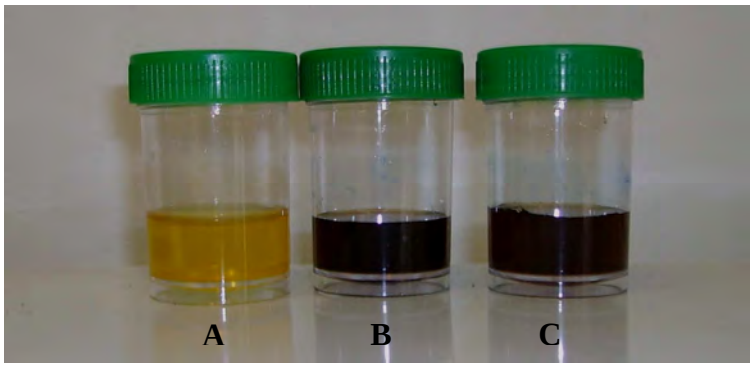

Figure 3. 3 (A) Control containing H_2PtCl_6, (B) reaction mixture with isolate 5456 extracellular fluid and H_2PtCl_6, (C) extracellular fluid from isolate 6377 incubated with H_2PtCI_6.

In the present study; the samples were analysed using UV spectroscopy and those results confirmed the reduction of H_2PtCl_6. To confirm the presence of nanoparticles, samples were analysed using transmission electron microscopy.

3.2.2.2 TEM identification and size distribution of platinum nanoparticles

Nanoparticles produced using the extracellular fluid extracted from isolate 5456 were extremely large with some nanoparticles approximately 185 nm in size (Figure 3.4 A). This isolate produced a wide variety of nanoparticles from triangles, squares and spherical nanoparticles (Figure 3.4 B, C). The particles shown in those images, and other similar images, show that the particle sizes range from 1-200 nm, with the majority larger than 200 nm (Figure 3.4 D). The nanoparticles produced from the extracellular fluid extracted from isolate 6377 were much different with the majority of the nanoparticles being circular in shape (Figure 3.5). The particle size histogram indicates that the range of nanoparticles ranges from 1-40 nm, with the majority falling in the 10-20 nm range (Figure 2.5 D).This indicates that the mechanism responsible for nanoparticle formation differs for the different isolates. There appeared to be no control in the size of nanoparticles, with many particles being formed outside the nanometre range for isolate 5456 (Figure 3.4 A, D). The nanoparticles produced by isolate 6377 appeared to be more mono-dispersed and uniform size, as the nanoparticles are all circular and the vast majority in the mean particle size range of 10-20 nm.

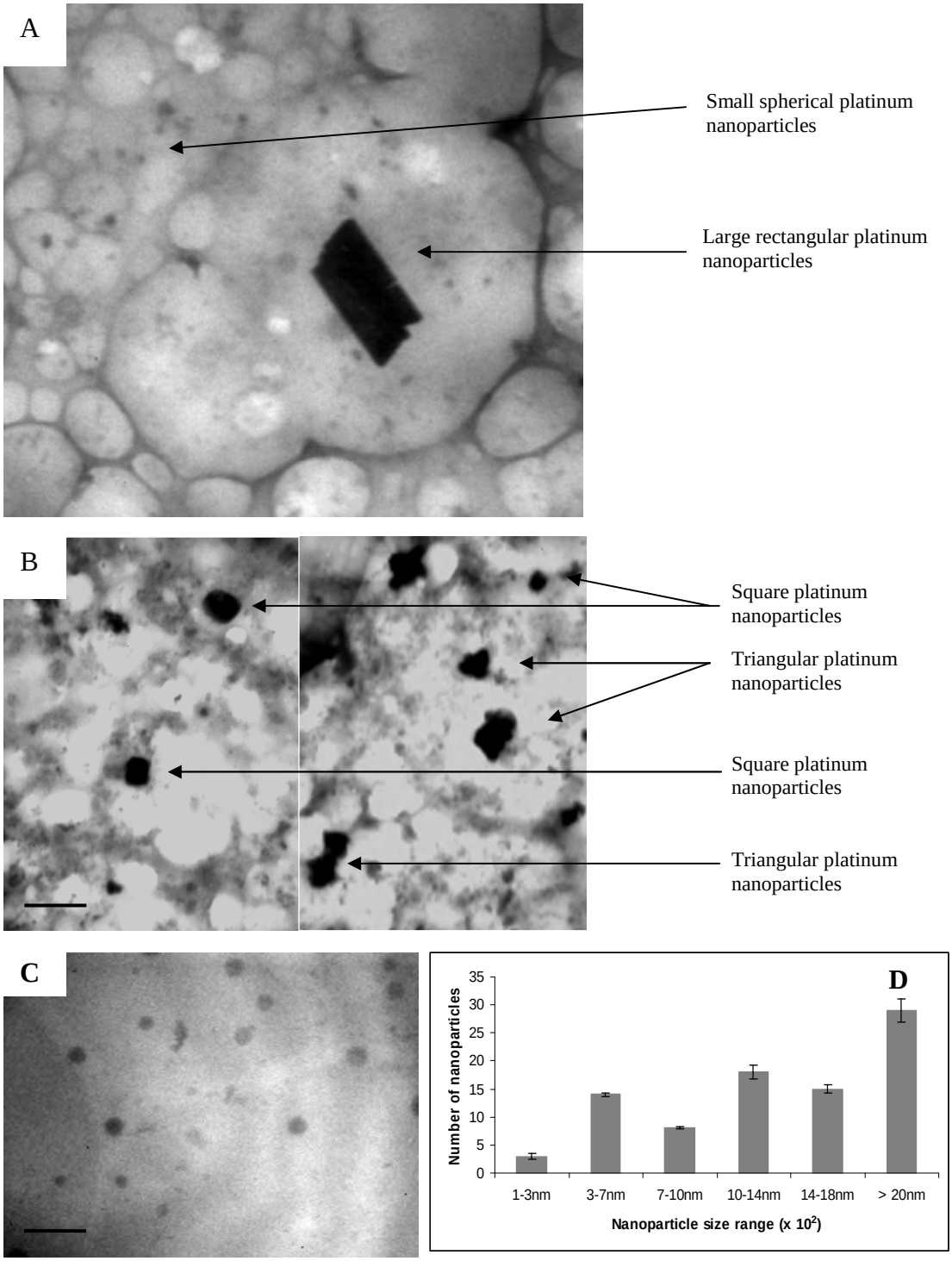

Figure 3. 4 Platinum nanoparticles with different shapes produced by the extracellular fluid obtained from isolate 5456. (A) Triangular and square, magnification = 80 000x, (B) large nanoparticles produced with smaller nanoparticles surrounding it, magnification = 40 000x, (C) Higher magnification of the smaller circular nanoparticles surrounding B, magnification = 100 000x, scale bar = 200 nm, (D) Particle size distribution histogram from the TEM micrographs. All scale bars are 1000 nm unless other wise stated. All error bars represent SE.

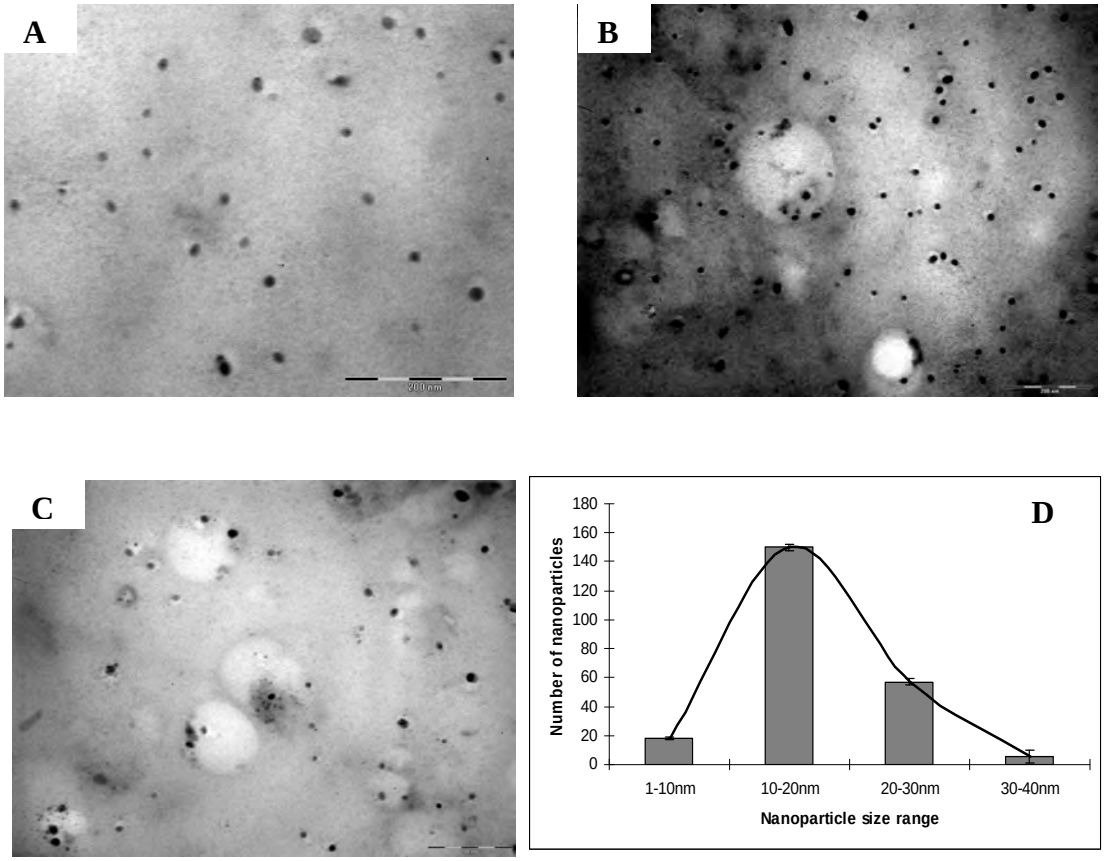

Figure 3. 5 Transmission electron micrographs recorded from drop-cast films of the platinum nanoparticle solution formed by the reaction of H_2PtCl_6 with the extracellular fluid from *F.oxysporum* isolate 6377 at different magnifications (A) 80 000x and (B) 85 000x. (C) 100 000 X. (D) Particle size distribution histogram determined from the TEM micrographs A, B and C.

3.3 Summary

In this chapter it has been shown that:

i. *F. oxysporum* can be used to produce platinum nanoparticles.
ii. The results indicate that factors secreted by the fungus into the extracellular fluids, are responsible for platinum nanoparticle formation.

The exact mechanism responsible for extracellular platinum nanoparticle formation is not clearly understood though, literature has indicated that using biological methods, amino acids (Mandal *et al*., 2001; Selvakannan *et al*., 2003) and proteins or enzymes (Gole *et al*., 2001a; Gole *et al*., 2001b; Gole *et al*., 2002) are some of the biomolecules which are hypothesised to be responsible for nanoparticle formation.

It is also hypothesised that these amino acids, proteins or enzymes behave similarly to the stabilising agents such as citrate salts, PVP and thiols, used in traditional "wet" chemical preparations of nanoparticles. These stabilising salts bind to the atoms exposed on the nanoparticle surfaces, leading to capping and preventing the uncontrolled growth of nanoparticles (Duff *et al*., 1995). Therefore the focus of Chapter 4 is to investigate the "factor" responsible for platinum nanoparticle formation.

INVESTIGATION OF THE "FACTORS" RESPONSIBLE FOR PLATINUM NANOPARTICLE FORMATION

4. Introduction

Research in nanotechnology deals mainly with the synthesis and stabilisation of various nanoparticles by chemical and physical processes. With the advancement of nanobiotechnology, research has highlighted new methods to produce nanoparticles using biological systems. Whilst various studies have been initiated on identification of microorganisms as possible nanofactories, very little work has been conducted on the actual mechanisms of nanoparticle formation in microorganisms. One of the initial findings was that exposure of *F.oxysporum* to aqueous $CdSO_4$ solution yielded quantum CdS dots (Ahmad *et al*., 2002), with results indicating that a NADH dependant enzyme was responsible for the quantum dot formation. Subsequent studies, in the reduction of $AuCl_4$ and Ag^+ ions, suggest the role of reductases released into solution by the fungus *F.oxysporum* (Mukherjee *et al*., 2002; Ahmad *et al*., 2003a). This has lead to the opening up of a novel fungal-enzyme based *in vitro* approach to nanoparticle formation. Recent findings (Mukherjee *et al*., 2001; Ahmad *et al*., 2002; Senapati *et al.*, 2005) have indicated that NADH and NADH-dependant enzymes are important factors in the biosynthesis of metal nanoparticles. The reduction is suggested to be initiated by electron transfer from the NADH by NADH-dependant reductase enzymes. Currently only a nitrate reductase has been identified to be directly responsible for the biosynthesis of silver nanoparticles but up to the present date (2007), no mechanism, has been elucidated for platinum nanoparticle formation in *F.oxysporum*.

As discussed in Chapters 2 and 3, a hydrogenase enzyme has been hypothesised to be responsible for platinum nanoparticle formation, thus, the following chapter includes the investigation, identification and purification of the enzyme/protein responsible for platinum nanoparticle formation. Purification of proteins is one of the most fundamental steps in the study of their function and expression. Hydrogenases were first described by Stephenson and Strickland in 1931 as a bacterial enzyme that catalysed the reversible oxidation of hydrogen.

They were subsequently found in a number of anaerobic and aerobic prokaryotes (Ueno *et al*., 1999), including algae, aerobic N_2 fixers, aerobic autotrophs, anaerobic fermentative bacteria, photosynthetic bacteria and the anaerobic sulphate reducing bacteria (Kow and Burris, 1984). The physiological functions of most prokaryotic hydrogenases are to oxidize hydrogen gas and reduce electron acceptors while another function is to maintain the intracellular pH and redox potentials at suitable levels by hydrogen gas production (Ueno *et al*., 1999).

The methods used in the purification and characterisation of enzymes should be reliable, rapid, and efficient during the purification steps (Willson, 1999). The purification of a protein is normally based on the structural and functional properties of the protein and its intended use, and this greatly influences the purification steps that are used. By definition, a protein is pure when it contains only a single protein species, though in practice, it is more or less impossible to achieve 100 % purity (Wilson and Walker, 1994). Contamination levels of between 5 to 10 % with other proteins is, however, generally acceptable. This is an important point, since each purification step inevitably involves the loss of the target protein. As a result any extra (and unnecessary) purification step that increases the purity of the target protein, to say 90 to 98 % may result in insufficient amount of protein for further work (Willson, 1999). The purification steps used in this study will be briefly described so as to gain an understanding of their principles.

4.1 Enzyme purification

4.1.1 Concentration of cell free extract

Small volumes of concentrated protein are easier to work with for subsequent purification procedures (Roe, 2001). The main aim of concentrating proteins during purification is to minimise protein loss by non-specific adsorption to container walls or column matrices. There are three main concentration methods that have been widely used.

4.1.1.1Freeze drying

Freeze drying, often referred to as lyophilisation, is a dehydration process which entails the removal of water from a frozen sample by sublimation. This process produces a dry powdered enzyme extract which is much more stable than the aqueous

extract (Roe, 2001). One of the major disadvantages of this method is that it is a lengthy procedure that may result in loss of enzyme activity.

4.1.1.2 Polyethylene Glycol (PEG)

Polyethylene glycol is an organic polymer which is often used in enzyme purification. Precipitation by the PEG is one of the simplest and most rapid methods of concentrating solutions as it does not require specialized apparatus (Roe, 2001) The mechanism of action involves addition of water miscible organic polymers which absorb water from the protein extract. The molecular weight of the polymer should be greater than 4000; normal polymers used are 6000 and 20 000. This technique is advantageous in that it does not interfere with subsequent purification steps and it does not affect enzyme activity (Willson, 1999)

4.1.2 Size exclusion chromatography (SEC)

Size exclusion chromatography (SEC) is a chromatographic procedure in which particles are separated based on their size. It is usually applied to large molecules or macromolecular complexes such as proteins and industrial polymers. The basic principle is that molecules are partitioned between solvent and stationary phase of defined porosity. The separation process is carried out using a porous gel matrix (in bead form) packed into a column surrounded by solvent. Molecules too large to pass through the gel are excluded and eluated first from the column. However, the smaller molecules within the fractionation range of the gel, penetrate the pores, and appear as the last components on a chromatogram. Apart from size-based separation, separation also depends on their shape, as elongated proteins (due to their higher hydration radius) pass through faster than compact globular proteins of the same molecular weight. Thus, the separation mechanism of SEC involves both molecular shape and mass of the molecules, and therefore can be used to determine molecular shape in solution and consequently as a monitor for denaturation (Wilson and Walker, 1994).

4.1.3 Ion exchange chromatography (IEC)

This is the most widely used form of chromatography that relies on the charge-charge interactions between oppositely charged particles in proteins and amino acids (Wilson and Walker, 1994). These molecules contain ionisable groups that carry a net positive or negative charge that is exploited in their separation.

IEC is carried out in columns made up of charged groups that are covalently attached to a support matrix. There are two types of ion exchangers: cation and anion exchangers. Cationic exchangers possess negatively charged groups that attract positively charged cations. These exchangers are also called acidic ion exchangers because their negative charges result in ionisation of acidic groups. Anion exchangers contain positively charged groups that attract negatively charged anion groups and they normally result from the association of protons with basic groups and as such are also referred to as basic ion exchangers (Wilson and Walker, 1994).

The mechanism of ion exchange chromatography is made up of five distinct steps:

a) The rapid diffusion of the ion to exchange surface in homogenous solutions.

b) Diffusion of the ion through the matrix structure of the exchanger to the exchange site which is highly dependent on the degree of cross linkage of the exchanger and the concentration of the solution. This is considered to be the rate limiting step of ion exchange chromatography.

c) The next step involves the exchange of ions at the exchange site, which occurs instantaneously at equilibrium. The more highly charged the ionised molecule to be exchanged, the tighter it binds and the less readily it is displaced by other ions.

d) The exchanged ions then diffuse through the exchanger to the surface.

e) The final step is the selective desorption by the eluent and diffusion of the molecule into the external eluent. This is achieved by changes in the pH and/ or ionic concentration or by affinity elution (i.e. in cases where an ion has greater affinity for the exchanger than that bound onto the matrix when it was introduced into the system (Wilson and Walker, 1994).

Traditionally IEC and SEC are used individually or concurrently during the purification procedure though sometimes SEC and IEC are combined. In this study, Sephacryl S-200 is used as it separates protein molecules by size, as well as by ion exchange of charges on the protein molecules.

4.2 Enzyme characterisation

Potential application of enzymes as catalysts for biotechnological processes necessitates their characterisation so as to determine their maximum activity. Physiological properties of enzymes that influence activity include stability to temperature change, pH, catalytic properties, size (molecular weight), charge (electrophoretic mobility), and binding partners (substrates and co-factors) (Wilson and Walker, 1994; Willson, 1999).

4.2.1 Sodium dodecyl sulphate-polyacrylamide gel electrophoresis (SDS-PAGE)

SDS-PAGE is the most widely used method for analysing protein mixtures qualitatively and for monitoring protein purification. This method is based on the separation of proteins according to size, and is used to determine the relative molecular mass of proteins as well as the purity of the protein during each purification step. The target protein sample is boiled in buffer containing β-mercaptoethanol and the anionic detergent SDS (CH_3-$(CH_2)_{10}$-CH_2OSO_3-Na^+). The mercaptoethanol disrupts the tertiary structure of the protein by cleaving the disulphide bridges, while the SDS binds strongly to and denatures the protein. This results in the opening up of the protein into a rod – shaped structure with a series of negatively charged SDS molecules of constant charge density per unit mass, thus facilitating electrophoretic mobility (Wilson and Walker, 1994). The samples are loaded onto a stacking gel which concentrates the protein sample into a sharp band before it enters the main separating gel. This is achieved by utilizing differences in ionic strength and pH between the electrophoresis buffer and the stacking gel, a phenomenon known as isotachophoresis. An electric current is passed through and the proteins migrate through the gel and interact with the ampholytes (electrostatic interaction). Along the gel, each protein encounters its isoelectric point; and the migration of that particular protein stops. This results in each protein species concentrating at that point thereby forming a very sharp band (Voet and Voet, 1995; Roe, 2001). The distance migrated by the protein is measured and a plot of $\log_{10}$ polypeptide molecular weight versus the relative mobility (R_f) of the standards and target protein are used to calculate the relative molecular mass of the target protein (Hames and Rickwood, 1981).

4.3 Qualitative analysis of platinum nanoparticles

4.3.1 Scanning Transmission Electron Microscopy (STEM)

The advancement in electron microscopy techniques such as scanning transmission electron microscope (STEM) techniques, has led to the advancement in the characterisation of nanodevices, nanoparticles and other nanosystems (Liu, 2005).When an electron nanoprobe in the STEM is focused onto an atomic size sample, all scattered electrons are collected, and a variety of electron, electromagnetic and other signals are generated (Figure 4.1).

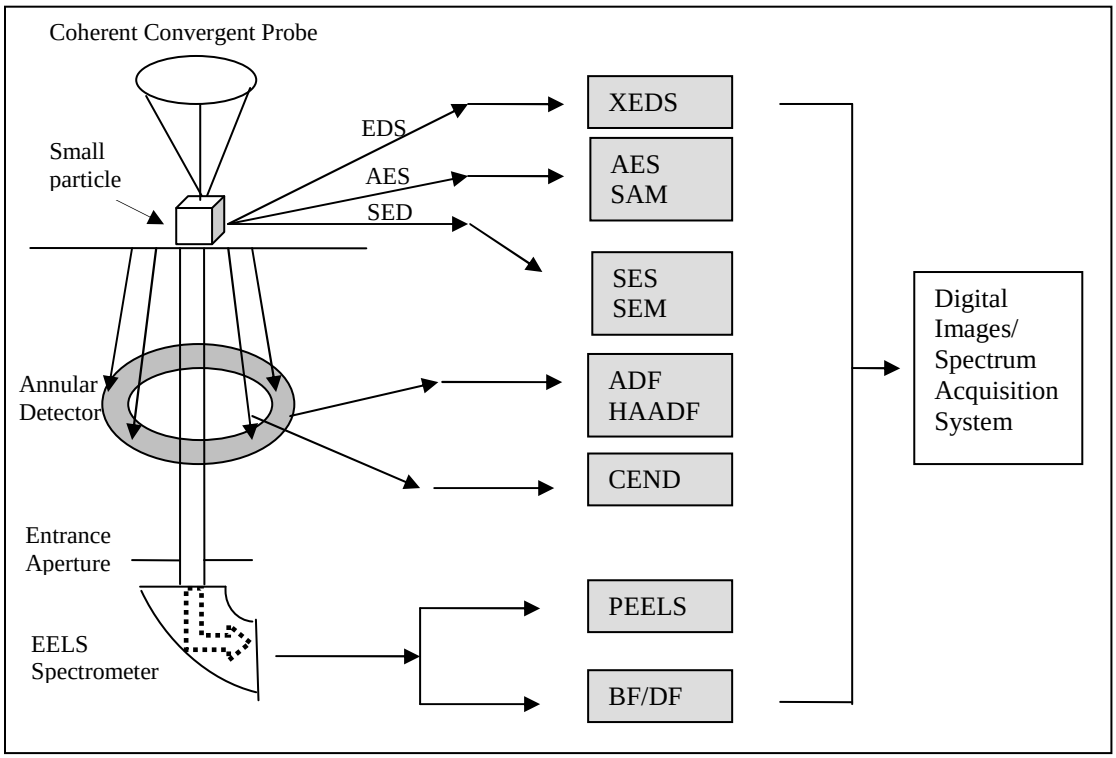

Figure 4. 1 A schematic (adapted from Liu, 2005) illustrating the different signals inside a STEM used to form high-resolution images, X-ray energy dispersive spectroscopy (XEDS); Aüger electron spectroscopy (AES), scanning Aüger microscopy (SAM), secondary electron spectroscopy (SES), secondary electron microscopy (SEM), annular dark field (ADF), high-angle annular dark-field (HAADF), coherent electron nano-diffraction (CEND), parallel electron energy-loss spectroscopy (PEELS), bright field (BF) and dark field (DF).

Elastically scattered electrons are collected by an annular detector and provide the elastic dark-field signal. The coherent bright-field signal arising from unscattered and low-angle elastically scatted electrons are collected (Engel and Colliex, 1993). All of these signals, discriminated in scattering angle and energy loss, yield various structural and chemical information and are captured simultaneously in different channels (Liu, 2005). These can be used to produce images and diffraction patterns (Figure 4.1), or spectroscopic information by using digital image or spectrum acquisitions systems such as X-ray energy dispersive spectroscopy (XEDS).

4.3.2 Atomic Force Microscopy (AFM)

The atomic force microscope is used to solve processing and materials problems in a range of technologies such as the electronics, biological, automotive, aerospace, chemical and energy industries. The principle on how an atomic force microscope works (Figure 4.2) is based on an atomically sharp stylus (tip) with an approximate radius of 1-2 nm, which is scanned over the surface of a specimen, with feedback mechanisms enabling the piezo-electric scanners to maintain the tip at a constant force (obtain height information) or height (obtain force information) over the surface (Müller *et al*., 1996; Morris *et al*., 1999).

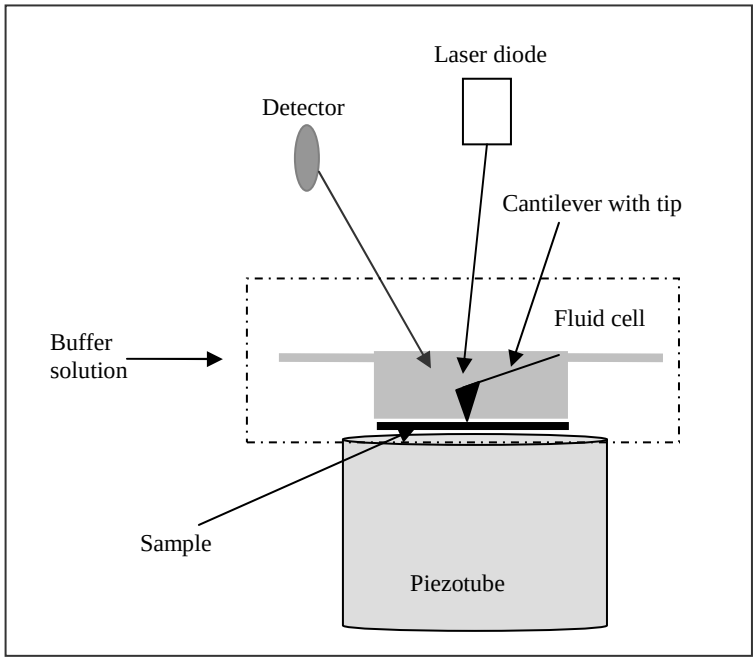

Figure 4. 2 Schematic representation of a typical atomic force microscope, adapted from Müller *et al*. (1996).

A diode laser emitting a laser beam is deflected off the attached cantilever into a dual element photodiode that measures the difference between light intensities between the upper and lower photo detectors, converting it into voltage (Figure 4.2). The photodiode signal, through software control from a servo system, controls the movement of the piezo-electric transducer, and in this way, the applied force between the stylus and the sample can be kept constant within tenths of a piconewton (Muller *et al.*, 1996). Depending on the atomic force microscope design, scanners are utilised to translate either the sample under the cantilever or the cantilever over the sample, and thus the height of the sample is measured. Three dimensional topographical maps of the sample surface area are then constructed by plotting the sample height against the horizontal tip position.

Three of the most common AFM mode techniques are described (Muller *et al*., 1996; Ricci and Braga, 2004).

a) Contact mode – during this mode the stylus scans the sample in close contact with the surface. The deflection off the cantilever is sensed and compared, in a feedback amplifier, to the desired value of deflection. In this mode electrostatic and surface tension forces drag the tip, damaging the surface and distorting the image (Ricci and Braga, 2004). Thus contact mode imaging is influenced by frictional and adhesive forces compared to the other two modes. In constant force mode the tip is constantly adjusted to maintain a constant deflection, and thus a constant height above the sample surface. It is the constant adjusting that is displayed as data though sometimes the tip is allowed to scan without these adjustments and thus only deflection is measured (Muller *et al*., 1996)

b) Non contact mode – is used in situations where the stylus contact might alter the sample in subtle ways. In this mode the tip hovers between 50-150 Angstrom above the sample surface, however the attractive forces from the sample are substantially weaker than forces used during contact mode (Ricci and Braga, 2004) Thus the tip is given a few oscillations so that detection methods can be used to detect the small forces between the tip and the sample by measuring the change in amplitude, phase or frequency of the oscillating cantilever. Non contact mode provides low resolution and can also

be hampered by a contamination layer (water vapour) that interferes with the oscillation (Muller *et al*., 1996)

c) Dynamic force mode – this mode is also referred to as tapping mode, and allows high resolution topographic imaging of sample surfaces that can be easily damaged (Ricci and Braga, 2004). During scanning the oscillating tip alternately contacts the surface and lifts off, as the oscillating cantilever begins to intermittently contact the surface, the cantilever oscillation is reduced due to energy loss caused by contact between tip and surface. This reduction in oscillation is used to identify and measure surface features (Muller *et al*., 1996).

4.4 Materials and Methods

4.4.1 Materials

Coomasie Brilliant Blue Stain, DEAE Sephacel and Sephacryl S-200 were obtained from Sigma-Aldrich (South Africa). A standard molecular weight marker peqGOLD 10-200 kDa was obtained from Optima Scientific (South Africa). UV analyses were carried out on a PowerWave microplate spectrophotometer (Bio-Tek Instruments) with 96 well plates, operated at 1nm using the KC Junior software programme. TEM analysis and imagery were performed on a JEOL JEM-1210 transmission electron microscope operated at an accelerated voltage of 100kV. Snake skin dialysis tubing was obtained from Pierce, Rockford (Illinois, USA).

4.4.2 Fungal strain and culture conditions

The same protocol was followed as described in section 2.4.2.

4.4.3 Hydrogenase Assay

Hydrogenase activity was measured using a protocol as described in literature (De Lacy *et al.*, 2000; Ngwenya and Whiteley, 2006; Rashamuse and Whiteley, 2007). The assay was determined spectrophotometrically at 604 nm, at room temperature by the reduction of methyl viologen (ε_{604nm} = 13.9 $mM^{-1}cm^{-1}$; electron acceptor) with H_2 gas (electron donor) in the presence of Tris-HCl buffer (50 mM, pH 7.5). The assay was carried out in a stoppered cuvette contained in a final volume of 3.105 ml; 3 ml (1 mM) methyl viologen which was pre-activated by bubbling with H_2 gas for 15

minutes at 1 atm, 30 $ml^{-1}min^{-1}$, sodium dithionite (5 µl, 100 mM) which was added into the cuvette to eliminate residual O_2 and the reaction was started by addition of 100 µl of pre-activated cell free extract. One unit of activity was defined as the amount of hydrogenase that catalysed the reduction of 1 µmol of methyl viologen per min per ml in the presence of excess hydrogen.

4.4.4 Protein determination

Protein was quantified by the Bradford method (Roe, 2001), using bovine serum albumin (BSA) as a standard and described in Appendix B.

4.4.5 Preparation of the cell free extract

The mycelial mass was separated from the MGYP broth by centrifugation (10 000 x g, 4 °C, 25 min) and the settled mycelia (10 g) was washed three times with sterile ddH_2O and re-suspended in Tris-HCI buffer (pH 7.5, 50mM; 100 ml). Cell integrity was disrupted by sonication (10W, 30 s intervals, 4 min). The lysate (1g biomass/10 ml ddH_2O) was incubated in Erlenmeyer flasks, covered in aluminium foil in a constant environment room (28 °C, 96 hr). Following the end of the incubation period, the fungal mycelial mass was removed from the extracellular solution by centrifugation (10 000 x g, 4 °C, 25 min), the fungal mycelial mass was discarded and the cell free extract was used for further analyses.

4.4.6 Concentration of the cell free extract

The concentration procedures reported here are those that showed the best results from several attempts made in this study. A preliminary study divided the supernatant into two 15 ml portions; one part was concentrated with PEG and the other by freeze drying. The method producing the best results was used thereafter.

4.4.6.1 Polyethylene glycol (PEG 20 000) concentration

The cell free extract (15 ml) was sealed in dialysis tubing that was then placed in a beaker and covered completely with a dry matrix of PEG 20 000. The sample was left to stand (4 °C, 3h) as the water was removed from the cell free extract until the desired volume (5ml) was obtained. The concentrated sample was assayed for protein concentration and hydrogenase activity.

4.4.6.2 Freeze drying

The sample (15 ml) was poured into a freeze drying flask and frozen by gently swirling the flask in liquid nitrogen for 10 min. The sample was then transferred onto a freeze dryer and dried at - 40 °C overnight. The powdered extract was re-suspended in a minimal amount of ddH_2O (5 ml) and assayed for protein and hydrogenase activity.

4.4.7 Separation of "factors" using ion exchange chromatography

The concentrated sample (5 ml) was applied onto a DEAE - Sephacel column (1.5 cm x 20 cm). The column was pre-washed with buffer Tris-HCl buffer (pH 7.6, 50 mM) and equilibrated until A_{280} of the eluate had reached baseline. The sample was applied and eluated with 0-1 M NaCl in the same buffer. Fractions (4 ml) eluated at 2 $mlmin^{-1}$ were assayed for protein concentration. Those that contained protein were collected and assayed for hydrogenase activity, pooled together, and were dialysed overnight in 10 times sample volume Tris-HCl buffer (pH 7.6, 10 mM) to remove any residual NaCl.

4.4.8 Purification of the hydrogenase using size exclusion and ion exchange chromatography on Sephacryl S-200.

The concentrated sample (5 ml) was applied onto a Sephacryl S-200 column (3 cm x 30 cm). The column was pre-washed with buffer Tris-HCI buffer (pH 7.5, 50 mM) and equilibrated until A_{280nm} of the eluate reached baseline. The sample was applied and eluated with a 0-1 M NaCI gradient in the same buffer. Fractions (4 ml) eluated at 2$mlmin^{-1}$, were collected and assayed for protein concentration. Those that contained protein were assayed for hydrogenase activity.

4.4.9 SDS-PAGE analysis of S-200 hydrogenase fractions

The effectiveness of the purification process was determined by running SDS-PAGE on samples exhibiting hydrogenase activity. Samples from each purification step (20 µl) and a standard molecular weight marker (10-200 kDa), were electrophoresed on 10 % SDS-PAGE at 120 V. The gels were stained with coomasie brilliant blue R-250 staining solution, then destained in methanol: acetic acid: water (1:1:8 v/v/v) destaining solution (Appendix C). The molecular weight of the partially purified hydrogenase was determined using a standard curve of log molecular weight versus distance migrated (Appendix C).

4.4.10 Characterization of the hydrogenase

4.4.10.1 pH profile

The optimum pH for the hydrogenase was established by re-suspending the partially purified enzyme (100 µl) in different pH buffers (3 ml), sodium acetate (pH 4- 5.5, 50 mM); sodium phosphate buffer (pH 6-6.5, 50 mM); Tris-HCI buffer (pH 7-9, 50 mM) and bicarbonate buffer (9.5-11, 50 mM). Hydrogenase activity was determined in each of the samples at the different pH levels as previously described in section 4.4.3.

4.4.10.2 Temperature profile

The temperature optimum of the partially purified hydrogenase enzyme was determined over a range of 10-70 °C. The reaction mixture was prepared as previously described in section 4.4.3. The reaction was started by addition of hydrogenase suspension (100 µl) pre-activated with gaseous H_2 at the different temperatures.

4.4.10.3 Thermal stability

The optimum pH and temperature were used to determine the optimal thermal stability of the enzyme. Hydrogenase activity at time zero was considered to be 100 % relative activity, and its activity measured at 10 min intervals for 90 mins.

4.4.10.4 Kinetic parameters (V_{max} and K_m)

The kinetic properties were determined by varying the substrate (methyl viologen, 3 ml) concentration between the ranges 0-10 mM. Hydrogenase activity was determined at each substrate concentration as previously described in section 4.4.3.

4.4.10.5 Effect of H_2PtCI_6 on hydrogenase activity

Hexachloroplatinic acid (1 and 2 mM) was added into the reaction mixture at each substrate (methyl viologen) concentration to determine if H_2PtCI_6 had any inhibitory effect or if the partially purified hydrogenase had a higher affinity for it than methyl viologen. Hydrogenase activity was carried out previously described (section 4.4.3).

4.4.11 Platinum nanoparticle synthesis

During the synthesis of platinum nanoparticles, hydrogenase containing fractions and those fractions high in protein composition but no hydrogenase activity were exposed to an aqueous solution containing a carbonate buffer (0.05 M, pH 9) and H_2PtCI_6 (20 mM) in Erlenmeyer flasks. Conditions for nanoparticle synthesis were maintained at pH 9 and the flasks were placed in an incubator shaker (65 °C, 180 rpm). The reduction of metal ions was routinely monitored during a 24 hr period by measuring the UV absorbance of the solution at 285 nm by periodic sampling of aliquots of the aqueous solution.

4.4.12 Analysis of platinum nanoparticles

4.4.12.1 Quantitative analysis using UV spectroscopy

The same protocol was followed as described in section 2.4.4

4.4.12.2 Qualitative analysis using TEM

The same protocol was followed as described in section 3.1.4.2

4.4.12.3 Qualitative analysis using STEM

Samples were suspended on an aluminium stub and allowed to air dry for 10 mins and scanned on a scanning transmission electron microscope. Once it was identified that heavy metal deposits were visible, the sample was diluted (100 x) with sterile ddH_2O and suspended on a holey carbon grid. Once nanoparticles were identified, XEDS was applied to identify if those were actual platinum nanoparticles.

4.4.12.4 Qualitative analysis using AFM

The diluted sample (section 4.4.12.3) was used for AFM studies incorporating two methods of detection - the contact mode and the dynamic mode. The former was used for small, high speed atomic resolution scans, whilst the latter was used to improve the lateral resolution of the soft sample surface (due to enzyme). Images were captured and viewed in the height, deflection and friction plane.

4.5 Results and Discussion

4.5.1 Identification of the 'factors"

4.5.1.1 Concentration of the extract

The effect of three concentration methods on the hydrogenase activity was investigated. The use of ammonium sulphate precipitation was not successful as all activity was lost. Literature indicates that polyethylene glycol stabilises enzyme activity (Harris, 2001), however in this study there was a significant loss of activity with only 10 % of the enzyme recovered. The best enzyme yield was obtained using freeze drying and consequently this was the method of choice during the purification of the "factors". During this investigation isolate 6377 was used for the protein purification.

4.5.1.2 Separation of the "factors" using ion exchange chromatography

DEAE Sephacel is a weak anion exchanger and separates proteins on the basis of their charge. Separation is obtained since different substances have different degrees of interaction with the ion exchanger due to differences in their charges, charge densities and distribution of charge on their surfaces. A summary of the purification protocol with freeze drying followed by dialysis and subsequent purification on Sephacel is shown in Table 4.1. The first step of freeze drying resulted in a loss of specific activity from 184.37 to 47.80 $nmolmin^{-1}mg^{-1}$. Activity could have been lost by the reduction in viscosity caused by the withdrawal of water molecules from the cell free extract.

Table 4. 1 Purification table of the hydrogenase containing peaks

Purification Step	Volume (ml)	Total Protein (mg)	Total Activity (U)	Specific Activity (U/mg)	Recovery %	Purification Fold
Crude	100	1.90	350.3	184.37	100	1
Freeze drying & dialysis	15	1.35	64.53	47.80	18.4	0.26
DEAE Sephacel[1]	5	0.96	30.74	32.02	8.78	0.17

[1] = DEAE Sephacel are the pooled fractions of peaks 2 (fractions 36-48) and 3 (fractions 56-60).

The elution profile yielded four distinct peak areas – peak 1 (fractions 23-29) eluting at 0.3 M NaCl, peak 2 (fractions 36-48) eluting at 0.5 M NaCl, peak 3 (fractions 56-60) eluting at 0.6 M NaCl and peak 4 (fractions 68-77) eluting at 0.75 M NaCl following the absorbance reading at 280 nm (Figure 4.3). These peak areas indicate the presence of four different proteins or similar proteins differing by only one charged amino acid. The hydrogenase assay was performed on all fractions and only two of the four peak areas (peaks 2 and 3) were active. All the hydrogenase containing fractions were pooled together and only 8.78 % of the hydrogenase was recovered with a very low purification fold of 0.17 (Table 4.1).

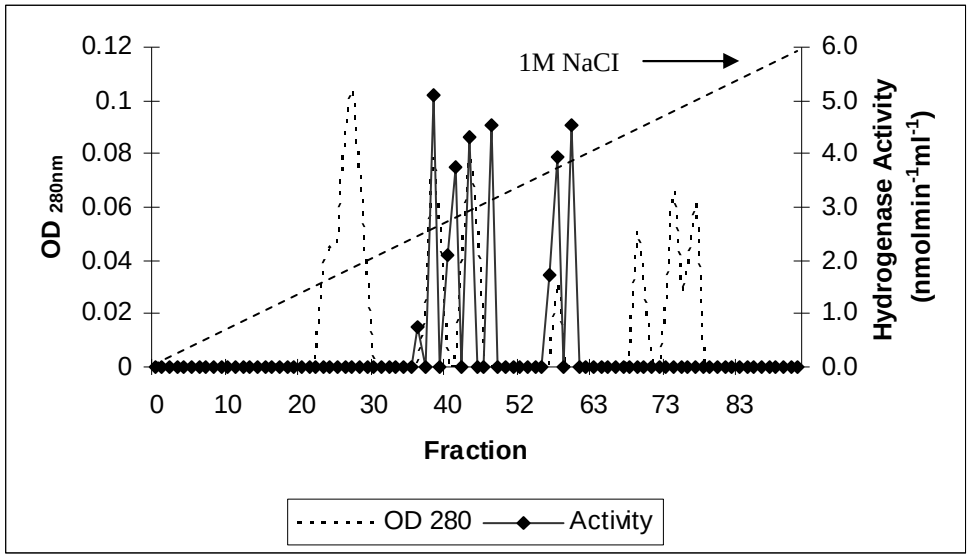

Figure 4. 3 DEAE-Sephacel ion-exchange chromatography after freeze drying. Column dimension (1.5 x 20 cm); Flow rate: 2 mlmin^{-1}. Peak 1 = fractions 23-39, peak 2 = fractions 36-48, peak 3 = fractions 56-60 and peak 4 = fractions 68 – 77. The fractions were eluated by gradient addition of NaCI (0-1M) with Tris-HCI buffer (pH 7.5, 50 mM).

Presence of the two hydrogenase active peaks indicates either the presence of two different hydrogenases or a single hydrogenase dimer. The dimer hydrogenase could have had the two subunits eluated separately. Although 4 peaks were identified only those two with hydrogenase activity were used for further purification. The other two non hydrogenase peaks will be discussed in section 4.5.5.1 on page 98.

4.5.2 Purification of the hydrogenase using combination size exclusion – ion exchange chromatography.

A summary of the hydrogenase purification with dialysis, freeze drying and Sephacryl S-200 size exclusion-ion exchange chromatography is shown in Table 4.2. The first purification step of freeze drying increased the specific activity from 13.84 to 25.74 Umg^{-1} as it managed to remove the water that constituted the aqueous sample as well as contaminating proteins as seen by the decrease in protein concentration from 7.89 to 3.78 mg. The fold purification increased slightly indicating that the target protein had been slightly 'cleaned up'. The freeze dried extract was then loaded onto a Sephacryl S-200 size-exclusion-ion exchange column.

Table 4. 2 Purification table for the hydrogenase fractions

Purification Step	Volume (ml)	Total Protein (mg)	Total Activity (U)	Specific Activity (Umg^{-1})	Recovery %	Purification Fold
Crude	100	7.89	109.20	13.84	100.00	1.00
FD and Dialysis	15	3.78	97.30	25.74	89.1	1.86
S200 F50-55	10	1.07	2.76	2.58	2.53	0.19
S200 F65-70	10	1.05	1.46	1.39	1.34	0.10

$1U = 1nmolmin^{-1}ml^{-1}$

The elution profile is shown in Figure 4.4. Two main protein peak areas were observed, peak 1 (fractions 50-55, eluated with 0.65 M NaCl) and peak 2 (fractions 65-70 eluated with 0.85 M NaCl) with hydrogenase activity. There was a significant decrease in fold purification for both peak areas, from 1.86 to 0.19 (fraction peak 50-55) and 0.10 (fraction peak 65-70) during the purification step with Sephacryl S-200. Hydrogenase enzymes are considered very unstable, and a rapid purification protocol is required to minimise the loss of enzyme. Previous attempts at the purification of the hydrogenase, from the present study, indicated that an increased flow rate of the eluate affects the resolution of the chromatogram. The elution profile (Figure 4.4) shows that at $2mlmin^{-1}$ there were over 50 fractions (100 mins) before the hydrogenase was eluated and this could explain the low enzyme recovery (Table 4.2). Studies were performed with SDS- PAGE to determine the molecular weight of the hydrogenase enzyme (s) purified in this study.

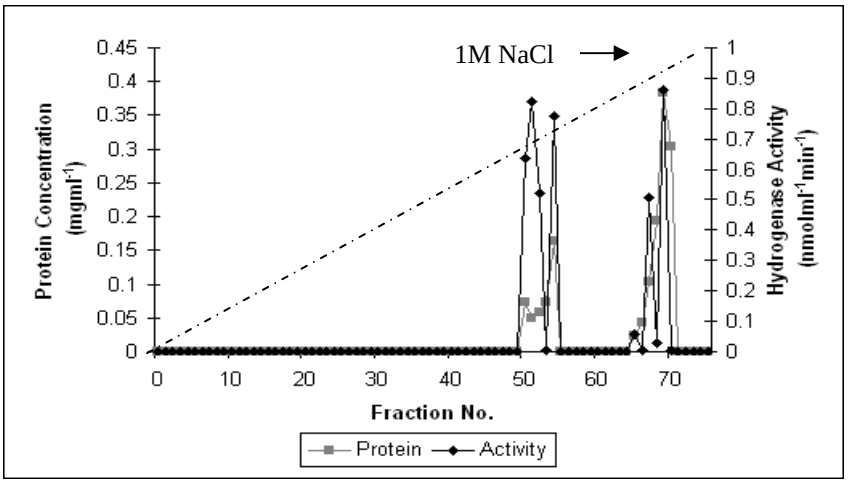

Figure 4. 4 Sephacryl S-200 size exclusion - ion exchange chromatography after freeze drying. Column dimension (3 x 30 cm); Flow rate: 2mlmin^{-1}. The hydrogenase activity was eluated by gradient addition of NaCl (0-1 M) with Tris-HCl buffer (pH 7.6, 50 mM).

4.5.3 SDS-PAGE molecular weight analysis

The results (Figure 4.5) with pooled fraction peaks (50-55) indicate two distinct protein bands of 44.5 and 29.4 kDa, whilst with fraction peaks 65-70 only a single band of 29.4 kDa was observed. It appears that the dimer was eluated first, followed by the single subunit. The Ni-Fe class of hydrogenases have been identified to contain dimeric subunits (Winter *et al*., 2005) and thus supports the likelihood of the "factor", in the present study, being identified as the same.

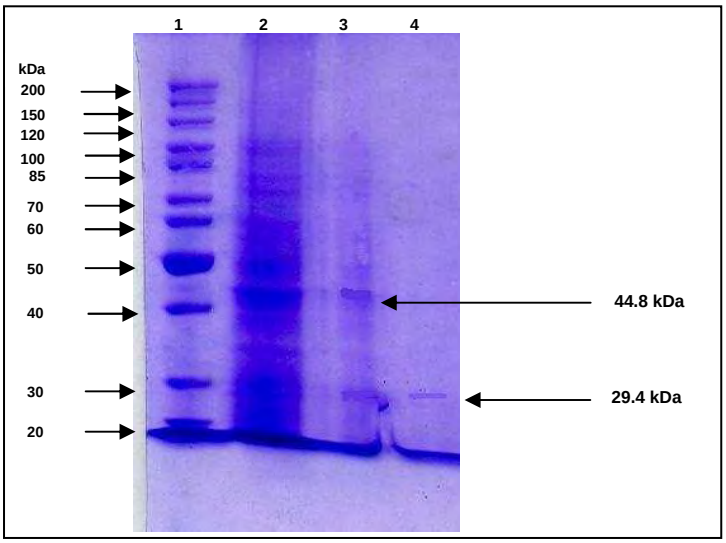

Figure 4. 5 10 % SDS-PAGE analysis of purified hydrogenase. Lane 1: Molecular weight markers. Lane 2: Freeze dried extract. Lane 3: Sephacryl S-200 fractions pool 50 - 55. Lane 4: Sephacryl S-200 fractions pool 65-70.

4.5.4 Characterization of the hydrogenase

4.5.4.1 pH optimum profile

The majority of enzymes normally exhibit a strong dependence of activity on the pH of the medium (Clark and Switzer, 1977), thus it is important to optimise the pH of a hydrogenases have been isolated in a variety of organisms including fungi, bacteria and algae. As habitats of the microorganisms differ in environmental conditions, the pH profile was investigated over a range of 4-11 with the use of various buffers coherent with each pH level. Enzymes have been known to operate within the pH of the organism that they are produced in as a result the hydrogenase purified in this study had an optimal pH that corresponded with the conditions under which *F.oxysporum* was cultured. The hydrogenase purified in this study had an optimal pH of 7.5 (Figure 4.6 A). Previous studies on hydrogenase characterisation had also found the optimal pH to be in the pH range 7-8 (Rashamuse and Whiteley, 2007; Ngwenya and Whiteley, 2006), thus it may be deduced that hydrogenase enzymes function optimally in a slightly alkaline environment, and thus it can be suggested that pH dependence of hydrogenase reactions is the consequence of the changes in degrees of ionisation of the functional groups in the enzyme and the substrate (Clark and Switzer, 1977).

4.5.4.2 Temperature profile

A maximum hydrogenase activity was observed at 38 °C. Previous studies on hydrogenase characterisation had also found the optimal temperature to be in the 35-40 °C range (Ngwenya and Whiteley, 2006; Rashamuse and Whiteley, 2007). The temperature curve follows a characteristic bell shape (Figure 4.6 B) which is typical of enzyme kinetics in which the rate of enzymatic reaction increases as the temperature increases, this being achieved by increase in the rate at which enzyme and substrate 'collide' or become in contact with one another (Walker, 2000). The downside to this reaction, however, it should be noted that at higher temperatures (greater than 50 °C), there is disruption of the quaternary structure of the protein resulting in inactivation and subsequent denaturation of the enzyme.

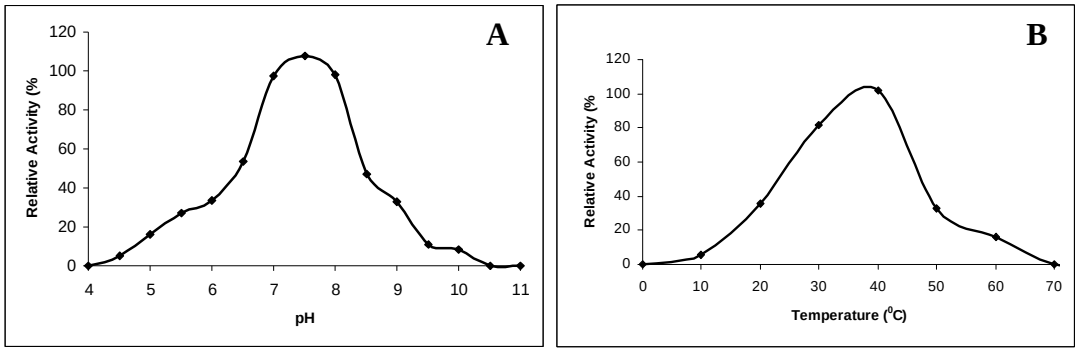

Figure 4. 6 (A) pH profile and (B) temperature profile of the purified hydrogenase enzyme (100 % activity = 2.63 nmolmin^{-1}ml^{-1})

4.5.4.3 Thermal stability of the hydrogenase

The thermal stability of the purified hydrogenase was investigated at optimum pH (7.5) and temperature (38 °C). Minimal activity loss was observed during the initial 10 minutes, but thereafter, activity steadily decreased as incubation time increased (Figure 4.7). The evident loss in activity observed could have been caused by the loss of protective matrices, which normally protect the hydrogenase enzyme *in vivo* as consequence of the isolation and purification steps carried out during the course of the study (Ngwenya and Whiteley, 2006; Rashamuse and Whiteley, 2007). External forces (such as changes in pH and temperature) could also result in progressive denaturation of the enzyme by altering the structural integrity of the hydrogenase. After 50 minutes 70 % of the activity had been lost after which little change in activity occurred. The hydrogenase purified in this study had a half life of 36 minutes ($t_{1/2}$ = 36).

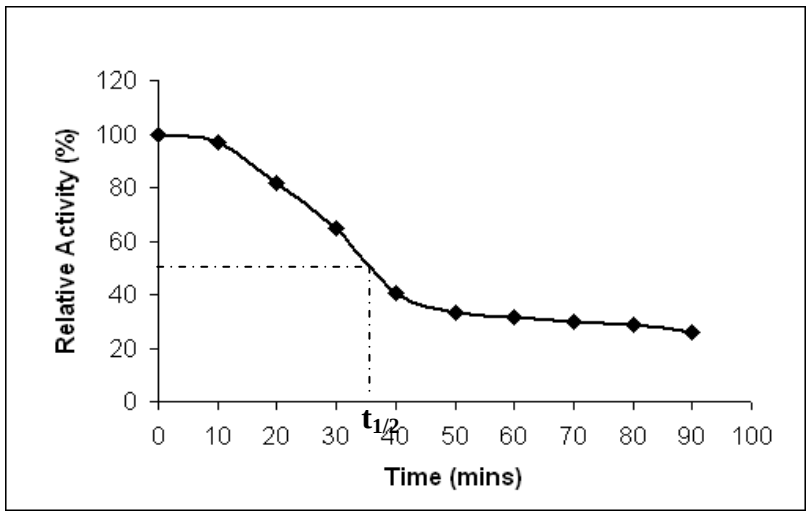

Figure 4. 7 Thermal stability of hydrogenase enzyme (100 % activity = 2.59 nmolmin^{-1}ml^{-1})

Hydrogenase enzymes are highly sensitive to oxygen and thus all studies are conducted carefully to minimize oxygen exposure. The relatively short life of the purified hydrogenase confirms our earlier thought that with a decreased flow rate, although enzyme resolution improved, hydrogenase activity drastically decreased (Table 4.2). The low enzyme yield obtained could be attributed to the lack of thermal stability during exposure to oxygen (Kamachi *et al*., 1995). The low hydrogenase yields obtained during the purification protocol (Table 4.1) is a consequence of the lack of thermal stability of the hydrogenase.

4.5.4.4 Kinetic parameters

An investigation into the effect of substrate concentration on the activity of hydrogenase was investigated by measuring hydrogenase activity over a range of methyl viologen concentration (0-10 mM). A typical increase in substrate concentration resulted in a proportional increase in activity until substrate saturation was achieved (Figure 4.8).

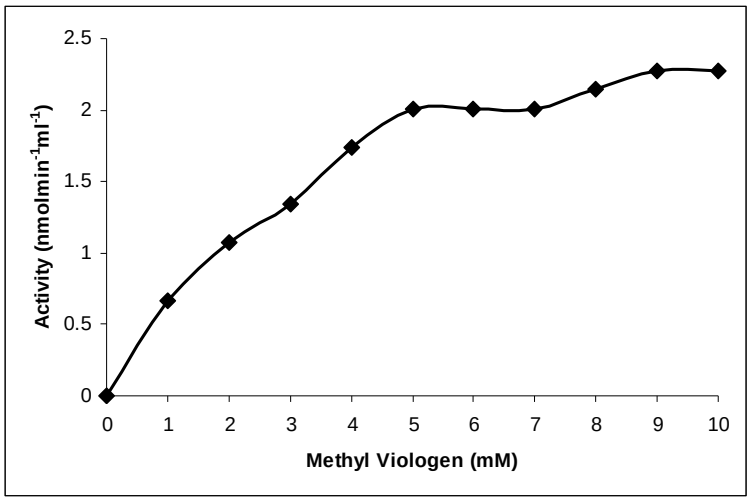

Figure 4. 8 Michaelis-Menten plot of hydrogenase enzyme activity versus methyl viologen concentration.

Hydrogenase activity of the enzyme purified in this study was rather low with a maximum activity (V_{max}) of 3.16 $nmolmin^{-1}ml^{-1}$ (Figure 4.9), while a Michaelis constant (K_m) value of 3.64 mM was recorded (Figure 4.9). These findings suggest that the purified enzyme could catalyse a range of substrates and thus could be useful for the bioreduction of metal salts to produce nanoparticles.

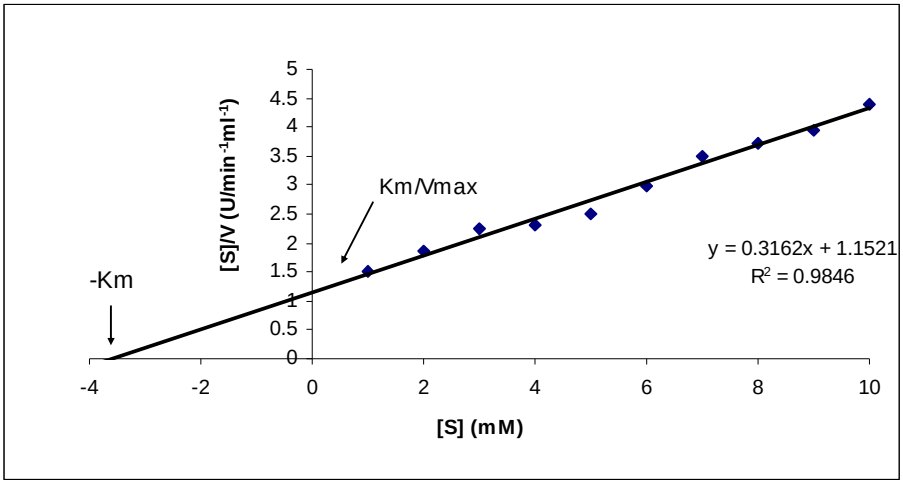

Figure 4. 9 Hanes-Woolf plot of hydrogenase enzyme activity versus methyl viologen concentration

4.5.4.5 Affinity of hydrogenase for hexachloroplatinic acid

The affinity of the hydrogenase enzyme for H_2PtCI_6 was determined by including H_2PtCI_6 to a lowered final concentration of either 1 or 2 mM with the substrate methyl viologen (0-10 mM, 3 ml). The results indicate that with the inclusion of 2 mM H_2PtCI_6, the V_{max} decreased drastically from 3.16 to 0.140 nmolmin^{-1}ml^{-1} (Figure 4.10), and the K_m value decreased from 3.64 mM to 1.89 mM (Figure 4.11), thus indicating that the hydrogenase had a higher affinity for H_2PtCI_6 than methyl viologen. It can be proposed that H_2PtCI_6 can be a suitable electron acceptor, thus may be reduced to form platinum nanoparticles.

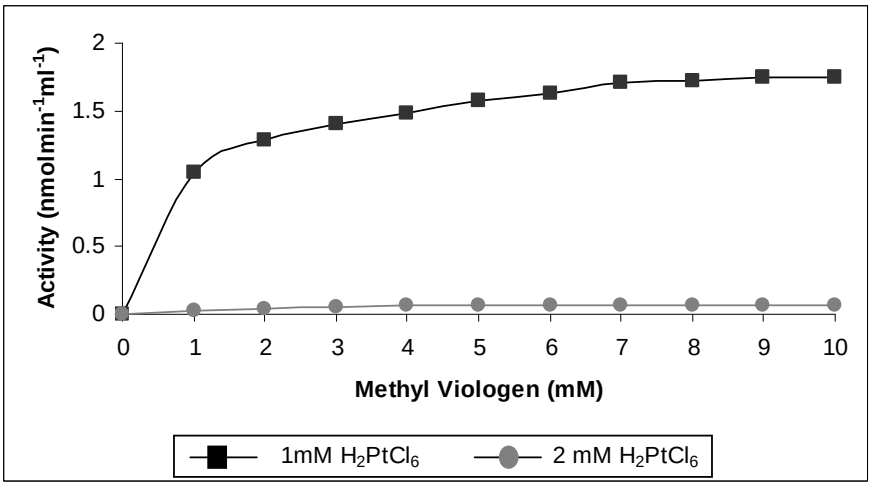

Figure 4. 10 Michaelis- Menten plot of hydrogenase enzyme activity versus methyl viologen concentration in the presence of both 1 and 2 mM H_2PtCl_6

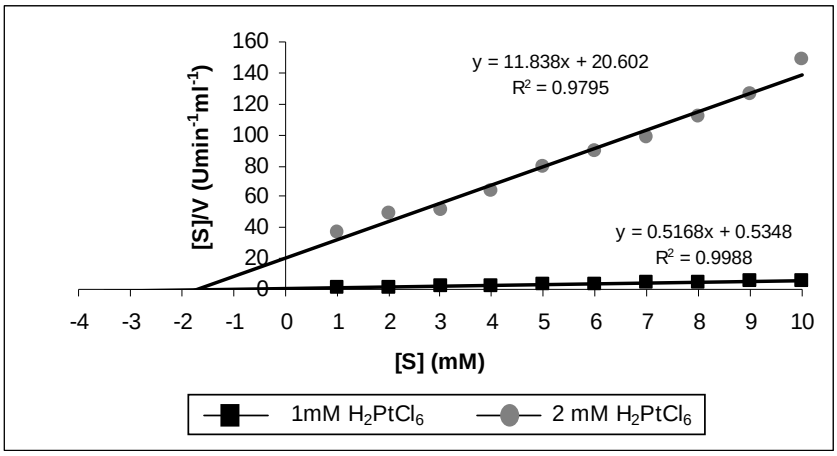

Figure 4. 11 Hanes-Woolf plot of hydrogenase enzyme activity versus methyl viologen concentrations in the presence of 1 and 2 mM H_2PtCI_6

4.5.5 Synthesis of platinum nanoparticles

4.5.5.1 Quantitative analysis using UV spectroscopy

Pooled fractions of the hydrogenase (fractions 50-55, Figure 4.4) and non hydrogenase pooled fractions (fraction 23-39, Figure 4.3) were compared in their ability to reduce H_2PtCI_6 and produce nanoparticles. Samples were routinely removed from flasks over a 24 hr period to monitor the bioreduction of H_2PtCI_6.

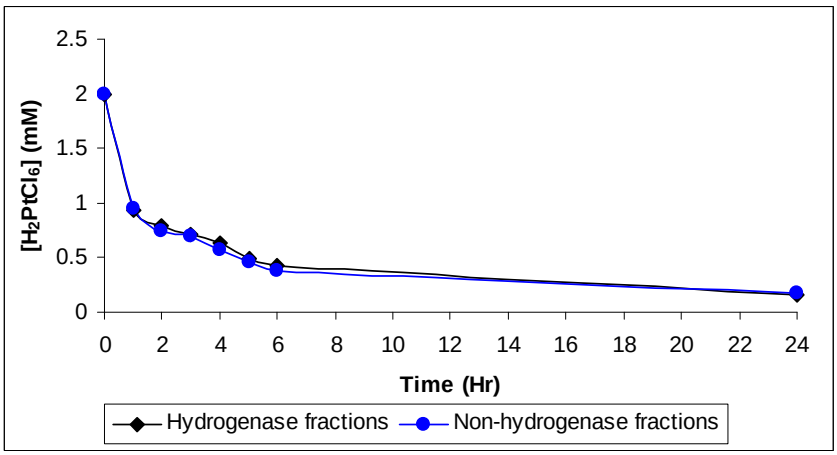

Figure 4. 12 Bioreduction of H_2PtCI_6 (2 mM) with pooled hydrogenase containing fractions (50 -55) and non hydrogenase containing fractions (23-39).

The results indicate that there was no difference in the ability of the different pooled fractions to reduce H_2PtCI_6. The hydrogenase and non hydrogenase fraction pools both reduced the platinum chloride levels from 2 to 0.94 mM after 1 hr (Figure 4.12), and within 24 hrs the H_2PtCI_6 levels had dropped below 0.16 mM for both pooled fractions.

These interesting and somewhat unexpected results indicate that both a hydrogenase and one or more unknown enzyme in *F.oxysporum* maybe responsible for the reduction of H_2PtCI_6 into platinum nanoparticles.

4.5.5.2 Qualitative analysis of using TEM

Sample aliquots removed during the time study (section 4.5.5.1) were analysed for platinum nanoparticle formation. Transmission electron micrographs show that nanoparticles were produced by both the hydrogenase pooled fraction and the pooled non hydrogenase fractions though the shape of the nanoparticles produced by the different fraction pools was distinctly different. Platinum nanoparticles produced by the non hydrogenase fractions 23-39 (Figure 4.13), were all uniform and spherical in shape. The size range distribution was from a few nanometres to particles of about 180 nm. The majority of nanoparticles were between 200-800 nm (Figure 4.13 B), with the mean nanoparticle size in the 400-600 nm range. In comparison the nanoparticles produced by the hydrogenase pooled fraction were of varied shaped, with circular, triangular and pentagonal nanoparticles being produced (Figure 4.14).

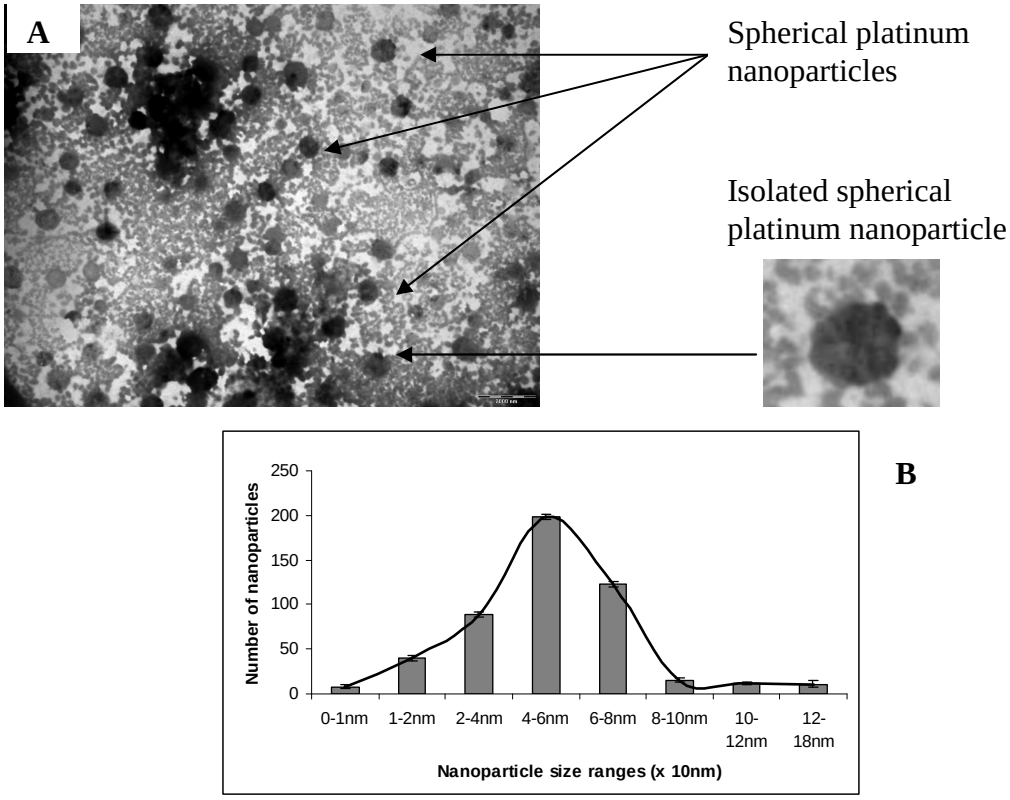

Figure 4. 13 (A) Platinum nanoparticles produced by pooled non hydrogenase fractions 23-39. Magnification = 6 000x, scale bar represents 2000 nm. (B) The size distribution histogram of platinum nanoparticles produced by pooled fractions 23-39. all error bars represent the SE.

The hydrogenase pooled fractions also produced circular nanoparticles over a wide size distribution with the majority of nanoparticles being between 200-800 nm, though the mean size range was 400-600 nm (Figure 4.14).

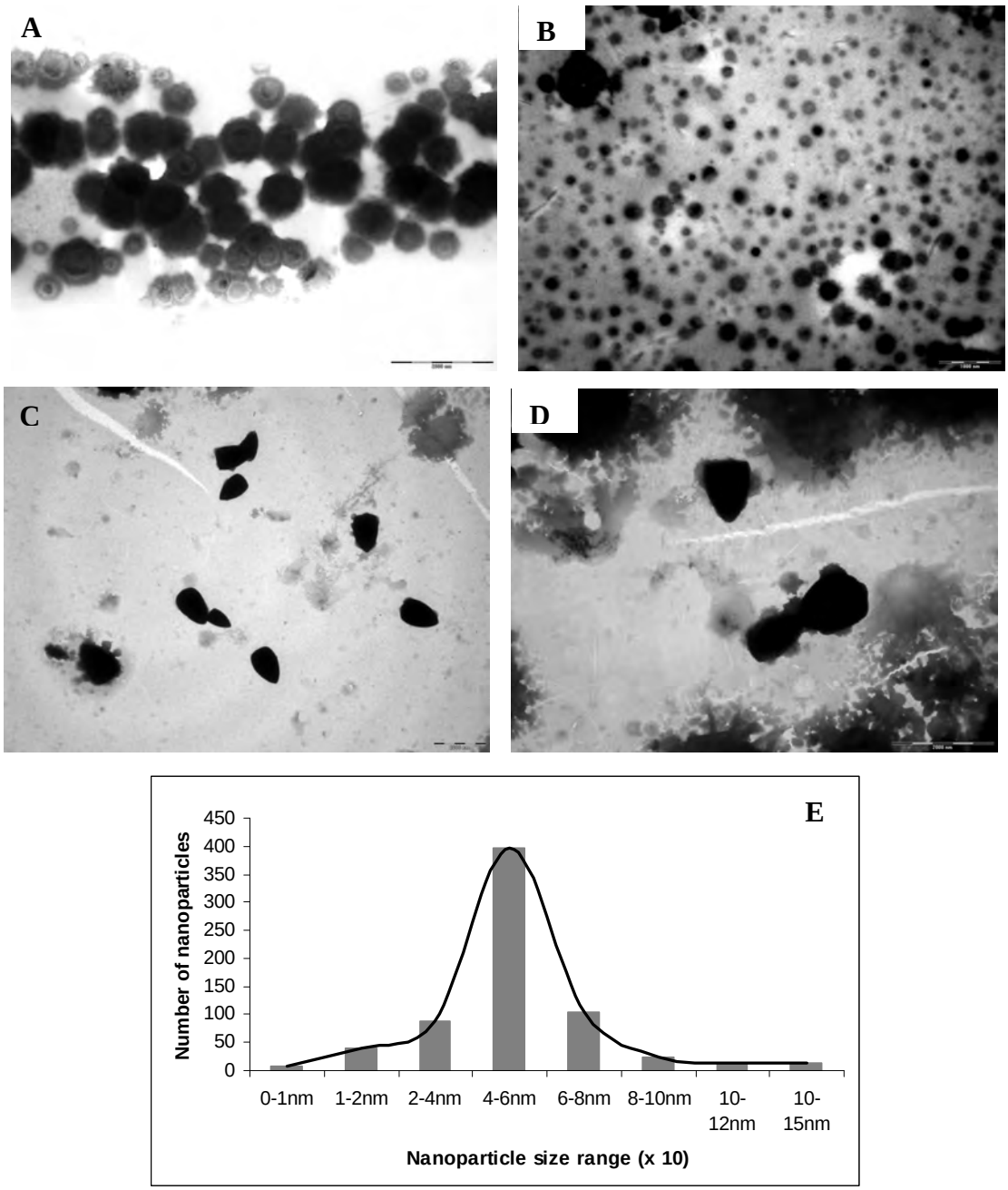

Figure 4. 14 Transmission electron micrographs of platinum nanoparticles produced by hydrogenase pooled fractions. (A and B) Circular nanoparticles, magnification = 12 000x. (C) Pentagonal nanoparticles, magnification = 6 000x. (D) Triangular nanoparticles, magnification = 12 000x. All scale bars represent 2000 nm. (E) The size histogram of spherical platinum nanoparticles. All error bars represent the SE.

Micrographs of the nanoparticles, using only the non hydrogenase fractions 23-39, produced monodisperse nanoparticles that were not aggregated. The nanoparticles were clearly monodisperse and did not accumulate in groups and lumps. This is contrary to nanoparticles produced from the hydrogenase fractions as these nanoparticles were found aggregated and bound to each other as well as, what appears to be extrapolymeric substances (hydrogenase) (Figure 4.15).

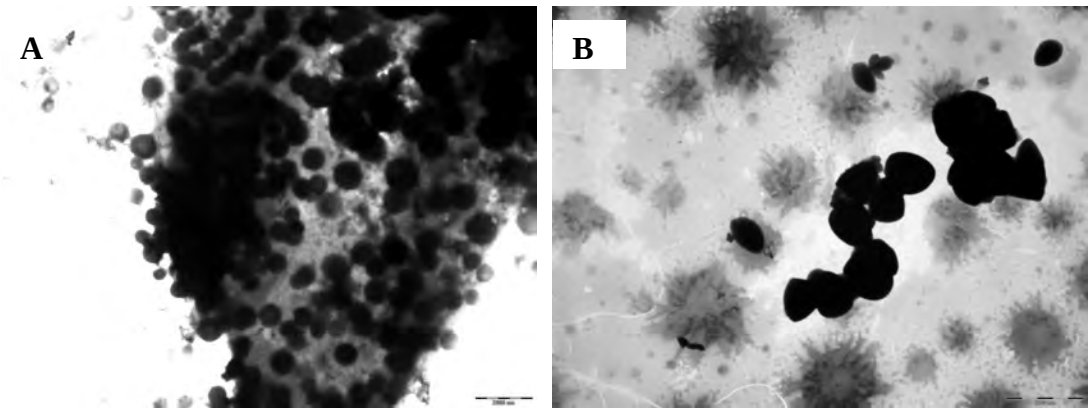

Figure 4. 15 Micrographs showing (A) circular nanoparticles bound to the enzyme and (B) pentagonal nanoparticles closely attached to each other. Magnification = 6 000x, all scale bars represent 2000 nm.

4.5.5.3 Qualitative analysis using STEM coupled with XEDS, of the nanoparticles synthesised by the hydrogenase

The 24 hr sample containing platinum nanoparticles produced from the hydrogenase containing fractions was analysed using STEM. The enzyme-platinum nanoparticle sample was scanned though the hydrogenase coated most of the nanoparticles and could not be viewed clearly at all. The platinum nanoparticles seemed to be coated with the enzyme (Figure 4.16) as the white areas on the micrograph represent the metallic platinum which is reflected due to the diffraction of the electron beam from the metallic surface. The micrograph indicated that heavy metal deposits were visible, however due to the density of the enzyme, a 100x dilution of the hydrogenase-nanoparticle solution was made with ddH_20, and the solution was suspended on a carbon grid. The grid contained holes of varying sizes, thus most of the larger particles and the enzyme solution passed through whilst the smaller particles remained on the grid. Triangular platinum nanoparticles were clearly visible, and the nanoparticles appeared white as a result of the electron deflection off the metallic surfaces.

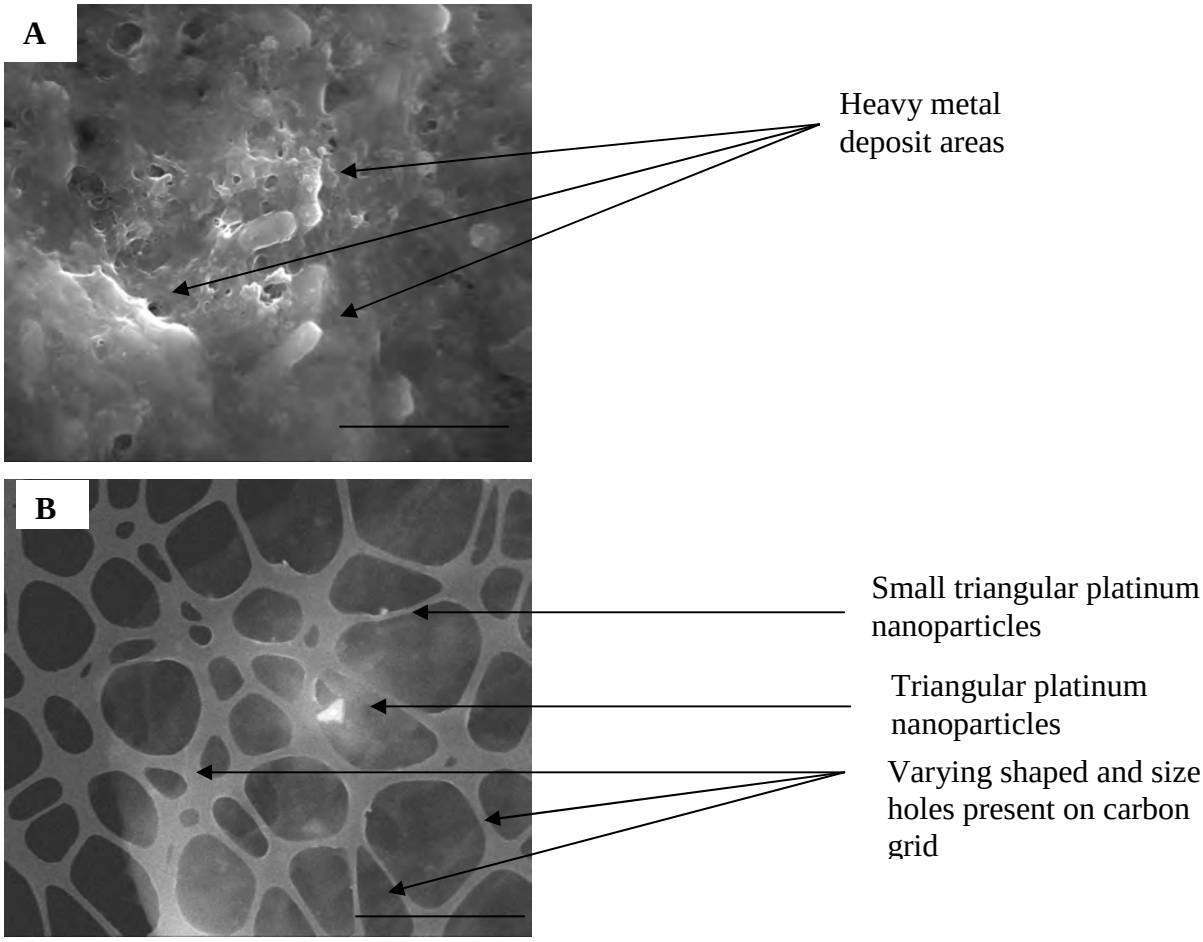

Figure 4. 16 Scanning transmission micrograph of (A) undiluted hydrogenase-platinum nanoparticle solution, magnification = 50 000x and the scale bar represents 2 µm. (B) 100x diluted hydrogenase-nanoparticle solution on a carbon grid, magnification = 32 000x and the scale bar represents 3 µm.

These triangular nanoparticles were spot scanned with X-ray energy dispersive spectroscopy (XEDS) (Figure 4.17), confirming the presence of elemental platinum (Pt^0) in the sample, and supporting our initial hypothesis that H_2PtCI_6 is bioreduced by a hydrogenase to produce platinum nanoparticles. Also present in the sample were carbon and oxygen, which is expected when working with a source derived from a carbon based life form, chloride obviously expected as H_2PtCI_6 was reduced to form platinum nanoparticles with the release of chloride ions. The scan also identified aluminium, and this is as a result of the sample being mounted on an aluminium stub during analyses on the STEM. There are currently three classes of recognised hydrogenases and one of these classes consists of the Ni-Fe hydrogenase, it is thus hypothesised that the observed nickel peaks are indicative of the class of hydrogenase used for this platinum nanoparticle synthesis.

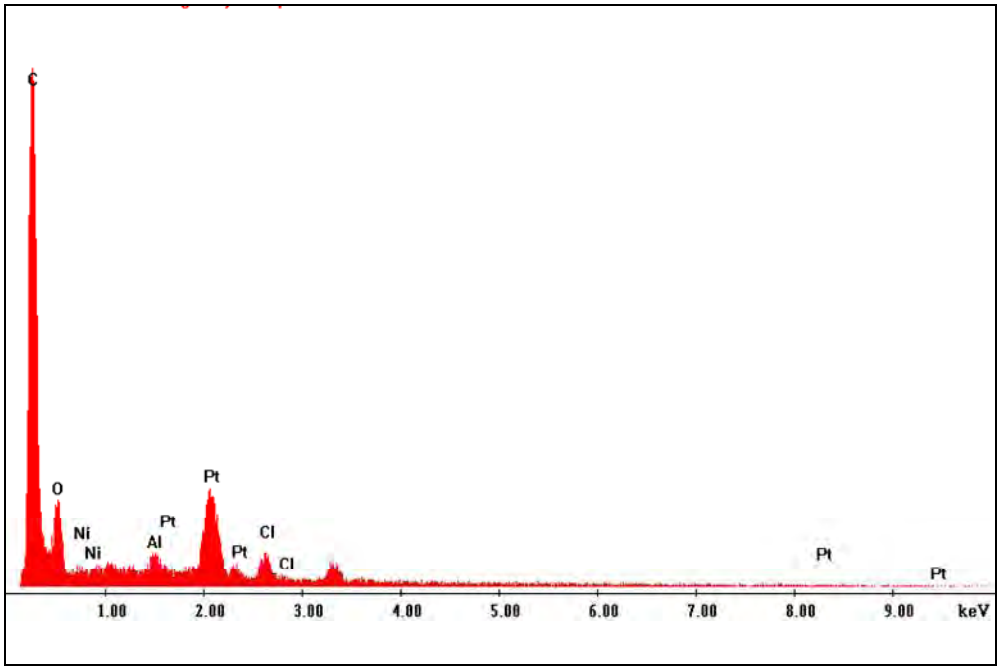

Figure 4. 17 X-ray energy dispersive spectroscopic spot scan of the platinum nanoparticles visualised on the holey grid.

4.5.5.4 Qualitative analysis of platinum nanoparticles using AFM

Groups of nanoparticles were visualised using the atomic force microscope. The 100 x diluted sample used during STEM was analysed using AFM. Particles being in the nano-range are incredibly difficult to visualise as images were viewed at 5um. The results obtained indicate the presence of large amounts of protein (as a result of the hydrogenase enzyme). Two methods of analyses were used, contact and dynamic mode. The first and foremost mode of operation, contact mode is widely used (Figure 4.18). In Figure 4.18, clusters of light white-like dots are platinum nanoparticles and are shown both in perspective view and top view with 3D information being incorporated in both views. In the perspective view, the three dimensional nature of the image is obvious, whilst in the top view; the intensity of the colour reflects the height of the nanoparticles. The AFM can distinguish between different materials thus providing spatial distribution on composite materials and information of material homogeneity. Therefore in the 3D image (Figure 4.18), platinum areas appear yellow and graduate to a lighter colour (dependant on height on the nanoparticle) and the hydrogenase appears red.

The colour gradient from red (enzyme) to yellow (nanoparticles), with the particles graduating in colour from yellow to light yellow to white, indicates an increase in deflection and therefore height. The lighter in colour the nanoparticles are, the larger they are or the more they stick out from the surface.

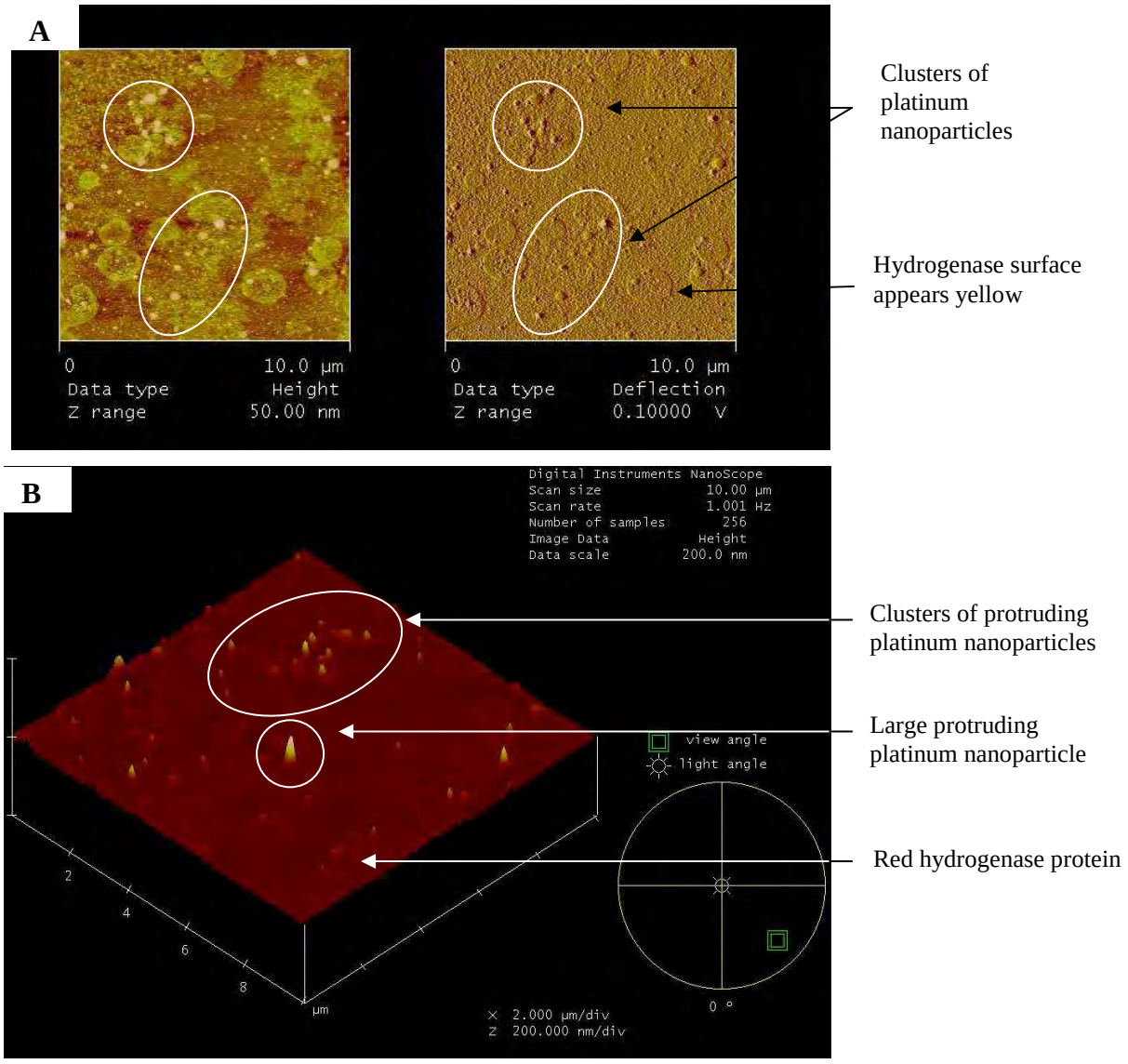

Figure 4. 18 Atomic force micrographs obtained using constant force mode (A) Two dimensional image data expressed in height and deflection. (B) Three dimensional image illustrating platinum nanoparticles.

In addition to the constant force mode, the dynamic force (tapping) mode was also applied to the sample. The tip of the electrode intermittently tapped the surface and was used to improve lateral resolution of the soft enzyme sample. The use of the dynamic force mode results in the elimination of drag and therefore increased sample resolution.

Phase imaging was used in conjunction with tapping mode, providing nanometre scale information about the surface structure. Both the tapping mode topography and phase images were viewed side-by-side in real time and, the resolution of phase imaging is comparable to the full resolution of tapping mode AFM, thus acting as a real-time contrast enhancement technique. Phase imaging highlighted edges and was not affected by the large scale height differences thus providing a clearer observation of fine features, such as sharper nanoparticle edges (Figure 4.19 A).

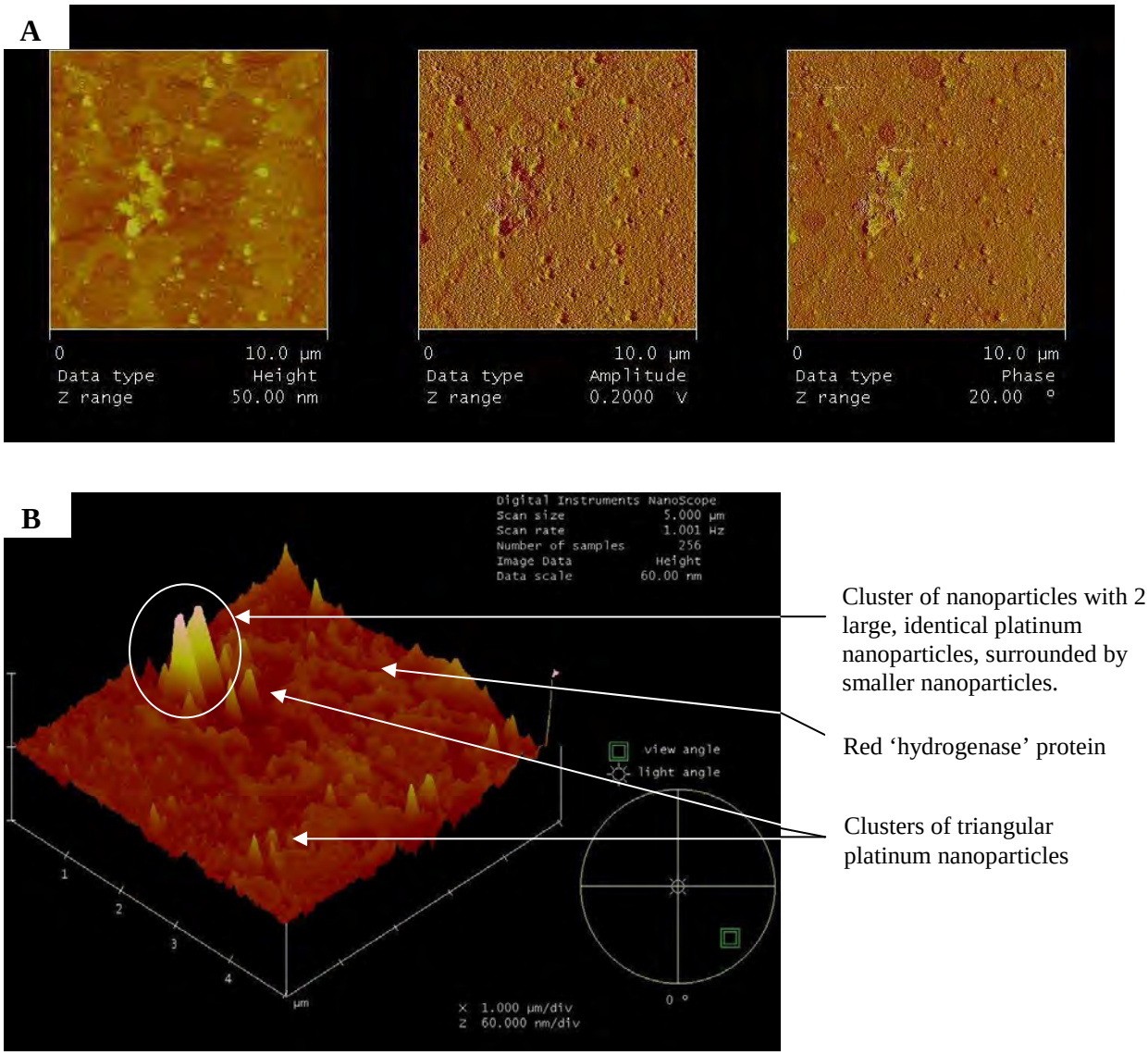

Figure 4. 19 Atomic force micrographs obtained using the dynamic force mode: (A) Two dimensional topographic image view expressed in height, amplitude and with phase imaging, with clusters of platinum nanoparticles encircled (B) 3D topographic phase image view of platinum nanoparticles.

As with constant force mode, a colour gradient corresponding to difference in substrate type was observed. All nanoparticles appear light yellow in the height data image (Figure 4.19 A) and the surrounding enzyme a darker shade of yellow. In the 3D image (Figure 4.19 B) the enzyme appears red with nanoparticle appearing yellow, but some nanoparticles have white tips, and this is as a result of the amplitude of the different nanoparticles. Some particles are larger and thus an increase in height results in a lighter colour (white) (Figure 14.9 B).

4.6 Summary and Conclusions

From the identification, purification and characterization studies it can be concluded that:

a) More than one protein is responsible for platinum nanoparticle formation in *F.oxysporum.*
b) One of those enzymes is a hydrogenase.
c) The molecular weight of the 2 subunit hydrogenase was determined to be 29.4 and 44.5 kDa, which is in the same magnitude as Ni-Fe hydrogenases previously purified (Nicolet *et al*., 2000).
d) The purified hydrogenase showed optimal temperature and pH at 38 °C and 7.5 respectively.
e) The enzyme displayed poor thermal stability over time with a $t_{1/2}$ = 36 minutes.
f) The kinetic parameters V_{max} and K_m were determined to be 3.16 and 3.64 mM respectively
g) The hydrogenase had a higher affinity for H_2PtCI_6 than the methyl viologen substrate.

The purified hydrogenase was used in subsequent experiments for the reduction of higher concentration platinum salts to produce nanoparticles under various conditions.

ENZYMATIC REDUCTION OF PLATINUM SALT TO PRODUCE PLATINUM NANOPARTICLES

5. Introduction

The field of nanotechnology is one of the most active areas in material science research. Innovative applications of nanoparticles and nanomaterials are rapidly emerging, and hence the synthesis of nanoparticles and their self assembly maybe regarded as the cornerstone of nanotechnology (Gardea-Torresdey *et al*., 2002). Therefore new methods to produce nanoparticles are constantly being researched and developed. Biomaterials and biological structures have been shown to act as active units for the synthesis of nanoparticles (Ahmad *et al*., 2002; Mukherjee *et al*., 2002; Bhainsa and D'Souza, 2006; Lengke *et al*., 2006; Shahverdi *et al*., 2007), however the mechanism of nanoparticle formation in these biological media is unknown. It has been hypothesised that various biosynthetic products such as α-hydroxy carboxylic acids or reduced co-factors could play an important role in the reduction of metal salts producing nanoparticles (Willner *et al*., 2006).

A new and emerging area in nanobiotechnology includes the use of biomaterials, specifically enzymes, as the active components for the synthesis and growth of nanoparticles. Hydrogen peroxide (H_2O_2), generated during the biocatalytic oxidation of substrates in the presence of molecular oxygen by oxidase enzymes have been shown to reduce $AuCI_4$ producing Au nanoparticles (Willner *et al*., 2006). Various redox reactions utilise the different oxidised and reduced nicotinamide adenine dinucleotide (phosphate) (NAD $(P)^+$/NAD(P)H) cofactor systems (Willner *et al*., 2006). These NADH and NADPH cofactors were found to synthesis Au nanoparticles by the reduction of $AuCI_4$ (Xiao *et al*., 2004). A review article (Willner *et al*., 2006) discussed the various types of enzymes such as oxidases, hydroxylases, hydrolytic proteins and NAD $(P)^+$ dependant enzymes that were used as biocatalysts for the synthesis of metallic nanoparticles. The ability of NiFe hydrogenase from *Desulfovibrio fructosovorans* to reduce technetium (VII) (De Luca *et al*., 2001) has been demonstrated previously and the mechanisms of enzymatic reduction of metal ions by chemotrophic bacteria have been proposed (Lovely *et al*., 1993; Lloyd *et al*., 2000; Lloyd, 2003).

The key role of hydrogenase, in the process of enzymatic corrosion, has also been discussed (Bryant and Laishley, 1993; Da Silva *et al*., 2002) with the hydrogenase isolated from *Clostridium pasteurianum* (Bryant and Laishley, 1993). The properties of hydrogenases from *Thiocapsa roseopersicina* and *Lamprobacter modestohalophilus* (Zorin, 1986; Zadvorny *et al*., 2004) are very similar to those from sulphate reducing bacteria, which are known to be involved in the process of metal ions reduction (De Luca *et al*., 2001; Michel *et al*., 2001). During the current study metal ion reduction was studied over a short time period using purified hydrogenases from *F.oxysporum* (Chapter 4).

Although enzymatic transformation of metal salts to produce nanoparticles appears to be more superior over other processes, it has its limitations. The fact that enzymes work best at specific optimum conditions is one major problem associated with the use of this technique. Metal salts at different pH, temperature and other physio-chemical composition may tend to inhibit or retard the activity of the redox enzyme. Another controlling factor for theses enzymes, including the hydrogenases, is the electrochemical potential that reflects the ability of reducing or oxidising equivalents (Elliot *et al*., 2002). Other ligands that may be present in metal salt preparations may also affect the activity of the hydrogenase. With these disadvantages in mind, the enzymatic reduction of metallic salts to produce nanoparticles is a novel technique and is still in its infancy. This chapter is aimed at evaluating the ability of the purified hydrogenase to reduce platinum salts thereby producing platinum nanoparticles.

5.1 Materials and Methods

5.1.1 Materials

Hexachloroplatinic acid (IV) (H_2PtCI_6) and platinum (II) chloride ($PtCI_2$) were obtained from Sigma-Aldrich, South Africa. All other reagents which were of analytical grade were obtained from either Merck or Sigma-Aldrich (South Africa). All ddH_20 used in the experiments was obtained from a Millipore Milli-Q system. UV spectroscopy measurements were recorded on a PowerWave microplate spectrophotometer (Bio-Tek Instruments) with 96 well plates, operated at 1nm using the KC Junior software programme. TEM analysis and imagery were performed on a JEOL JEM-1210 transmission electron microscope operated at an accelerated voltage of 100kV.

5.1.2 Methods

5.1.2.1Experimental Conditions

Two experimental procedures were carried out during the course of this study. In the first study, the parameters optimal for platinum nanoparticle formation pH 9, 65 °C (Riddin *et al*., 2006) were used. In the second study, parameters optimal for hydrogenase activity (Chapter 4, pH 7.5, 38 °C) were utilised. For the purpose of this chapter the first experiment will be referred to as POPN (parameters optimal for platinum nanoparticle formation) and POHA (parameters optimal for hydrogenase activity).

5.1.2.1 Effect of metal salt concentration on platinum salt reduction (using the purified hydrogenase)

During the experimental set up, the purified hydrogenase (300µl) was added into sealed flasks containing carbonate buffer (4.2ml, 0.05 M, pH 9)

i. H_2PtCI_6 (20 mM, 500 µl)
ii. H_2PtCI_6 (200 mM, 500 µl)
iii. $PtCI_2$ (20 mM, 500 µl)
iv. $PtCI_2$ (200 mM, 500 µl)
v. ddH_20 (500µl) (Control)

Flasks were incubated in orbital shakers (100 rpm, 24 hrs) at the specific experimental conditions.

5.1.2.2 Quantitative analysis of platinum salt reduction

Samples were removed periodically during the 24 hr period and analysed using UV spectroscopy at 285 nm (H_2PtCl_6) and 290 nm ($PtCl_2$). The concentration of H_2PtCl_6 and $PtCl_2$ before, and after reaction, can be established from a standard curve at this wavelength (Appendix A).

5.1.2.3 Qualitative analysis of platinum nanoparticles

The same protocol was similar to methods described in section 3.1.4.2

5.2 Results and Discussion

5.2.1 Quantitative analysis of the platinum reduction using UV spectroscopy

5.2.1.1Reduction of platinum (IV) salt (H_2PtCI_6)

The rate of enzymatic reduction of H_2PtCI_6 was different with the different set of experimental parameters. During POPN at low H_2PtCI_6 concentration (2 mM) 0.60 mM was present in the reaction vessel after 8 hours, with 70 % of the platinum salt being converted to nanoparticles (Figure 5.1). The rate of bioreduction proceeded faster during POPN as at 24 hours, approximately 0.22 mM of the H_2PtCI_6 was reduced. At a higher platinum salt concentration (20 mM), during POPN, resulted in a reduction of H_2PtCI_6 from 20 to 2.31 mM (Figure 5.2), within 8 hours, and thereafter no further reduction was noticed.

With a low H_2PtCI_6 concentration (2 mM), during POHA, the reduction rate was much slower although those conditions were optimal for enzymatic activity (Figure 5.1). With POHA at 8 hours, 1.34 mM H_2PtCI_6 was present in the reaction vessel, with only 33 % of the platinum salt being converted to platinum nanoparticles. These results are unusual, as theoretically, the reduction rate of H_2PtCI_6 should proceed at the faster rate during POHA as the enzyme would be fully functional. However the platinum (IV) salt appears to be efficiently reduced during conditions suitable for nanoparticle formation, although the elevated temperature and pH would have denatured the enzyme substantially. With a high H_2PtCI_6 concentration, during POHA, there was a reduction from 20 mM to 18.37 mM, at 8 hrs, resulting in a less than 8 % reduction (Figure 5.2).

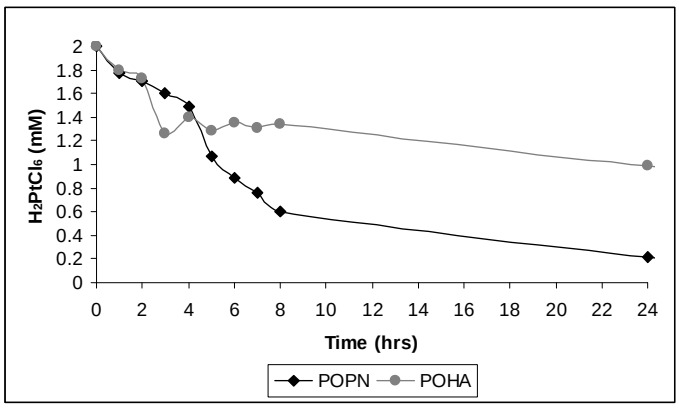

Figure 5. 1 Enzymatic reduction of H_2PtCI_6 (2 mM) in the presence of purified hydrogenase during optimal conditions for platinum nanoparticle formation (POPN) and hydrogenase activity (POHA).

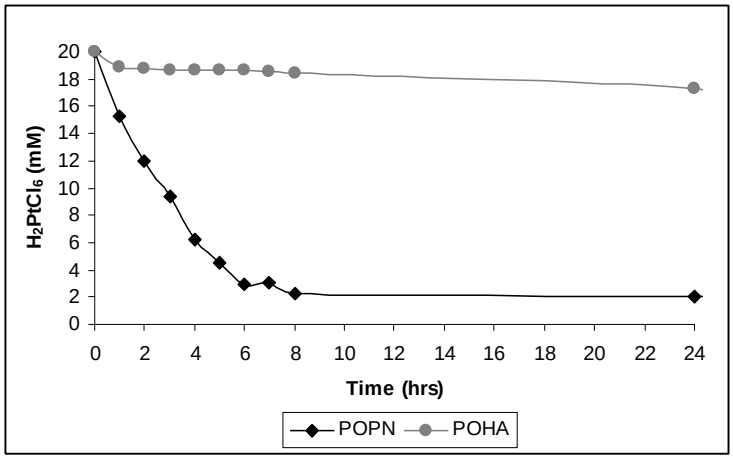

Figure 5. 2 Enzymatic reduction of H_2PtCI_6 (20 mM) in the presence of purified hydrogenase during optimal conditions for platinum nanoparticle formation (POPN) and hydrogenase activity (POHA)

5.2.1.2 Reduction of platinum (II) salt ($PtCI_2$)

Within an hour with POPN 1.02 mM $PtCl_2$ at an initial concentration of 2mM concentration was reduced (Figure 5.3); however no further reduction took place during the 24 hr period. However with an initial concentration of $PtCl_2$ at 20 mM with POPN the $PtCl_2$ levels had decreased to 1.97 mM within 8 hours, with over 95 % of the salt being reduced (Figure 5.4).

$PtCl_2$ reduction, under conditions optimal for enzyme production (POHA), was much slower as only 1.26 mM of the platinum salt was reduced after 3 hrs from an initial 2 mM concentration (Figure 5.3). However after 7 hours less than 0.12 mM of $PtCl_2$ remained in the reaction vessel with over 90 % reduction. However with an initial concentration of $PtCl_2$ at 20 mM with POHA the reduction proceeded more slowly with a less than 9 % reduction of the $PtCl_2$ after 8 hrs (Figure 5.4). There was a further gradual reduction of 20 % of the $PtCl_2$ salt over the next 16 hrs though no noticeable change was recorded thereafter.

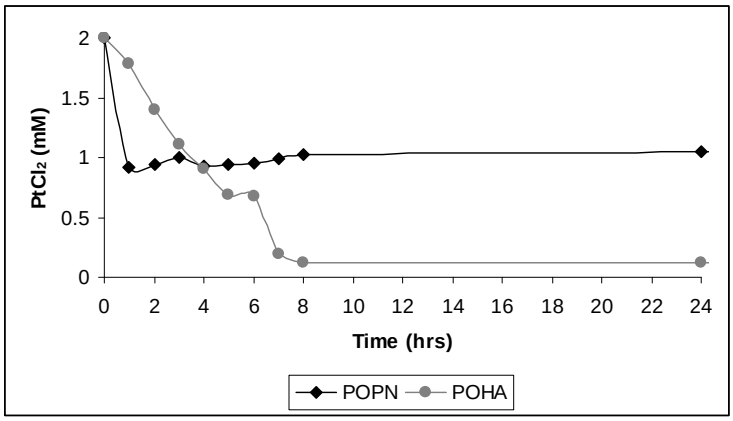

Figure 5. 3 Enzymatic reduction of $PtCl_2$ (2 mM) in the presence of purified hydrogenase during optimal conditions for platinum nanoparticle formation (POPN) and hydrogenase activity (POHA).

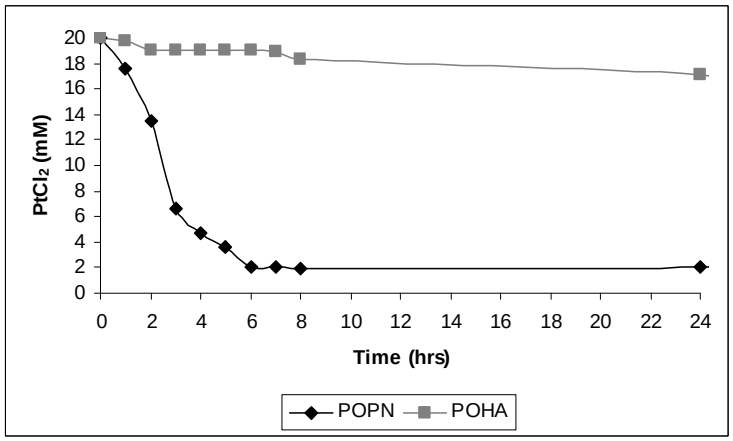

Figure 5. 4 Enzymatic reduction of $PtCl_2$ (20 mM) in the presence of purified hydrogenase during optimal conditions for platinum nanoparticle formation (POPN) and hydrogenase activity (POHA).

Any reduction process resulting in the formation of nanoparticles has to be efficient and cost effective. From the results (Figure 5.1-5.4) the maximum reduction of the platinum salts appears to occur during the first eight hours of the reduction processes. The results indicate that a pH 9 and temperature 65 °C appears to be optimal for H_2PtCl_6 reduction and subsequent platinum nanoparticle synthesis (Figure 5.5 A), however with $PtCl_2$ the results obtained were different. With a low initial $PtCl_2$ concentration (2 mM) optimal conditions are pH 7.5 and temperature 38 °C, and with a high initial concentration (20 mM) POPN were favoured (Figure 5.5 B).

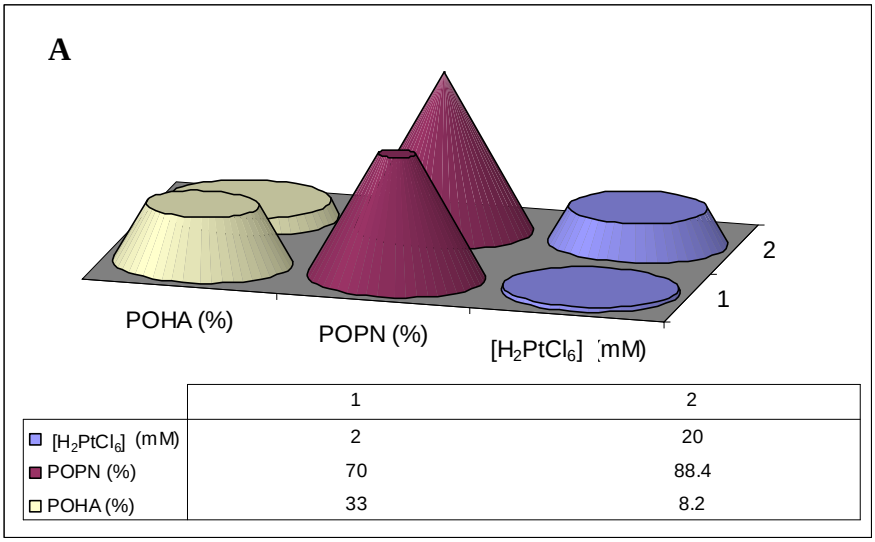

	1	2
$[H_2PtCl_6]$ (mM)	2	20
POPN (%)	70	88.4
POHA (%)	33	8.2

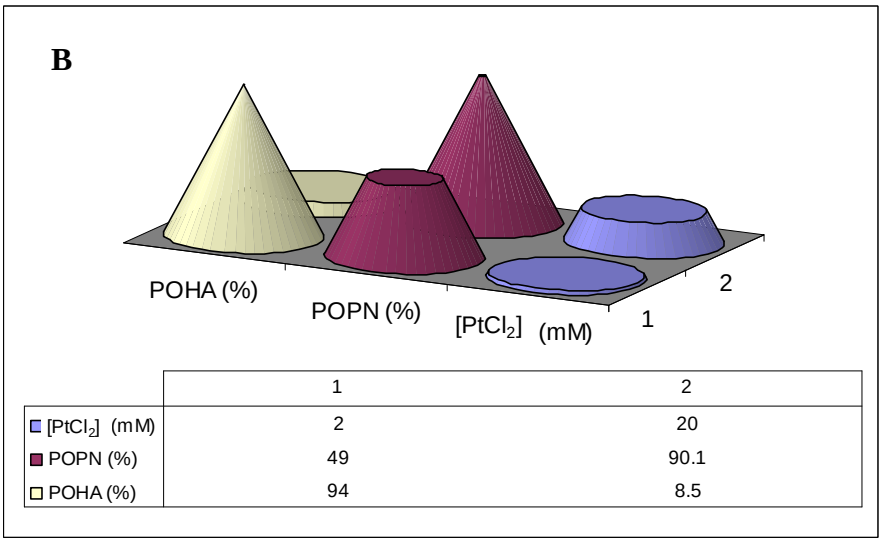

	1	2
$[PtCl_2]$ (mM)	2	20
POPN (%)	49	90.1
POHA (%)	94	8.5

Figure 5. 5 (A) H_2PtCl_6 and (B) $PtCl_2$ reduction (%) during the first eight hours of the bioreduction process with parameters optimal for platinum nanoparticle formation (POPN) and parameters optimal for hydrogenase activity (POHA).

It appears as though the hydrogenase does not have to function at optimum in order to reduce the platinum salts to produce nanoparticles. The results indicate that the combination of pH and temperature could be important in the ability of the hydrogenase to reduce the platinum salts. The results obtained using H_2PtCl_6 were different to the results obtained when a platinum (II) salt was used. H_2PtCl_6 has a 4^+ oxidation state, and the metal (Pt) centres adopt an octahedral geometry, thus forming a polymer wherein half of the chloride ligands bridge between the platinum atoms (Cotton, 1997). As a result of its polymeric structure H_2PtCl_6 dissolves only upon breaking of the chloride bonds.

Increased temperature and pH (POPN) could break these bonds and thus more platinum ions would be available for nanoparticle reduction. Studies have also suggested that the active sites of proteins maybe responsible for nanoparticle formation (Yoshimura, 2006). Thus the pH, temperature and metal ion concentration alters the orientation and possibly the interaction of the amino groups surrounding the active site of the hydrogenase resulting in reduction and nanoparticle formation (Riddin *et al.*, 2006).

5.2.2 Qualitative analysis of nanoparticles formation using transmission electron microscopy

5.2.2.1 Reduction of platinum (IV) (H_2PtCl_6)

With a low initial H_2PtCl_6 concentration (2 mM), varied irregular shaped and triangular nanoparticles were produced (Figure 5.6) with POPN. The larger nanoparticles produced were similar to other metallic nanoparticles synthesised where often referred to as nanoplates, and these were between 100-180 nm in size. The triangular particles were much smaller between 30-60 nm in size.

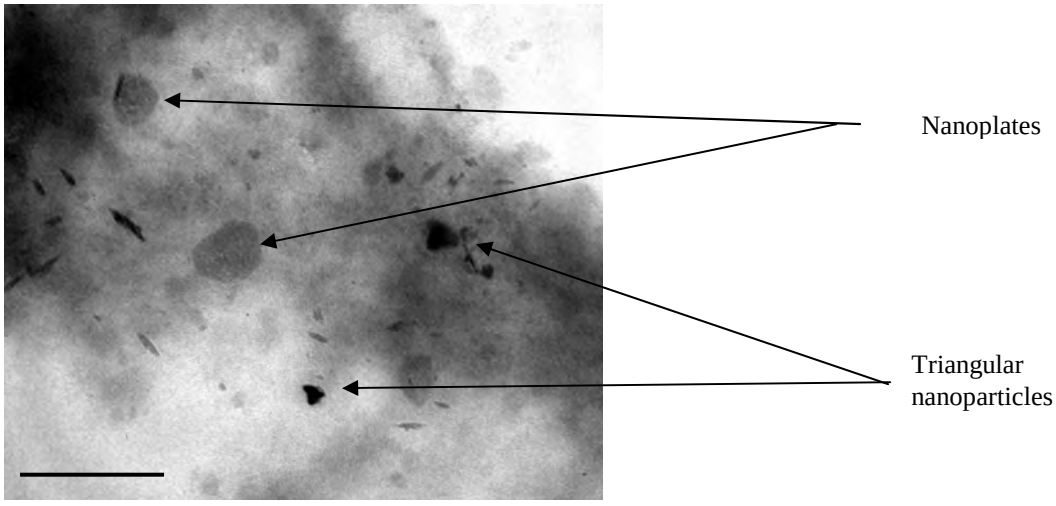

Figure 5. 6 Nanoplates and triangular nanoparticles produced after 24 hour incubation. Scale bar represents 250 nm, magnification = 60 000x

Besides nanoplates and triangular nanoparticles, particles in the shape of rods generally referred to as nano-rods 20 -100 nm in length and 10-25 nm in width were identified (Figure 5.7), and smaller spherical nanoparticles were produced (Figure 5.7).

The results indicate that in the presence of the enzyme under condition ideal for particle formation, the formation of the different shape and size nanoparticles was uncontrollable.

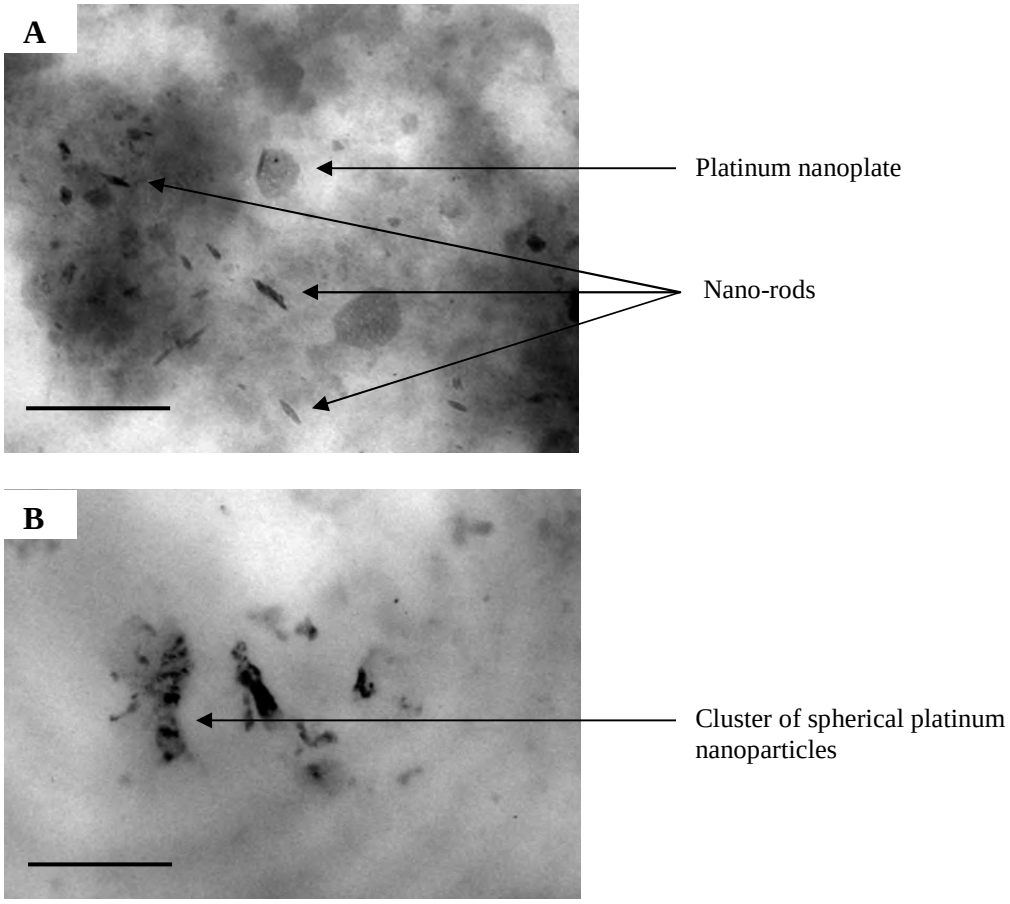

Figure 5. 7 Nanoparticles produced during the reduction of H_2PtCl_6 (2 mM) with POPN. (A) Platinum nano-rods (B) closely assembled spherical nanoparticles. All scale bars represent 500 nm, magnification = 50 000x (A) and 60 000x (B).

An excessive number of spherical nanoparticles were also produced (Figure 5.8 A). A histogram of nanoparticle size analysis of these nanoparticles indicated that the size distribution was between 100-180 nm, with very few nanoparticles larger than 180 nm (Figure 5.8 B). The vast majority of the spherical nanoparticles however were between the 70-180 nm with the mean nanoparticle size between 100-140 nm.

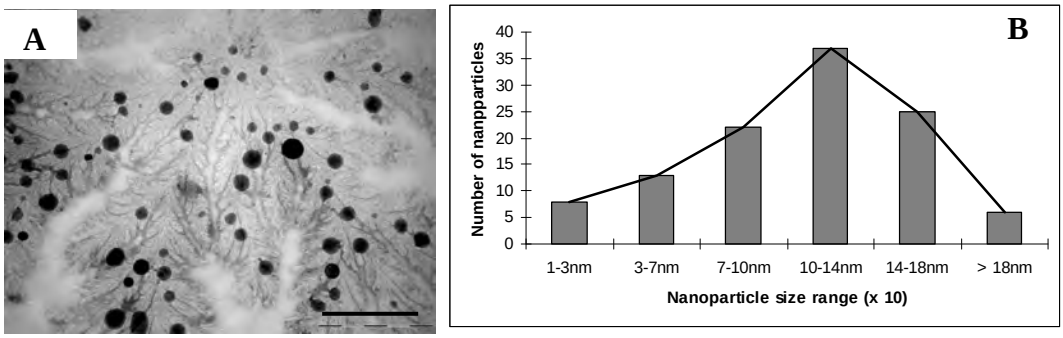

Figure 5. 8 (A) Spherical platinum nanoparticles produced during the reduction of H_2PtCI_6 (2 mM) with POPN. Scale bars represent 1000 nm, and magnification = 25 000x. (B) Histogram of platinum nanoparticle size analysis.

With POHA, triangular and irregular shaped nanoparticles were clearly identified (Figure 5.9), although the former nanoparticles produced were larger and not as widely dispersed. The irregular shaped nanoparticles seemed to be caught in the midst of a specific shape formation such as triangles and squares (Figure 5.9 A), indicating that the platinum nanoparticles had not fully nucleated.

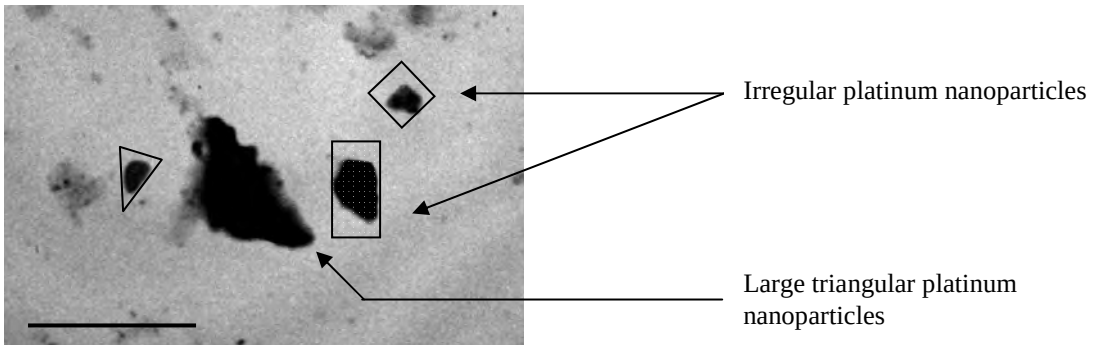

Figure 5. 9 Triangular and irregular platinum nanoparticles produced during the reduction of H_2PtCI_6 (2 mM) during POHA, magnification = 10 000x and the scale bar represents 2000 nm.

In comparison to a previous study the vast majority of particles formed were nanorods (Figure 5.10). The platinum nanoparticles were self assembled in a lattice formation (Figure 5.10 B), with small circular nanoparticles found between the lattices. The nano-rods produced during this study were similar to those platinum nanorods produced using vitamin B (Nadagouda and Varma, 2006).

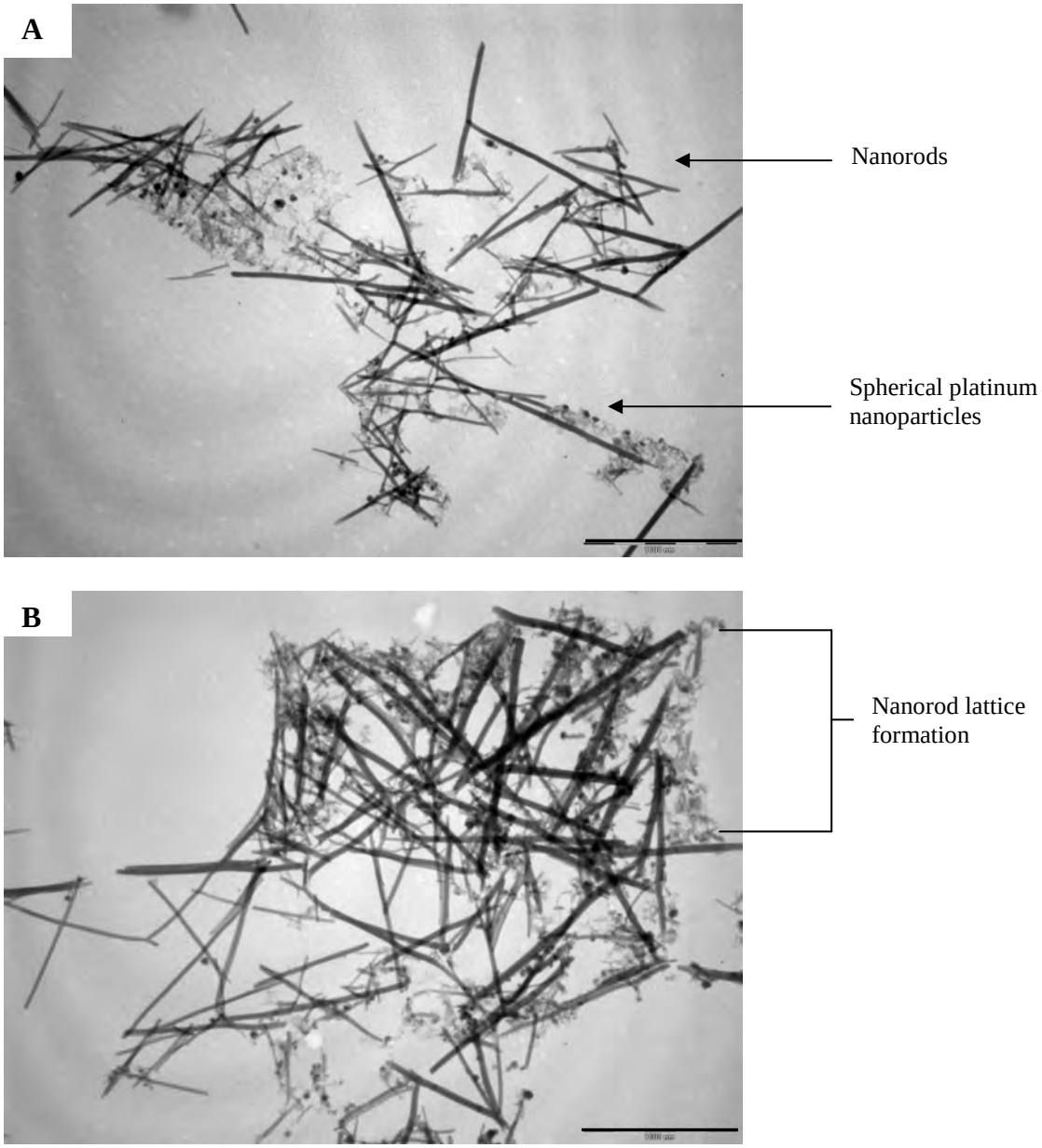

Figure 5. 10 (A) Platinum nanorods produced during the reduction of H_2PtCl_6 (2 mM) at conditions optimal for hydrogenase activity (POHA). (B) Nanorods assembled in a lattice-like formation. All scale bars represent 1000 nm and magnifications = 25 000x.

The nanoparticles produced during the reduction of H_2PtCI_6 (20 mM) with POPN also resulted in the synthesis of a mixture of triangular and square platinum nanoparticles (80-100 nm) and nanoplates between 200 -500 nm in size (Figure 5.11 A). These nanoplates appeared to be stacked close to each other or on top of each other and where much larger than those produced using the 2 mM H_2PtCI_6. The observed stacking of nanoplates could occur as a result of an overlap in nucleation times and subsequent attachment of the nanoparticles particles resulting in aggregation.

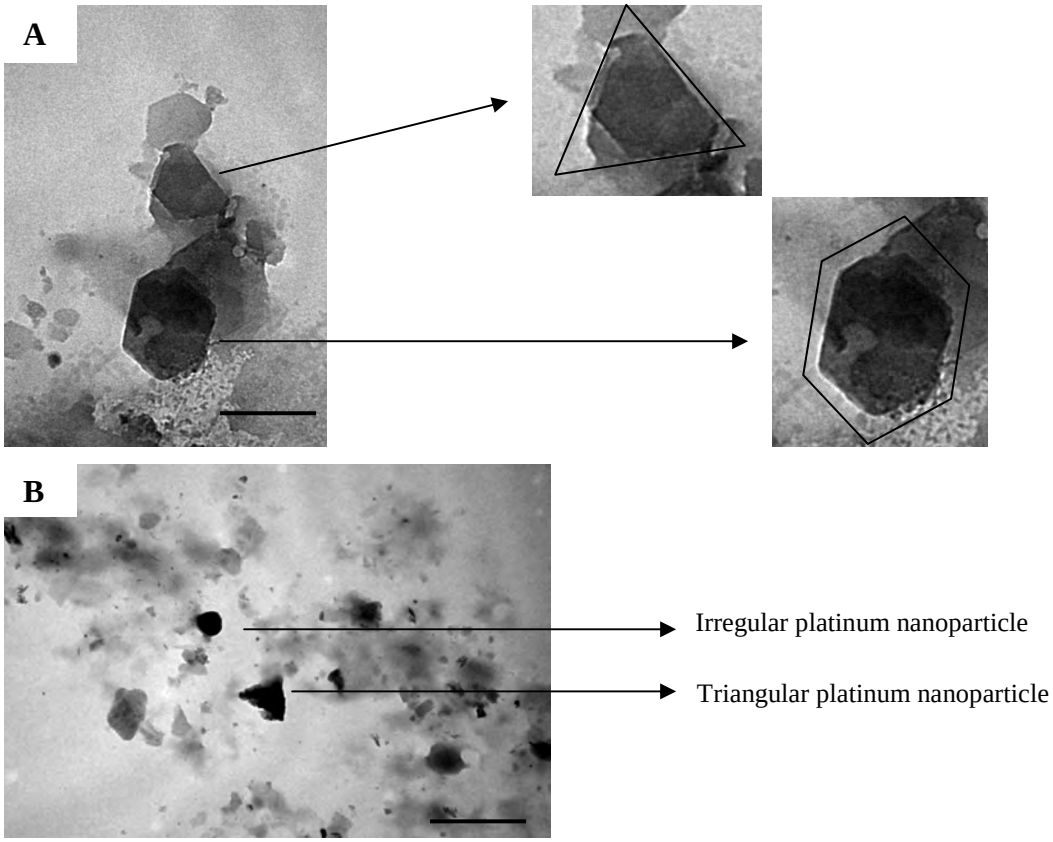

Figure 5. 11 (A) Platinum nanoplates and (B) triangular and irregular shaped platinum nanoparticles produced during the reduction of H_2PtCl_6 (20 mM) during parameters optimal for platinum nanoparticle formation (POPN). All scale bars represent 1000nm and magnifications = 80 000x.

As hypothesised earlier if the nanoparticle is synthesised in the active site of the enzyme, which acts as a template, all nanoparticles should be uniform in shape and size. However other smaller triangular nanoparticles were also formed as well as other irregular shaped nanoparticles (Figure 5.11 B). Nanoparticles resembling quantum dots were also synthesised (Figure 5.12 A), and the histogram representing the size distribution of these quantum dot like structures were between 1-90 nm, with the mean nanoparticle size between 40-50 nm (Figure 5.12 B)

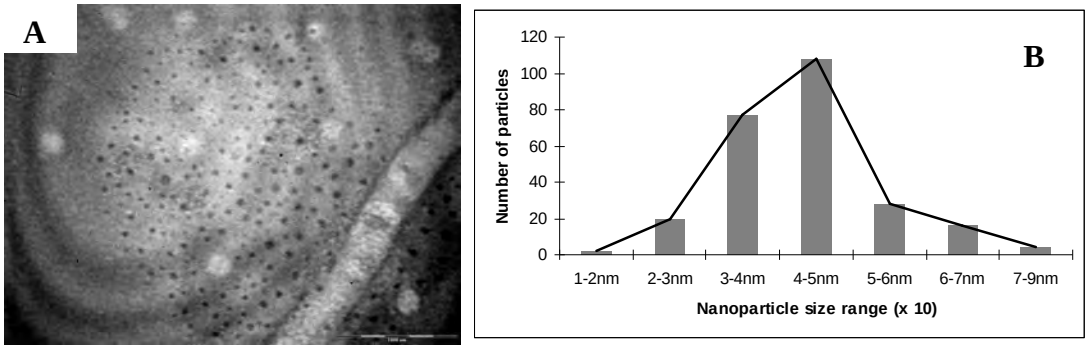

Figure 5. 12 Platinum quantum dots produced during the reduction of H_2PtCI_6 (20 mM) using parameters optimal for platinum nanoparticle formation (POPN). Scale bars = 1000 nm, and magnification = 100 000x. (C) Histogram of platinum nanoparticle size analysis.

The platinum nanoparticles produced during the reduction of H_2PtCI_6 (20 mM) with POHA were similar to those particles discussed earlier, with triangular (70 – 120 nm) and irregular shaped nanoparticles produced (Figure 5.13 A, B). Particles were closely associated to each other sometimes lying on top of each other (Figure 5.13 A) whilst other irregular shaped nanoparticles were more monodisperse and not closely associated to each other (Figure 5.13 B).

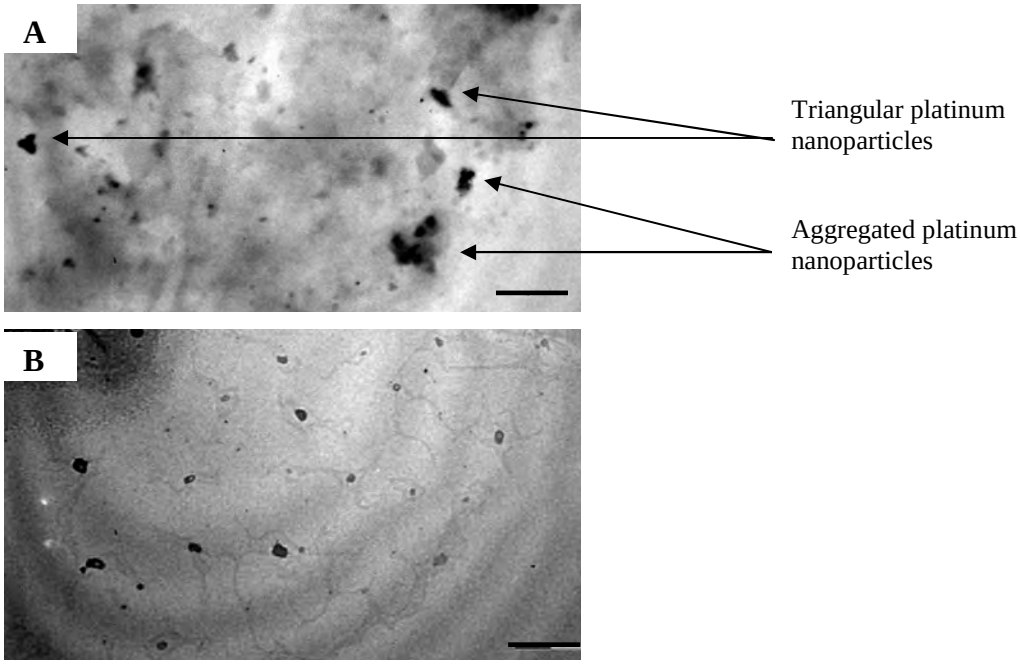

Figure 5. 13 Platinum nanoparticles produced during the reduction of H_2PtCI_6 (20 mM) during parameters optimal for hydrogenase activity (POHA). (A) Triangular and aggregated irregular shaped nanoparticles, magnification = 60 000x. (B) Monodisperse nanoparticles, magnification = 50 000x. All scale bars represent 1000 nm.

A number of spherical particles were also found (Figure 5.14 A). These nanospheres were monodisperse and not closely associated with each other. The histogram representing the nanosphere size range indicates that the nanoparticles were dispersed over a broad size range from 10- 100 nm (Figure 5.14 B), with the majority of the particles were between the size range of 30–60 nm and the mean particle size around 50-60 nm.

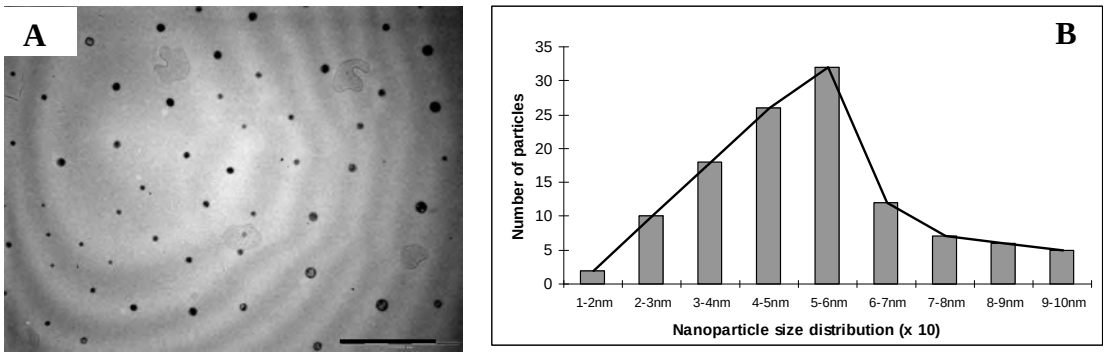

Figure 5. 14 (A) Platinum nanospheres produced during the reduction of H_2PtCI_6 (20 mM) during conditions optimal for hydrogenase activity (POHA). Scale bar represents 1000 nm and magnification = 10 000x. (B) Histogram illustrating the nanosphere size range.

5.2.2.2 The reduction of platinum (II) chloride ($PtCI_2$)

The bioreduction of $PtCI_2$ (2 mM) produced nanoparticles that were distinctly different to those produced from H_2PtCI_6 (2 mM) with POPN (pH 9; 65°C). The nanoparticles produced were much larger with the majority of nanoparticles being rectangular and triangular in shape (Figure 5.15). The nanoparticles were aggregated and thus it was very difficult to distinguish one shape from the other. It appears as though there was some extrapolymeric substance ("factor") coats the nanoparticles keeping them closely attached to each other. Thus although nanoparticle were produced they were not mono-dispersed. Nanorods (1000 -2000 nm) were also formed and appeared similar to those produced during the reduction of H_2PtCI_6 (Figure 5.10), though the nano-rods produced by $PtCI_2$ (Figure 5.16) were not assembled in any kind of lattice formation. Nanorods and nano-lattices were produced by H_2PtCI_6 at conditions optimal for enzyme activity (pH 7.5 38 °C), however the nanorods produced using $PtCI_2$ were obtained at conditions optimal for nanoparticle formation (pH 9; 65°C). These results indicate that in addition to pH and temperature, the oxidation state of the platinum salt also plays a role.

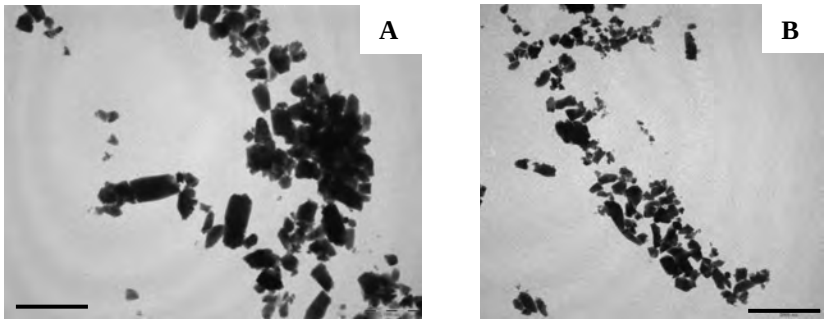

Figure 5. 15 (A and B) Platinum nanoparticles produced during the reduction of $PtCl_2$ (2 mM) during conditions optimal for particle formation (POPN). (A) Magnification = 15 000x and scale bar represents 1000 nm. (B) Magnification = 8 000x and scale bar represents 2000 nm.

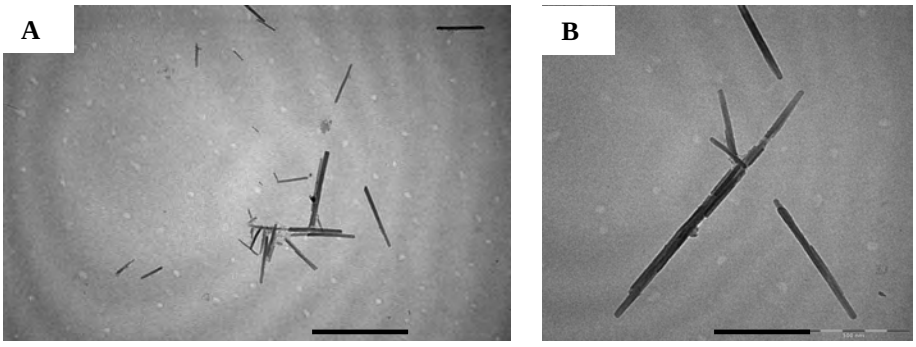

Figure 5. 16 (A and B) Nano-rods produced during the reduction of $PtCI_2$ (2 mM) during conditions optimal for particle formation (POPN). (A) Magnification = 30 000x and scale bar represents 1000 nm. (B) Magnification = 60 000x and scale bar represents 500 nm.

Although over 90 % of $PtCl_2$ (2 mM) was reduced using the purified hydrogenase with POHA, the nanoparticles was not as defined as those produced with POPN. The nanoparticles were closely associated to the extracellular polymeric material ("factor") and many of the nanoparticles could not be clearly seen. Larger triangular nanoplates were formed (Figure 5.17 A) comparable to those produced during the reduction of H_2PtCI_6 (Figure 5.6), with irregular smaller nanoparticles also produced (Figure 5.17 B).

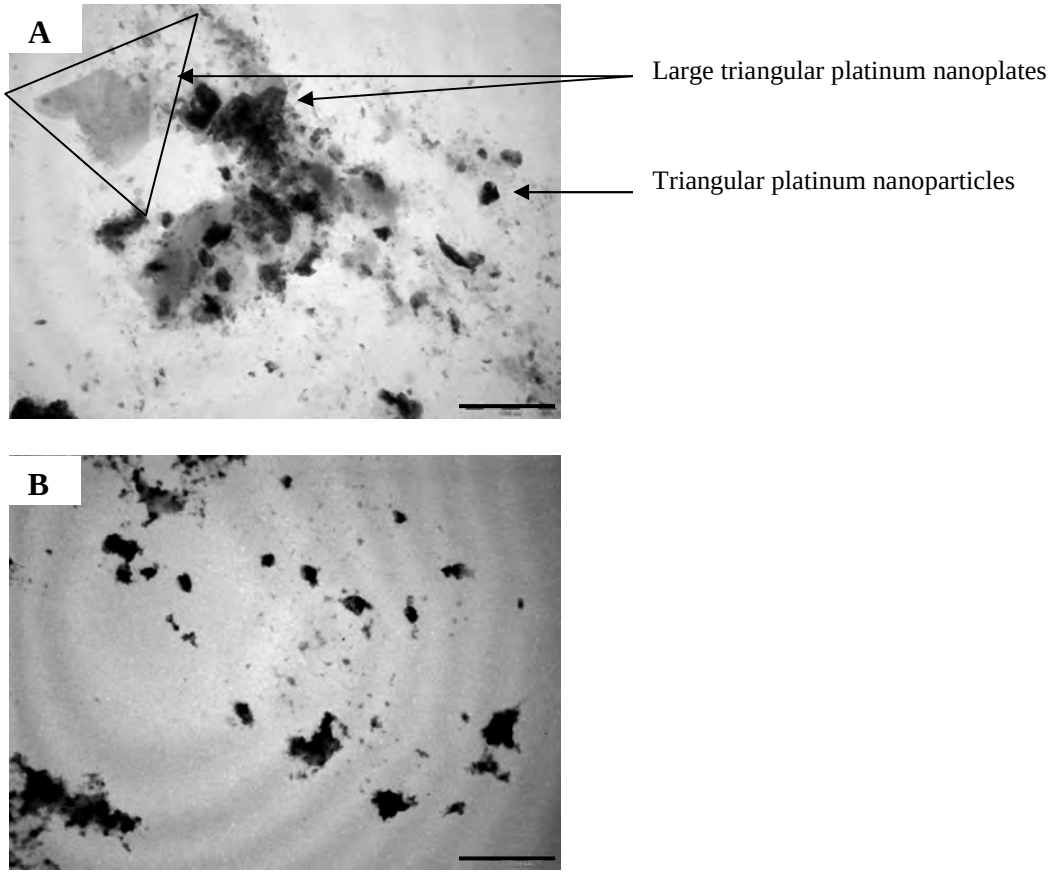

Figure 5. 17 (A) Platinum nanoplates and smaller undefined nanoparticles and (B) irregular platinum nanoparticles produced during the reduction of $PtCI_2$ during conditions optimal for hydrogenase activity (POHA). (A) Magnification = 20 000x and scale bar represents 1000 nm. (B) Magnification = 15 000x and scale bar represents 1000 nm.

With the higher concentration of $PtCl_2$ (20 mM) a large number of irregular platinum nanoparticles were formed during POPN (Figure 5.18). It was difficult to clearly identify what shape these nanoparticles were, however the majority of them were in the smaller nanoparticle range between 50-100 nm. Although irregular nanoparticles were identified other clearly defined nanoparticles were also identified. Triangular, spherical and square nanoparticles of varying size were produced during conditions optimal for platinum nanoparticle (POPN) (Figure 5.19). The large triangular nanoparticles (80 -110 nm) were surrounded by smaller spherical (15- 50 nm) and other irregular shaped nanoparticles (50-65 nm), indicating that the mechanism of nanoparticle formation had no control on the size or the shape of the platinum nanoparticles.

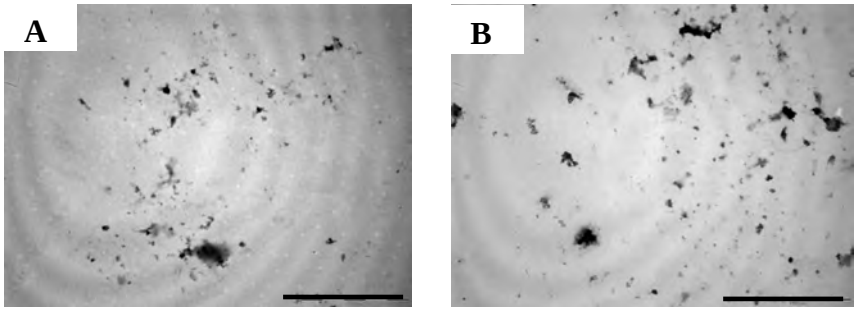

Figure 5. 18 Irregular shaped nanoparticles produced during the reduction of $PtCI_2$ (20 mM) during conditions optimal for platinum nanoparticle formation (POPN). (A) Magnification = 15 000x, (B) magnification = 25 000x. All scale bars represent 1000 nm.

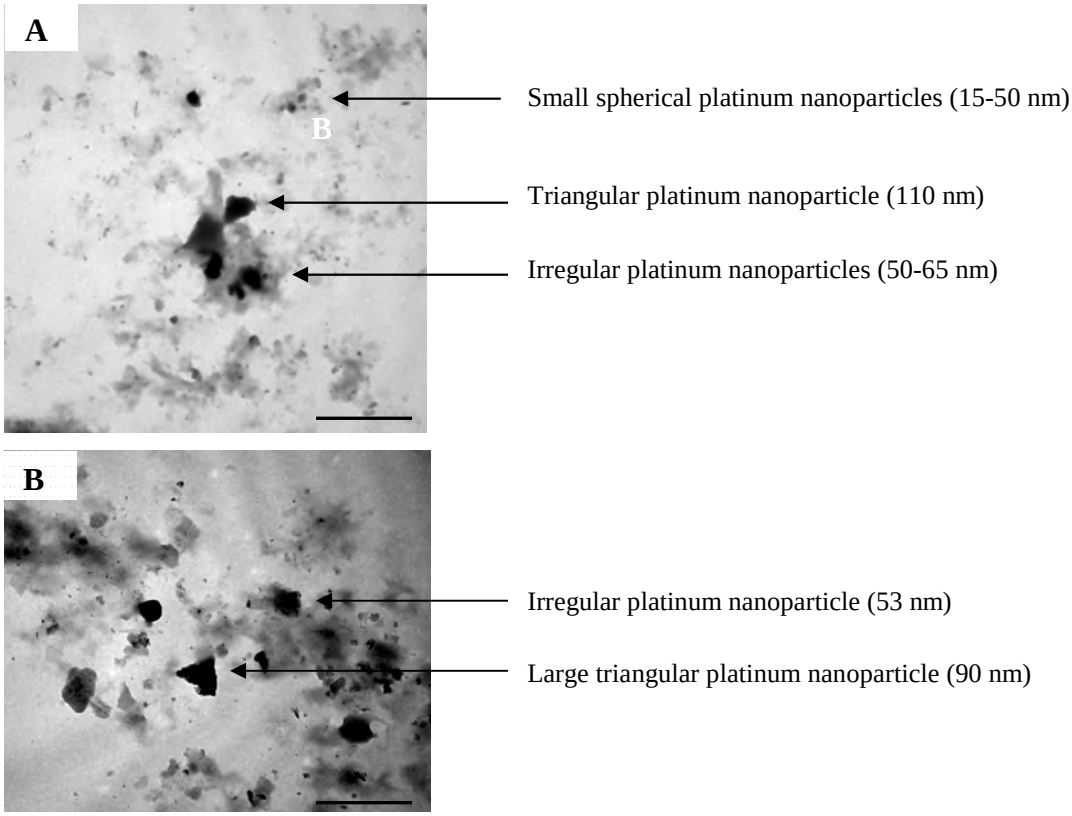

Figure 5. 19 Platinum nanoparticles produced during the reduction of $PtCI_2$ (20 mM) during conditions optimal for platinum nanoparticle formation (POPN) (A) Magnification = 10 000x, (B) magnification = 30 000x. All scale bars represent 200 nm.

The spherical nanoparticles (Figure 5.20 A) produced, were all in the range of 60 -100 nm and thus were the largest spherical nanoparticles produced during the entire study. The square nanoparticles were not distributed widely and only a few were identified with all of them in the 40-60 nm size range. (Figure 5.20 B).

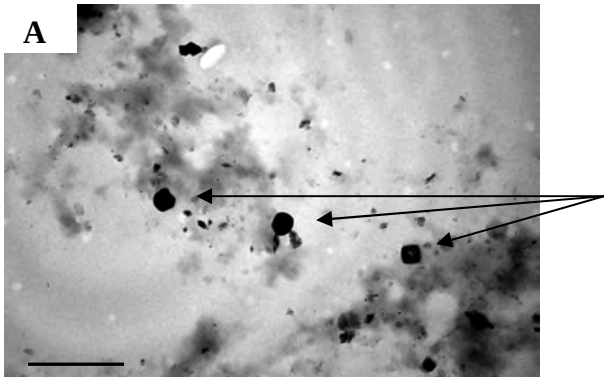

Spherical platinum nanoparticles (60-100 nm).

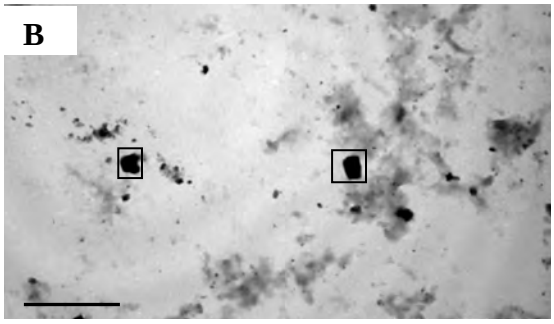

Figure 5. 20 Platinum nanoparticles produced during the reduction of $PtCI_2$ (20 mM) during conditions optimal for nanoparticle formation (POPN). (A) Spherical platinum nanoparticles magnification = 30 000x. (B) Square nanoparticles produced, magnification = 16 000x. All scale bars represent 1000 nm.

Unlike the other studies, the reduction of $PtCI_2$ (20 mM) with POHA produced only two types of nanoparticles (nanospheres and triangles). There were a greater majority of nanospheres formed with only a few triangles been identified. The nanospheres were monodisperse and uniformly shaped (Figure 5.21), whilst the triangles had distinct shape edges (Figure 5.22).

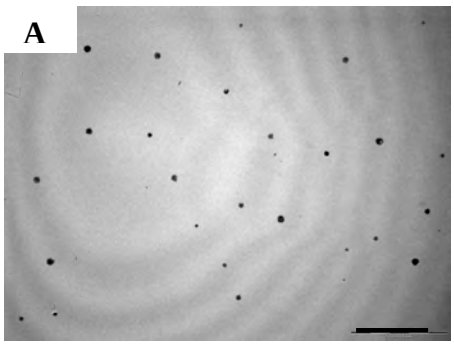

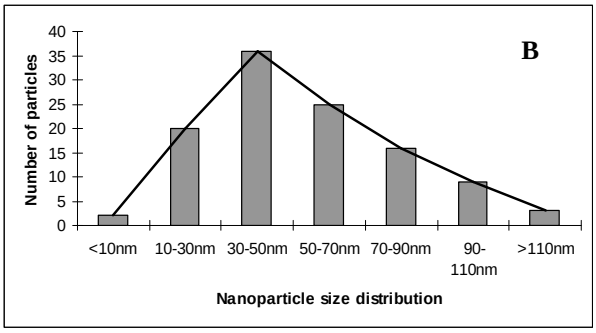

Figure 5. 21 (A) Spherical platinum nanospheres produced during the reduction of $PtCI_2$ (20 mM) during conditions optimal for hydrogenase activity (POHA), scale bar = 1 000 nm, magnification = 8 000x. (B) Histogram showing the size distribution of the nanospheres.

The histogram of the platinum nanospheres (Figure 5.21B) shows that there is a uniform distribution even though they were not mono-sized and particles were between 1-110 nm in size. The majority of the nanospheres were sized between 10-70 nm with the mean between 30-50nm. The triangular nanoparticles on the other hand appeared much larger between 100-150 nm (Figure 5.22). These results are unusual since a mixture of nanoparticle shape and sizes were produced with POPN, however with POHA only two types of particles were produced, indicating that the combination of pH and temperature is important in nanoparticle formation.

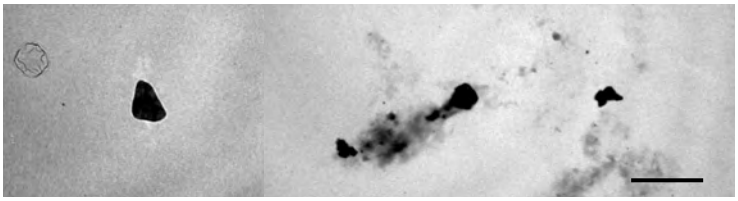

Figure 5. 22 Triangular platinum nanoparticles produced during the reduction of $PtCI_2$ (20 mM) during conditions optimal for hydrogenase activity (POHA). Scale bar = 1000 nm and magnifications = 20 000x.

5.3 Summary and General Discussion

Previous studies have shown that hydrogenases from *Ralstonia eutropha* (Da Silva *et al*., 2002) *Thiocapsa rosepersicina* (Nedoluzhko *et al*., 2000) have been demonstrated to reduce metal ions to produce nanoparticles. In the present work it was demonstrated that the Ni-Fe hydrogenase from *F.oxysporum* is capable of reducing platinum salts to produce nanoparticles. Zadvorny *et al*. (2006) suggested a direct electron transfer between metal/metal ions and the enzyme as a possible mechanism for the isolated hydrogenases to carry out redox transformations of metals.

A new type of technology has been described (Yoshimura, 2006), where the metal ions are reduced in the active sites of enzymes that catalyse their reduction. In nature, biological enzymes operate with very high selectivity. In the active site of an enzyme chemical transformation such as bond breaking and forming takes place, (Kung and Kung, 2004). Thus nanoparticle growth process is thought to occur in the protective environment of the enzyme active site, which could provide control over the nanoparticle size. What distinguishes enzymes is the environment of the active site, as often the active site is in a cavity formed by the protein.

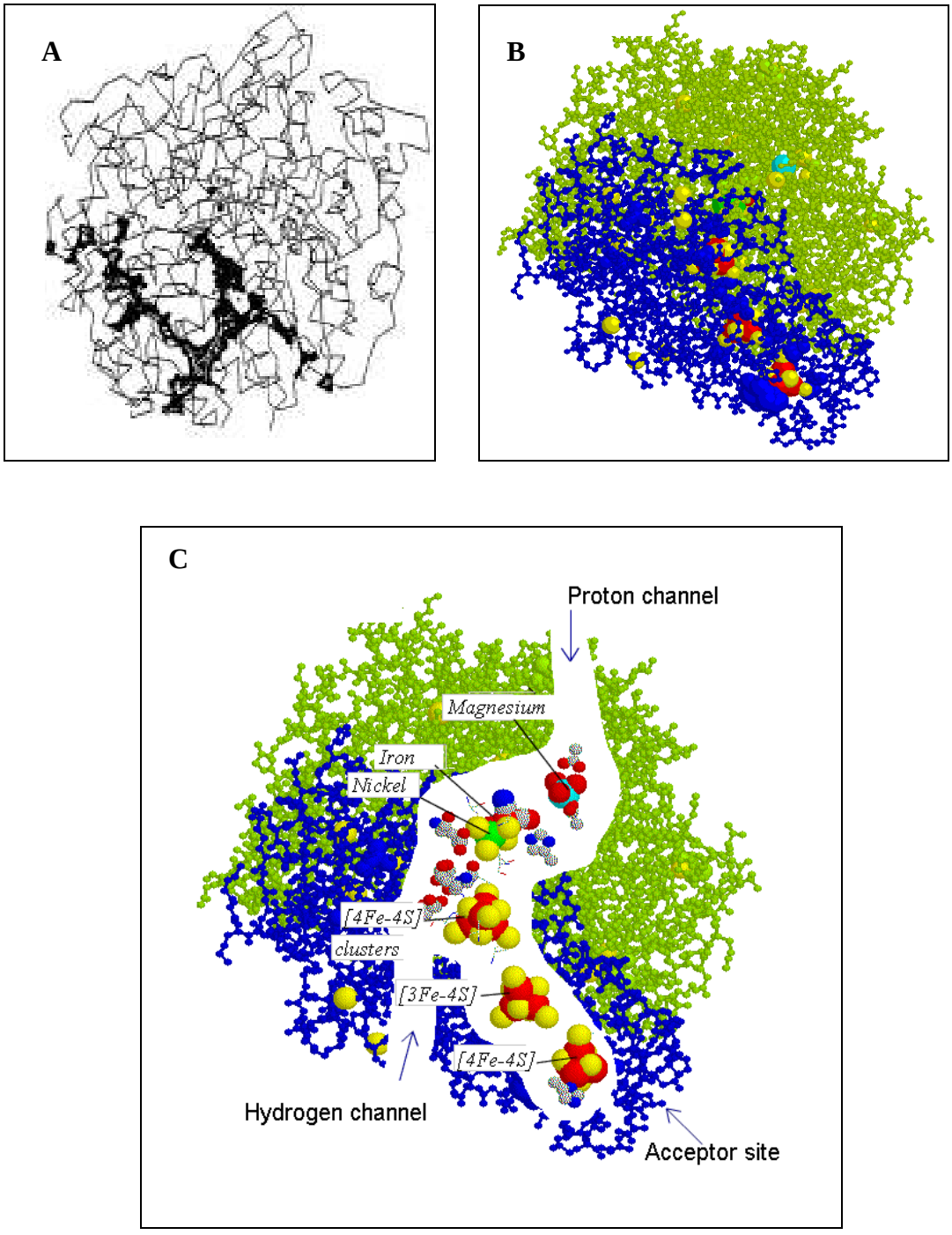

Figure 5. 23 Model of the Ni-Fe hydrogenase isolated from *Desulfovibrio gigas*. (A) Cavity map of *D. gigas* hydrogenase (Adapted from Montet *et al.*, 1998). (B and C) Identification of channels within the hydrogenase (Adapted from Cammack, 2007).

Previous studies elucidated transfer pathways between the active site and the molecular surface and a cavity map was calculated from the model of *Desulfovibrio gigas Ni-Fe* hydrogenase (Figure 5.23 A) (Montet *et al.,* 1998).

These results illustrated a network of hydrophobic channels whose shape roughly resembles the letter V and connected through their right and left sides, respectively (Figure 5.23 A). Those channels starting at the interface between the small and the large subunit of hydrogenase and extend from the bottom of the V motif to the protein surface (Figure 5.23 A) The left arm of the V is surrounded entirely by residues of the large subunit and the right is located in the N-terminal domain of the small subunit, provides another possible access to the active site (Figure 5.23 B, C) From this analysis, it appears that there are several putative entrance sites for gas diffusion connected by different channels to a unique entrance to the active site. These channels could serve as a passage way for metal ions, although the diameter of these channels is about 4.5 - 6 Å (0.45 – 0.60 nm). Along the wall of the cavity are functional groups that would help bind the reactant (platinum salt) and the product (nanoparticle). One of the most interesting and probably critical characteristic is that the enzyme is flexible (Eisenmeser *et al.,* 2002), such that the cavity, the active site, and the binding sites move during the course of the reaction to accommodate the addition and release of the reacting species. Thus in the synthesis of nanoparticles, it would be desirable to have complete control over the reactivity of the active site, the environment around the active site, the binding sites and their locations relative to the active site, and the path to access these functionalities (Kung and Kung, 2004). Complete control is required thereafter from the atomic scale to thousands of nanometre scale. Defining and controlling the active site is inadequate to afford complete control of nanoparticle formation as when using an enzyme the environment around the active site plays a critical role. The physiological role of metal oxidation and metal ions reduction is still unknown, though it could be related to general metal detoxification. Thus this type of hydrogenase could be considered as a new type of metal oxido-reductase, of valuable practical significance in nanoparticle synthesis.

GENERAL DISCUSSION AND CONCLUSION

The ability of microorganisms to reduce inorganic metals has opened up a new exciting green chemistry approach towards the development of natural "nano-factories". The elucidation of biochemical pathways leading to metal ion reduction and information of nanoparticles is essential in order to develop a bio-based nanoparticle synthesis method. In light of this on-going research, the current study investigated the "factors" in the fungus *Fusarium oxysporum* which were responsible for platinum nanoparticle formation. Therefore the thesis gives an account of

i. The intercellular biosynthesis of platinum nanoparticles using *F.oxysporum* biomass
ii. The extracellular synthesis of platinum nanoparticles
iii. Isolation and purification of one of the enzymatic "factors" responsible for platinum nanoparticle formation
iv. Using the purified "factor" to reduce platinum salts during various conditions to synthesis platinum nanoparticles.

Chapter 1 presents a general introduction about nanoscience, nanotechnology and their consequences in different fields of science. The different synthesis routes of nanomaterials were discussed. Based on a literature survey, the scope, objectives and aim of the present study were summarised at the end of the chapter.

Chapter 2 deals with the intercellular biosynthesis of platinum nanoparticles using *F. oxysporum*. The fungal biomass was exposed to the platinum salt and the initial response to the platinum salts was metal internalisation and subsequent reduction of H_2PtCI_6 to produce platinum nanoparticles. Changes in the morphology of the fungal cells were observed as a result of platinum chloride uptake and the observed localisation and distribution of platinum precipitates provided some evidence for a hydrogenase mediated bioreduction (Rashamuse and Whiteley, 2007) of platinum salts to produce nanoparticles. It is important that these nanoparticles are harvested from within the fungal biomass therefore it would be more practical if the metal ions exposed to the fungus could be produced outside the fungal biomass, leading to the formation of platinum nanoparticles in solution.

Chapter 3 investigated the possibility of producing platinum nanoparticles extracellulary. Factors secreted by the fungus into the extracellular fluids, were shown to be responsible for platinum nanoparticle formation. However the exact mechanism responsible for extracellular platinum nanoparticle formation is not clearly understood although, literature has indicated that biomolecules in nanobiotechnology using biological methods to synthesis nanoparticles (Mandal *et al*., 2001; Selvakannan *et al*., 2003; Gole *et al*., 2001a; Gole *et al*., 2001b; Gole *et al*., 2002) are hypothesised to be responsible for nanoparticle formation.

Chapter 4 investigated the enzymatic "factors" responsible for platinum nanoparticle formation. From the identification, purification and characterization studies it was concluded that more than one protein was responsible for platinum nanoparticle formation in *F.oxysporum*. Further purification of one of these enzymatic "factors" indicated that it was a hydrogenase enzyme. This enzyme was found to have 2 subunits of 29.4 and 44.5 kDa, which is in the same magnitude as Ni-Fe hydrogenases previously purified (Nicolet *et al*., 2000). The characterisation studies indicated that the purified hydrogenase had an optimal temperature and pH of 38 °C and 7.5 respectively, with a poor thermal stability over time with a $t_{1/2}$ = 36 minutes. During kinetic studies V_{max} and K_m were determined to be 3.16 $nmolmin^{-1}ml^{-1}$ and 3.64 mM respectively, with the hydrogenase expressing a higher affinity for H_2PtCI_6 than the methyl viologen substrate. The purified hydrogenase was used in subsequent experiments for the reduction of higher concentration platinum salts to produce nanoparticles under various experimental conditions.

Chapter 5: In this chapter the purified hydrogenase was exposed to platinum salts (H_2PtCl_6 and $PtCl_2$) with parameters optimal for platinum nanoparticle formation (POPN) and parameters optimal for hydrogenase activity (POHA). Various shape and sized platinum nanoparticles were synthesised during the various experimental treatments. The various combinations of platinum salt concentration, temperature and pH influenced the reduction of the salts and the results surprisingly indicated that conditions unfavourable for hydrogenase activity (POPN) were optimal for nanoparticle synthesis.

Future work involves:

a) Isolation, purification and identification of the other “factors” in *F.oxysporum* responsible for platinum nanoparticle formation.

b) Understanding the role and mechanism of the active site in nanoparticle synthesis

c) Synthesising a template using molecular imprinting to mimic the active site of the hydrogenase

d) Use of the template to produce platinum nanoparticle of a predefined shape and size.

e) Development of a method to quantify platinum nanoparticle formation.

REFERENCES

Ahmad, A., Mukherjee, P., Mandal, D., Senapati, S., Khan, M.I., Kumar, R. and Sastry, M. (2002) Enzyme mediated extracellular synthesis of CdS nanoparticles by the fungus *Fusarium oxysporum*. *Journal of American Chemical Society* **124**:12108-12109

Ahmad, A., Mukherjee, P., Senepati, S., Mandal, D., Khan, M.I., Kumar, R. and Sastry, M. (2003a). Extracellular biosynthesis of silver nanoparticles using the fungus *Fusarium oxysporum*. *Colloids and Surfaces B: Biointerfaces* **28**: 313-318

Ahmad, A., Senepati, S., Khan, M.I., Kumar, R. and Sastry, M. (2003b). Extracellular biosynthesis of monodisperse gold nanoparticles by a novel extremophilic actinomycete, *Thermomonospora* sp. *Langmuir* **19**: 3550-3553

Ahmad, A., Senepati, S., Khan, M.I., Kumar, R. and Sastry, M. (2005). Extra-/Intracellular biosynthesis of gold nanoparticles by an alkalotolerant fungus, *Tricothecium* sp. *Journal of Biomedical Nanotechnology* **1**: 47-53

Ahmad, A., Senepati, S., Khan, M.I., Kumar, R., Ramani, R., Srinivas, V and Sastry, M. (2003c). Intracellular synthesis of gold nanoparticle by a novel alkalotolerant actinomycete, *Rhodococcus* species. *Nanotechnology* **14**:824-828

Albracht, S.P.J. (1994). Nickel hydrogenases: in search of the active site. *Biochimica et Biophysica acta* **1188**:167-204

Alm, E. (2003). Implications of microbial heavy metal tolerance in the environment, *Reviews in Undergraduate Research* **2**:1-6

Armstrong, F.A. (2004). Hydrogenases: active site puzzles and progress. *Current Opinion in Chemical Biology* **8**:133-140

Bansal, V., Rautaray, D., Ahmad, A and Sastry, M. (2005). Biosynthesis of zirconia nanoparticles using the fungus *Fusarium oxysporum*. *Journal of Materials Chemistry* **14**:3303-3305

Beard, S.J., Hashim, R., Hernandez, J., Hughes, M. and Poole, R.K. (1997). Zinc (II) tolerance in *Escherichia coli* K-12: evidence that the *zntA* gene (*o732*) encodes a cation transport ATPase. *Molecular Biology* **25**:883-891

Beveridge, T.J. and Murray, R.G.E. (1980). Sites of metal deposition in the cell wall of *Bacillus subtilis*. *Journal of Bacteriology* **141**: 876–887.

Bhainsa, K.C. and D'Souza, S.F. (2006). Extracellular biosynthesis of silver nanoparticles using the fungus *Aspergillus fumigatus*. *Colloids and Surfaces B: Biointerfaces* **47**: 160-164

Bhat, J.S.A. (2003). Heralding a new future – Nanotechnology. *Current Science* **85**: 147-154.

Bhattacharya, D and Gupta, R.K. (2005). Nanotechnology and potential of microorganisms. *Critical Reviews in Biotechnology* **25**: 199-204

Bozzola, J.J. and Russell, L.D. (1999). Electron microscopy: principles and techniques for biologists. Jones and Bartlett publishers. Second edition. Pgs 1-18. Boston, USA

Braun, M., Burda, C., and El-Sayed, M.A. (2001). Variation of the Thickness and Number of Wells in the CdS/HgS/CdS Quantum Dot Quantum Well System. *Journal of Physical Chemistry A* **105**: 5548-5551.

Bruchez Jr., Moronne, M.M., Gin, P., Weiss, S. and Alivisatos, A.P. (1998). Semiconductor Nanocrystals as Fluorescent Biological Labels. *Science* **281**: 2013-2016

Bruins, M.R., Kapil, S and Oehme, F.W. (2000). Microbial resistance to metals in the environment. *Ecotoxicology and Environmental Safety* **45**:198-207.

Brust, M and Kiely, C.J. (2002). Some Recent Advances In Nanostructure Preparation From Gold and Silver Particles: A Short Topical Review. *Journal of Colloids and Surfaces A* **202**: 175-186

Bryant RD, Laishley EJ (1990). The role of hydrogenase in anaerobic biocorrosion. *Canadian Journal of Microbiology* **36**:259–264

Cao, G. (2004). *Nanostructures* and Nanomaterials: Synthesis, Properties and Applications, Imperial College Press, London, 2004.

Cammack, R. (2007). Mechanism of nickel-iron hydrogenase. www.kcl.ac.uk/ip/richardcammack/H2/animation/movie1.html

Chan, W.C.W. and Nie, S. (1998). Quantum Dot Bioconjugates for Ultra sensitive No isotopic Detection. *Science* **281**: 2016-2018

Chen, S. and Kimura, K. (2001). Synthesis of Thiolate-Stabilized Platinum Nanoparticles in Protolytic Solvents as Isolable Colloids. *Journal of Physical Chemistry B* **105**: 5397 - 5403;

Chen, X., Lou, Y., Samia, A.C., and Burda, C (2003). Coherency Strain Effects on the Optical Response of Core/Shell Heteronanostructures. *Nanotechnology Letters* **3**: 799-803

Clark, J.M., and Switzer, R.L. (1977). Experimental Biochemistry. Second Edition, W.H.Freeman and Company, NY, USA. p82 – 83.

Clausen, K. (2001). Enzymatic degumming by a novel microbial phospholipase. *European Journal of Lipid Science and Technology* **103**:333-340.

Cotton, S.A. (1997). Chemistry of precious metals. Pgs (173-273). Chapman and Hall Publishers.

Da Silva S, Basseguy R, Bergel A (2002). The role of hydrogenases in the anaerobic microbiologically influenced corrosion of steels. *Bioelectrochemistry* **56**:77–79

Dameron, C.T., Reese, R.N., Mehra, R.K., Kortan, A.R., Carroll, P.J., Steigerwald, M.L., Brus, L.E. and Winge, D.R. (1989). Biosynthesis of cadmium sulphide quantum semiconductor crystallites *Nature* **338**: 596- 597

De Lacey A.L., Santamaria E., Hatchikian E.C., and Fernandez V.M., (2000). Kinetic characterization of *Desulfovibrio gigas* hydrogenase upon selective chemical modification of amino acid groups as a tool for structure-function relationships. *Biochimica et Biophysica Acta* **1481**: 371-380

De Luca G, de Philip P, Dermoun Z, Rousset M, Vermeglio A (2001). Reduction of technetium (VII) by *Desulfovibrio fructosovorans* is mediated by the nickel–iron hydrogenase. *Applied Environmental Microbiology* **67**:4583–4587

De Windt, D., Aelterman, P. and Verstraete, W. (2005). Bioreductive deposition of palladium (0) nanoparticles on *Shewanella oneidensis* with catalytic activity towards reductive dechlorination of polychlorinated biphenyls. *Environmental Microbiology* **7**:314-325

Dowling, A (2004). Nanoscience and nanotechnology: opportunities and uncertainties. A report by The Royal Society and The Royal Academy of Engineering, London.

Doyle, M.E. (2006) Nanotechnology: A brief literature review. Food research institute briefings. University of Wisconsin-Madison 1-10. www.wisc.edu/fri/

Duff, D.G., Edwards, P.P. and Johnson, B.F.G (1995). Formation of a Polymer-Protected Platinum Sol: A New Understanding of the Parameters Controlling Morphology. *Journal of Physical Chemistry* **99**:15934-15944

Duran, N., Marcato, P.D., Alves, O.L., de Souza, G.I.H. and Esposito, E. (2005). Mechanistic aspects of biosynthesis of silver nanoparticles by several *Fusarium oxysporum* strains. *Journal of Nanobiotechnology* **3**:8-14

Ehrlich, H.L. (1997). Microbes and metals. *Applied microbiology in biotechnology* **48**:687-692

Eisenmeser, E.Z., Bosco, D.A., Akke, M. and Kern, D. (2002). Enzyme dynamics during catalysis. *Science* **295**: 1520-1523

Elliot, S.J., Leger, C., Pershad, H.R., Hirst, J., Heffron, K., Ginet, N., Blasco, F., Rothery, R.A., Weiner, J.H. and Armstrong, F.A. (2002). Detection and interpretation of redox potential optima in the catalytic activity of enzymes. *Biochimica et Biophysica Acta* **1555**: 54-59

Emory, S.R. and Nie, S. (1998). Screening and Enrichment of Metal Nanoparticles with Novel Optical Properties. *Journal of Physical Chemistry B* **109**: 493-497

Erhardt, D (2003). materials conservation: not-so-new technology. *Nature Materials* **2**: 509-510

Engel, A. and Colliex, C (1993). Application of scanning transmission electron microscopy to the study of biological structure. *Current Opinion in Biotechnology* **4**: 403-411

Fendler, J.H. (1998). Nanoparticles and nanostructured films: preparation characterisation and applications. John Wiley and Son.

Fendler, J.H. and Meldrum, F.C. (2004). The colloidal chemical approach to nanostructured materials. *Advanced materials* **7**: 607- 632

Gadd, G.M. (1993). Tansley Review No. 47 Interactions of fungi with toxic metals. *New Phytologist* **124**:25-60

Gao, M., Rogach, A.L., Kornowski, A., Kirstein, S., Eychmuller, A, Mohwald, and Weller, H (1998). Strongly Photoluminescent CdTe Nanocrystals by Proper Surface Modification. *Journal of Physical Chemistry B* **102**: 8360-8363.

Gardea-Torresdey, J.L., Parsons, J.G., Gomez, E., Peralta-Videa, J., Troianl, H.E., Santiago, P and Yacaman, M.J. (2002). Formation and growth of Au nanoparticles inside alfalfa plants. *Nanotechnology Letters* **2**:397-401

Gole, A., Dash, C., Ramakrishna, V., Shankar, S.R., Mandal, A.B., Rao, M. and Sastry, M. (2001a). Pepsin-gold conjugates: Preparation, characterisation and enzymatic activity. *Langmuir* **17**:1674-1679

Gole, A., Dash, C., Soman, C., Shankar, S.R., Rao, M. and Sastry, M. (2001b). On the preparation, characterisation and enzymatic activity of fungal proteases-gold colloid bioconjugates. *Bioconjugate Chemistry* **12**: 684-690

Gole, A., Vyas, S., Phadtare, S., Lachke, A. and Sastry, M. (2002). Studies on the formation of bioconjugates of *Endoglucannase* with colloid gold. *Colloids and Surfaces B: Biointerfaces* **25**:129-138

Granchinho, S.C.R., Franz, C.M., Polishchuk, E., Cullen, W.R., and reamer, K.J. (2002). Transformation of arsenic (v) by the fungus *Fusarium oxysporum* melonis isolated from the alga *Fucus gardneri*. *Applied Organometallic chemistry* **16**:721-726

Guarro, J. and Gene, J. (1995). Opportunistic fusarial infections in humans. European *Journal of Clinical Microbiology and Infectious Diseases***14**:741-754

Hames, B.D., and Rickwood, D. (1981). Gel electrophoresis of proteins: a practical approach. IRL Press Limited, London and Washington DC. p93 – 96.

Harrison, M.T., Kershaw, S.V., Rogach, A.L., Kornowski, A., Eychmuller, A., and Weller, H (2000). Wet Chemical Synthesis of Highly Luminescent HgTe/CdS Core/Shell Nanocrystals. *Advanced Materials* **12**:123

He, B., Ha, Y., Liu, H., Wang, K. and Lie, K.Y. (2007). Size control synthesis of polymer-stabilised water-soluble platinum oxide nanoparticles. *Journal of Colloid and Interface Science* **308**:105-111

He, S., Guo, Z., Zhang, Y., Zhang, S., Wang, J. and Gu, N. (2007). Biosynthesis of gold nanoparticles using the bacteria *Rhodopseudomonas capsulate*. *Materials Letters* doi:10.1016/j.matlet.2007.01.018

Henglein, A. (1993). Physicochemical Properties of Small Metal Particles in Solution: "Microelectrode" Reactions, Chemisorptions, Composite Metal Particles, and the Atom-to-Metal Transition. *Journal of Physical Chemistry* **97:** 5457-5471

Holmes, J.D., Smith, P.R., Evans-Gowing, R., Richardson, D.J., Russell, D.A., and Sodeau, D.J. (1995). Energy-dispersive X-ray analysis of the extracellular cadmium sulphide crystallites of *Klebsiella aerogenes*. Archives of Microbiology **163**:*143–147*

Huang, H and Yang, X. (2005). One-step, shape control synthesis of gold nanoparticles stabilized by 3-thiopheneacetic acid. *Colloids and Surfaces A, Physiochemical and Engineering Aspects* **255**: 11-17

Huang, J., He, C., Liu, X., Xiao, Y., Mya, K.Y. and Chai, J. (2004). Formation and characterisation of water soluble platinum nanoparticles using a unique approach based on the hydrosilylation reaction. *Langmuir* **20**:5145-5148

Huang, J., Liu, Z., Liu, X., He, C., Chow, S.Y. and Pan, J. (2005). Platinum nanoparticles from the hydrosilylation reaction: capping agents, physical characterisations, and electrochemical properties. *Langmuir* **21**:699-704

Ingelsten, H.H., Bagwe, R., Palmqvist, A., Skoglundh, M., Svanberg, C., Holmberg, K. and O Shah, D. (2001). Kinetics of the formation of nano-sized platinum particles in water-in-oil microemulsions. *Journal of colloid and interface science* **241**: 104-111

Jarvis, W.R. and Shoemaker, R.A. (1978). Taxonomic status of *Fusarium oxysporum* causing foot and root rot of tomato. *Phytopathology* **68**:1679-1680

Jeong, B.C., Hawees, C., Bonthrone, K.M. and Macaskie, L.E. (1997). Localization of enzymatically enhanced heavy metal accumulation by *Citrobacter* sp. and metal accumulation *in vitro* by liposomes containing entrapped enzyme. *Microbiology* **143**: 2497-2507

Ji, G. and Silver, S. (1995). Bacterial resistance mechanism for heavy metals of environmental concern. *Journal of industrial microbiology* **14**:61-75

Joerger, R., Klaus, T and Granqviat, C.G. (2000). Biologically produced silver-carbon composite materials for optically functional thin film coatings. *Advanced Materials* **12**:407-409

Joho, M., Inouhe, M., Tohoyama, H. and Murayama, T. (1998). Nickel resistance in yeast and other fungi. *Journal of industrial microbiology* **14**:64-168

Kagi, J.H.R. and Schäffer, A. (1988). Biochemistry of metallothionein. *Biochemistry* **27**:8509-8515

Kagi, J.H.R. (1991). Overview of metallothioneins. *Methods in enzymology* **205**:613-626.

Kamat, P.V. (2002). Photophysical, Photochemical and Photocatalytic Aspects of Metal Nanoparticles. *Journal of Physical Chemistry B* **106**:7729 – 7744

Kamachi, T., Uno, S., Hiraoshi, T. and Okura, I. (1995). Purification and properties of intact hydrogenase from *Desulfovibrio vulgaris* (Miyazaki). *Journal of Molecular Catalysis A: Chemical* **95**: 93 – 98.

Kashefi. K., Tor, J.M., Nevin, K.P. and Lovely, D.R. (2001). Reductive precipitation of gold by dissimilatory Fe (III) - reducing bacteria and archae. Applied Environmental Microbiology 67:3275-3279

Kato, H., Minami, T., Kanazawa, T. and Sasaki, Y. (2004). Mesopores created by platinum nanoparticles in zeolite crystals. Angewandte Chemie (International ed. in English) 43:1251-1254

Klaus, T., Joerger, R., Olsson, E and Granqviat, G.C. (1999). Silver based crystalline nanoparticles, microbial fabricated. *Proceedings of the National Academy of Science USA* **96**: 13611 – 13614

Klaus-Joerger T., Joerger, R., Olsson, E. and Granqvist, C.G. (2001). Bacteria as workers in the living factory: metal accumulating bacteria and their potential for materials science. *Trends in Biotechnology* **19**: 15-20

Knez, M and Gösele, U. (2006). Bionanoelectronics: Viruses show their good side. *Nature Nanotechnology* **1**:22-23

Konetzka, W.A. (1977). Microbiology of metal transformations In: Weinberg ED Microorganisms and minerals. New York Marcel Dekker Inc pg 317-342

Konishi, Y., Ohno, K., Saitoh, N., Nomura, T., Nagamine, S., Hishida, H., Takahashi, Y. and Uruga, T. (2007). Bioreductive deposition of platinum nanoparticles on the bacterium *Shewanella algae*. *Journal of Biotechnology* **128**: 648-653

Konishi, Y., Tsukiyama, T., Ohno, K., Saitoh, N., Nomura, T. and Nagamine, S. (2006). Intracellular recovery of gold by microbial reduction of $AuCI^{4-}$ ions using the anaerobic bacterium *Shewanella algae*. *Hydrometallurgy* **81**:24-29

Kow, Y.W. and Burris, R.H. (1984). Purification and properties of membrane bound hydrogenase from *Azotobacter vinelandii*. *Journal of Bacteriology* **159**:564-569

Kowshik, M., Ashtaputre, S., Kharrazi, Vogel, W., Urban, J., Kulkarni, S.K. and Paknikar, K.M. (2003). Extracellular synthesis of silver nanoparticles by a silver-tolerant yeast strain MKY3. *Nanotechnology* **14**: 95-100

Kumar, A., Joshi, H.M., Mandal, A.B., Srivastava, R., Adyanthaya, S.D., Pasricha, R. and Sastry, M. (2004). Phase transfer of platinum nanoparticles from aqueous to organic solutions using fatty amine molecules. *Journal of Chemical Science* **116**: 293-300

Kung, H.H. and Kung, M.C. (2004). Nanotechnology: applications and potentials for heterogeneous catalysis. *Catalysis Today* **97**:219-224

Leach, M.R. and Zamble, D.B. (2007). Metallocentre assembly of the hydrogenase enzymes. *Current Opinion in Chemical Biology* **11**: 159-165

Lengke, M.F., Fleet, M.E. and Southam, G. (2006). Synthesis of platinum nanoparticles by reaction of filamentous cyanobacteria with platinum (IV) - chloride complex. *Langmuir* **22**: 7318-7323

Leslie, J.F. and Summerell, B.A. (2006). The *Fusarium* laboratory manual. Blackwell Publishing, Iowa, USA.

Lewis, L.N. (1993). Chemical catalysis by colloids and clusters. *Chemical Reviews* **93**:2693 - 2730

Liu, J. (2005). Scanning transmission electron microscopy and its application to the study of nanoparticles and nanoparticle systems. *Journal of Electron Microscopy* **54**:251-278.

Liu, Z., Ling, X.Y., Su, X. and Lee, J.Y. (2004). Carbon supported Pt and PtRu Nanoparticles as catalysts for a direct methanol fuel cell. *Journal of physical chemistry B* **108**:8234-8240

Liu, Z., Shamsuzzoha, M., Ada, E.T., Reichat, M. and Nikles, D.E. (2007). Synthesis and activation of platinum nanoparticles with controlled size for fuel cell electrocatalysts. *Journal of Power Sources* **164**: 472- 480

Lloyd, J.R. (2003). Microbial reduction of metals and radionuclides. *FEMS Microbiology Reviews.* **27**:411-425

Lloyd, J.R., Lovely, D.L. and Macaskie, L.E. (2003). biotechnological application of metal-reducing microorganisms. *Advanced Applied Microbiology* **53**:85-128

Lloyd, J.R., Yong, P. and Macaskie, L.E. (1998). Enzymatic recovery of elemental palladium by using sulphate reducing bacteria. *Applied and Environmental Microbiology* **64**: 4607-4609

Lloyd, S.M., Lave, L.B. and Matthews, H.S. (2005). Life Cycle Benefits of Using Nanotechnology To Stabilize Platinum-Group Metal Particles in Automotive Catalysts. *Environmental Science & Technology* **39**:1384 – 1392

Lloyd, J.R., Sole, V.A., Van Praagh, C.V. and Lovely, D.R. (2000). Direct and Fe(II)-mediated reduction of technetium by Fe(III)-reducing bacteria. *Applied Environmental Microbiology* **66**:3743–3749

Lovely, D.R. and Phillips, E.J. (1992). Reduction of uranium by *Desulfovibrio desulfuricans*. *Applied and Environmental Microbiology* **58**: 850-856

Lovely, D.R., Widman, P.K., Woodward, J.C. and Phillips, E.J. (1993). Reduction of uranium by cytochrome c3 of *Desulfovibrio vulgaris*. *Applied Environmental Microbiology* **59**:3572–3576

Lyon, E.J., Shima, S., Boecher, R., Thauer, R.K., Grevels, F.-W., Bill, E., Roseboom, W. and Albracht, S.P.J. (2004). Carbon monoxide as an intrinsic ligand to iron in the active site of the iron-sulfur-cluster-free hydrogenase H_2-forming methylenetetrahydromethanopterin dehydrogenase as revealed by infrared spectroscopy. *Journal of American Chemical Society* **126**: 14239–14248.

Macaskie, L.E., Bonthrone, K.M., Yong, P. and Goddard, D.T. (2000). Enzymatically mediated bioprecipitation of uranium by a *Citrobacter* sp.: a concerted role exocellular lipopolysaccharide and associated phosphatases in biominreal formation. *Microbiology* **146**: 1855- 1867

Macaskie, L.E., Baxter-Plant, V.S., Creamer, N.J., Humphries, A.C., Mikheenko, I.P., Mikheenko, P.M., Penfold, D.W. and Yong, P. (2005). Applications of bacterial hydrogenases in waste decontamination, manufacture of novel bionanocatalysts and in sustainable energy. *Biochemical Society Transactions* **33**:76-79

Mandal, S., Gole, G., Lala, N., Gonnade, R., Ganvir, V. and Sastry M. (2001). Studies on the reversible aggregation of cysteine-capped colloidal silver particles interconnected via hydrogen bonds. *Langmuir* **17**: 6262-6268

Mann, S. (1995). Biominerilization and biomimetic materials chemistry. *Journal of Material Chemistry* **5**: 935-946.

Martino, E., Cerminara, S., Prandi, L., Fubini, B. and Perotto, S. (2004). Physical and biochemical interactions of soil fungi with asbestos fibres. *Environmental Toxicology and Chemistry* **23**:938-944

Matthey, J (2006). Precious metals division, Johnsson Matthey Publishing Company, London, UK

Mazzola, L. (2003). Commercialising nanotechnology. *Nature Biotechnology* **21**:1137-1143

Mejáre, M. and Bellow, L. (2001). Metal-binding proteins and peptides in bioremediation and phytoremediation of heavy metals. *TRENDS in Biotechnology* **19**:63-73

Michel, C., Brugna, M., Aubert, C., Bernadac, A. and Bruschi, M. (2001). Enzymatic reduction of chromate: comparative studies using sulphate-reducing bacteria. Key role of polyheme cytochrome c and hydrogenases. *Applied Microbiology Biotechnology* **55**:95–100

Mintek and Whiteley, C. (2006). Hypothesised mechanism of platinum nanoparticle formation. Private Communication

Misra, T.K. (1992). Bacterial resistance to inorganic mercury salts and organomercurials. *Plasmid* **27**:4-16

Montet, Y., Garcin, E., Volbeda, A., Hatchikians, C., Frey, M., and Fontecilla-Camps, J.C. (1998). Structural bases for the catalytic mechanism of Ni-Fe hydrogenase. *Pure and Applied Physical Chemistry* **70**: 25-31

Morris, V.J., Kirby, A.R. and Gunning, A.P. (1999). Atomic Force Microscopy, pp 1-132. Imperial College Press

Motte, L., Billoudet, F., Lacaze, E., Douin, J. and Pileni, M.P. (1997). Self organisation into 2D and 3D superlattices of nanosized particles differing by their size. *Journal of Physical Chemistry B* **101**: 138-144

Mukherjee, P., Ahmad, A, Mandal, D., Senepati, S., Sainkar, S.R., Khan, M.I., Pasricha, R., Ajayakumar, P.V., Alam, M., Kumar, R. and Sastry, S. (2001a). Fungus mediated synthesis of silver nanoparticles and their immobilisation in the mycelial matrix: a novel biological approach to nanoparticle synthesis. *Nano Letters* **1**:515- 519

Mukherjee, P., Senepati, S., Ahmad, A., Mandal, D., Sainkar, S.R., Khan, M.I., Pasricha, R., Ajayakumar, P.V., Alam, M, Sastry, M. and Kumar, R. (2001b). Bioreduction of AuCI4 ions by the fungus *Verticillium* sp. and surface trapping of the gold nanoparticles. *Chemie International Edition* **40**: 3585-3588

Mukherjee, P., Senepati, S., Mandal, D., Ahmad, A., Khan, M.I., Kumar, R. and Sastry, M. (2002). Extracellular synthesis of gold nanoparticles by the fungus, *Fusarium oxysporum*. *ChemBioChem* **5**: 461-463

Muller, D.J., Aebi, U. and Engel, A. (1996). Chapter 3: Imaging, measuring and manipulating native bimolecular systems with the atomic force microscope. In MSB Booklet – Frame Bones to Atoms 2nd Ed. M.E. Muller Institute for Microscopy. www.min.unibas.ch

Murata, K., Fukuda, Y., Shimosaka, M., Wantanabe, K., Saikusa, T., and Kimura,A. (1985). Phenotypic character of the methylglyoxal resistance gene in *Saccharomyces cervisiae*: expression in *Escherichia coli* and application to breeding wild-type strains. *Applied Environmental Microbiology* **50**:1200-1207

Murphy, R.J. and Levy, J.F. (1983). Production of copper oxalate by some copper tolerant fungi. *Transactions of the British Mycological Society* **81**:165-168

Murray, C.B., Norris, D.J. and Bawendi, M.G. (1993). Synthesis and characterisation of nearly monodisperse CdE (E = sulphur, selenium, tellurium) semiconductor nanocrystallites. *Journal of American Society* **115**:8706-8715.

Nadagouda, M.N. and Varma, R.S. (2006). Green and controlled synthesis of gold and platinum nanomaterials using vitamin B2: density assisted self assembly of nanospheres, wires and rods. *Green Chemistry* **8**: 516-518.

Nair, B. and Pradeep, T. (2002). Coalescence of nanoclusters and formation of submicron crystallites assisted by *Lactobacillus* strains. *Journal of Crystal Growth and Design* **2***:*293-298.

Nedoluzhko, A.I., Shumilin, I.A., Mazhorova, L.E., Popov, V.O. and Nikandrov, V.V. (2000). Enzymatic oxidation of cadmium and lead metals photodeposited on cadmium sulphide. *Bioelectrochemistry* **53**:61–71

Nelson, P.E., Toussoun, T.A. and Cook, R.J. (1981). *Fusarium*: diseases, biology and taxonomy. Pennsylvania State University Press, Pennsylvania, USA.

Ngwenya, N. and Whiteley, C.G. (2006). Recovery of rhodium (III) from solutions and industrial wastewaters by a sulphate reducing consortium. *Biotechnology Progress* **22**: 1604-1611

Nicolet, Y., Lemon, B.J., Fontecilla-Camps, J.C. and Peters, J.W. (2000). A novel FeS cluster in Fe-only hydrogenases. *Trends in Biochemical Scence* **25**: 138–143.

Nies, D.H. (1995). The cobalt, zinc, cadmium efflux system czcABC from *Alcaligenes eutrophus* functions as a cation-proton antiporter in *Escherichia coli*. *Journal of Bacteriology* **177**:2707-2712

Peng, Q., Dong, Y., Deng, Z and Li, Y. (2002). Selective Synthesis and Characterization of CdSe Nanorods and Fractal Nanocrystals. *Journal of Inorganic Chemistry* **41**:5249-5254.

Peng, Z. A., and Peng, X (2001). Formation of High-Quality CdTe, CdSe, and CdS Nanocrystals Using CdO as a precursor. *Journal of American Chemistry Society***123**: 183-184

Qi, L., Ma, J., Cheng, H and Zhao, Z (1997). Reverse Micelle Based Formation of $BaCO_3$ Nanowires. *Journal of Physical Chemistry* **101**:3460-3463

Qu, L., Peng, Z.A., and Peng, X (2001). Alternative Routes toward High Quality CdSe Nanocrystals. *Nanotechnology Letters* **1**: 333-337.

Qu, L., Yu, W.W., and Peng, X. (2004). In Situ Observation of the Nucleation and Growth of CdSe Nanocrystals. *Nanotechnology Letters* **4**: 465-469.

Rao, C.N.R. and Cheetham, A.K. (2001). Science and technology of nanomaterials: current status and future prospects. *Journal of Material Chemistry* **11**: 2887-2894

Rao, C.R.M and Reddi, G.S. (2000). Platinum Group Metals: occurrence, use and recent trends in their determination. *Trends in Analytical Chemistry* **19**: 565-586

Rao, C.N.R., Muller, A. and Cheetham, A.K. (2004). The Chemistry of Nanomaterials: Synthesis, Properties and Applications Volume 1, Wiley-VCH, Weinheim.

Rashamuse, K. and Whiteley (2007). Bioreduction of platinum (IV) from aqueous solution using sulphate reducing bacteria. *Applied Microbiology and Biotechnology* **75**: 1429-1435.

Ricci, D. and Braga, P.C. (2004). The basis of atomic force microscopy. In: Atomic Force Microscopy: Biomedical Methods and Application, pp 3-39. Humana Press

Riddin, T.L., Gericke, M., and Whiteley, C.G. (2006). Analysis of inter- and extracellular formation of platinum nanoparticles by *Fusarium oxysporum* f.sp. *Lycopersici* using response surface methodology. *Nanotechnology* **17**:1-8

Rivadulla, J.F., Vergara, M.C., Blanco, M.C., López-Quintela, M.A. and Rivas, J. (1997). Optical Properties of Platinum Particles Synthesized in Microemulsions *Journal of Physical Chemistry B* **101**:8997 – 9004

Roe, S. (2001). Protein purification techniques. Second Ed, Oxford University Press, Britain. Pgs 111 – 153.

Rogach, A.L., Kornowski, A., Gao, M., Eychmuller, A., and Weller, H (1999). Synthesis and Characterization of a Size Series of Extremely Small Thiol-Stabilized CdSe Nanocrystals. *Journal of Physical Chemistry B* **103**: 3065-3069.

Roh, Y., Lauf, R.J., McMillan, A.D., Zhang, C., Rawn, C.J., Bai, J., and Phelps, T.J. (2001). Microbial synthesis and the characterization of metal-substituted magnetites. *Solid State Communication* **110**:529-534.

Rosa, R.H., Miller Jr, D. and Alfonso, E.C. (1994).. The changing spectrum of fungal keratitis in South Florida. *Ophthalmology* **101**:1005-1013

Rouch, D.A., Lee, B.T.D and Morby, A.P. (1995). Understanding cellular responses to toxic agents: A model for mechanism choice in bacterial metal resistance. *Journal of Industrial Microbiology* **14**:132-141

Royal Society and The Royal Academy of Engineering (2003). Nanoscience and nanotechnology: opportunities and uncertainties. Royal Society London. www.nanotec.org.uk

Salata, O.V. (2004).Applications of nanoparticles in biology and medicine. *Journal of Nanobiotechnology* **2**:3-8.

Sangregorio, C., Galeotti, M., Bardi, U., and Baglioni, P. (1996). Synthesis of Cu_3Au Nanocluster Alloy in Reverse Micelles. *Langmuir* **12**: 5800-5802

Sarathy, K.V., Raina, G., Yadav, R.T., Kulkarni, G.U. and Rao, C.N.R. (1997). Thiol-Derivatized Nanocrystalline Arrays of Gold, Silver, and Platinum. *Journal of Physical Chemistry B* **101**:9876 - 9880;

Sastry, M., Ahmad, A., Khan, M.I. and Kumar, R. (2003). Biosynthesis of metal nanoparticles using fungi and actinomycete. *Current Science* **85**:162-170

Sastry, M., Ahmad, A., Khan, M.I. and Kumar, R. (2004). Microbial nanoparticle synthesis. In: Nanobiotechnology: Concepts, applications and perspectives. Niemeyer, C.M., and Mirkin, C.A. (Eds) Pgs 126-135. Wiley-VCH, Verlag GmbH & Co. kGaA, Weinheim.

Selvakannan, P.R., Mandal, S., Phadtree, S., Pasricha, R. and Sastry, M. (2003). Capping of gold nanoparticles by the amino acid lysine renders them water-dispersible. *Langmuir* **19**:3545-3549

Senepati, S., Ahmad, A., Khan, M.I., Sastry, M. and Kumar, R. (2005). Extracellular biosynthesis of bimetallic Au-Ag alloy nanoparticles. *Small* **1**:517-520

Shahverdi, A.R., Miniaeian, S., Shahverdi, H.R., Jamalifar, H. and Nohi, A.A. (2007). Rapid synthesis of silver nanoparticles using culture supernatants of *Enterobacteria*: A novel biological approach. *Process Biochemistry* **42**: 919-923

Shankar, S.S., Rai, A., Ankamwar, B., Singh, A., Ahmad, A and Sastry, M. (2004). Biological synthesis of triangular gold nanoprisms. *Nature Materials* **3**:482-488

Shim, M. and Guyot-Sionnest, P. (2001). Organic-Capped ZnO Nanocrystals: Synthesis and n-Type Character. *Journal of American Chemical Society* **123**: 11651-11654.

Shukla, N., Svedberg, E.B. and Ell, J. (2007). Surfactant isomerization and dehydrogenation of FePt nanoparticles. *Colloids and Surfaces A: Physiochemical and Engineering Aspects* **301**:113-116

Silver, S and Phung, L.T. (1996). Bacterial heavy metal resistance: new surprises *Annual Review in Microbiology* **50**:753-789

Smith, D.G. (1974). Tellurite reduction in *Schizosaccharomyces pombe*. Journal of *General Microbiology* **83**: 389-392

Southam, G. and Beveridge, T.J. (1996). The occurrence of bacterially derived sulphur and phosphorus within pseudocrystalline and crystalline octahedral gold formed *in vitro*. *Geochimica et Cosmochimica Acta* **60**:4369-4376.

Stallings, D.M. (2004). H_2: The fuel of the future Fe-Only hydrogenase structure and plausible mechanism. A literature seminar at the University of Alabama.

Stephenson, M. and Stickland, L.H. (1931). Hydrogenase: A bacterial enzyme activating hydrogen. *Biochemistry Journal* **25**: 205-214

Summerell, B.A. and Rugg, C.A. (1992). Vascular wilt of *Helichrysum* species caused by *Fusarium oxysporum*. *Australian Plant pathology* **21**:18-19

Talapin, D.V., Rogach, A.L., Kornowski, A., Haase, M., and Weller, H (2001). Highly Luminescent Monodisperse CdSe and CdSe/ZnS Nanocrystals Synthesized in a Hexadecylamine-Trioctylphosphine Oxide-Trioctylphospine Mixture. *Nanotechnology Letters* **1**:207-211.

Tang, Z., Geng, D. and Lu, G. (2005). Size controlled synthesis of colloid platinum nanoparticles and their catalytic activity for the electrocatalytic oxidation of carbon monoxide. *Journal of Colloid and Interface Science* **287**:159-166

Taton, T.A. (2002). Nanostructures as tailored biological probes. *Trends in Biotechnology* **20**:277-279.

Titchmarsh, J.M. (1993). Energy dispersive x-ray analysis EDX in the TEM/STEM. In: Electron probe microanalysis. Fitzgerald, A.G., Fabian, D.J. and Storey, B.E. (Eds) Pgs 275 – 280. CRC Press

Toshima, N., Nakata, K. and Kitoh, H. (1997). Giant platinum clusters with organic ligands: preparation and catalysis. *Inorganica Chimica Acta* **265**:149-153

Ueno, Y., Kurano, N. and Miyachi, S. (1999). Purification and characterisation of hydrogenase from the marine green alga, *Chlorococcum littorale*. *FEBS Letters* **443**:144-148

Valls, M. and de Lorenzo, V. (2000). Exploiting the genetic and biochemical capacities of bacteria for the remediation of heavy metal pollution. *FEMS Microbiology Reviews* **26**: 327-338

Vignais, P.M., Billoud, B. and Meyer, J. (2001). Classification and phylogeny of hydrogenases. *FEMS Microbiology Reviews* **25**: 455–501.

Vigneshwaran, N, Ashtaputre, N.M., Varadarajan, P.V., Nachane, R.P., Paralikar, K.M. and Balasubramanya, R.H. (2007). Biological synthesis of silver nanoparticles using the fungus *Aspergillus flavus. Materials Letters* **61**:1413-1418

Vigneshwaran, N., Kathe, A.A., Varadarajan, P.V., Nachane, R.P and Balasubramanya, R.H. (2006). Biomimetics of silver nanoparticles by white rot fungus *Phaenerochaete chrysosporium*. *Colloids and Surfaces B: Biointerfaces* **53:**55-59

Vo-Dinh, T. (2005). Protein technology: the new frontier in biosciences. In: Protein nanotechnology: protocols, instrumentation and applications. Pgs 1-3. Humana press. Totowa, new jersey, united states.

Voet, D. and Voet, J.G. (1995). Techniques for protein purification. In: Biochemistry, Second Edition. John Wiley and Sons, Inc., USA.

Wakatsuki, T., Hayakawa, S., Hatayama, T., Kitamura, T. and Imahara H. (1991). Purification and some properties of copper reductase from cell surface of Debaryomyces hansenii. *Journal of Fermentation and Bioengineering* **72**: 158-161

Walker, J.M. (2000). Protein structure, purification and characterization. In: Practical biochemistry, principles and techniques. Wilson, K. and Walker, J. (Eds). Fifth Edition, Cambridge University Press. UK.

Williams, D.B. and Carter, C.B. (1996). Transmission electron microscopy: A textbook for materials science. Plenum Press, New York

Willner, I., Baron, R. and Willner B. (2006). Growing metal nanoparticles by enzymes. *Advanced Materials* **18**:1109-1120

Willson, R.C. (1999). Purification and characterization of proteins. In: Manual of industrial and microbial biotechnology. Demain, A.L., Davies, J.E., Atlas, R.M., Cohen, G., Hershberger, C.L., Hu, W-S., Sherman, D.H., Willson, R.C. and Wu, J.H.D. (Eds). Second edition. ASM Press. Washington D.C. USA.

Wilson, K., and Walker, J. (1994). Practical Biochemistry Principles and techniques. Fourth Ed. Cambridge University Press, Britain.p17 – 18, 498 – 507.

Winter, G., Buhrke, T., Lenz, O., Jones, A.K., Forgber, M., and Friedrich, B. (2005). A model system for [NiFe] hydrogenase maturation studies: Purification of an active site containing hydrogenase large subunit without small subunit. *FEBS Letters* **579**: 4292 –4296.

Xiao, Y., Pavlov, V., Levine, S., Niazov, T., Markovitch, G. and Willner, I. (2004). Catalytic growth of Au nanoparticles by NAD (P) H cofactors: Optical sensors for NAD $(P)^+$-dependent biocatalyzed transformations. *Angewandte Chemie International Edition* **43**: 4519-4522

Yang, W., Ma, Y., Tang, J. and Yang, X. (2007). Green synthesis of monodisperse platinum nanoparticles and their catalytic properties. *Colloids and Surfaces A: Physiochemical and Engineering Aspects* **302**:628-633

Yong, P., Rowson, N.A., Farr, J.P.G., Harris, I.R. and Macaskie, L.E. (2002). Bioaccumulation of palladium by *Desulfovibrio desulfuricans*. *Journal of Chemical Technology and Biotechnology* **77**:593-601.

Yoshimura, H. (2006). Protein assisted nanoparticle synthesis. *Colloids and Surfaces A: Physiochemical and Engineering Aspects* **283**: 464-470

Zadvorny O.A, Zorin N.A., Gogotov I.N., Gorlenko V.M. (2004). Properties of Stable hydrogenase from the purple sulphur bacterium *Lamprobacter modestohalophilus. Journal of Biochemistry (Moscow)* **69**: 164-169

Zhang, J.Z., O'Neil, R.H. and Roberti, W.T. (1994). Femtosecond Studies of Photoinduced Electron Dynamics at the Liquid-Solid Interface of Aqueous CdS Colloids. *Journal of Physical Chemistry* **98**: 3859- 3864

Zorin NA (1986). Redox properties and active centre of phototropic bacteria hydrogenases. *Biochimie* **68**:97–10.

APPENDICES

Appendix A: Method of hexachloroplatinic acid determination

A1: Hexachloroplatinic acid stock solution

Dissolve 1 g of hexachloroplatinic acid (H_2PtCI_6) in 100 ml ddH_2O

A2: H_2PtCI_6 standard curve (0-20 mM)

Different H_2PtCI_6 concentrations were prepared from the H_2PtCI_6 stock solution ($10mgml^{-1}$) as shown in Table A1. H_2PtCI_6 standard curve generated by reading the absorbance at 285 nm (Figure 1). For the test sample, 200 µl of sample was the absorbance read at 285 nm.

Table A1: Preparation of H_2PtCI_6 standard curve

H_2PtCI_6 Stock solution (20 mM) (µl)	ddH_2O (µl)	H_2PtCI_6 Concentration (mM)
0	200	0
40	160	4
80	120	8
120	80	12
160	40	16
200	0	20

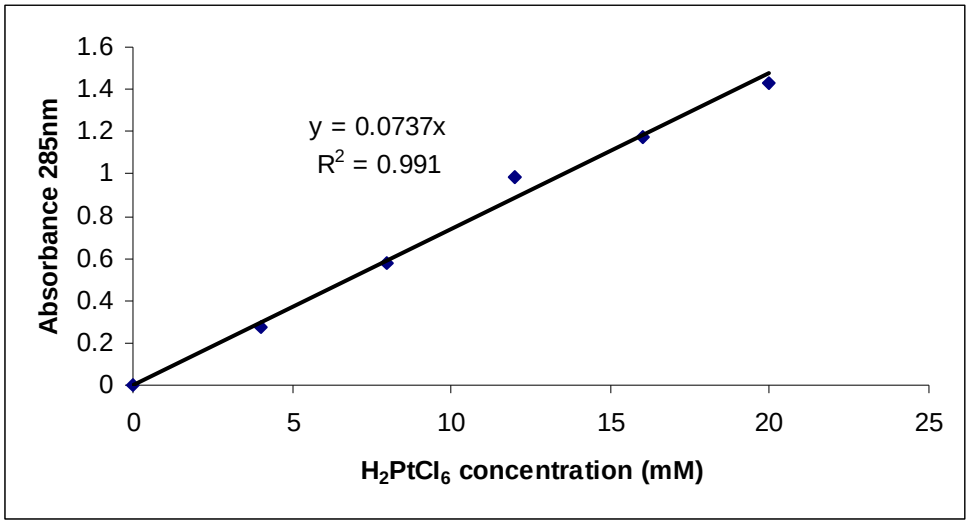

Figure I: H_2PtCI_6 standard curve (0-20 mM)

A3: H_2PtCI_6 standard curve (0-2 mM)

Different H_2PtCI_6 concentrations were prepared from the H_2PtCI_6 stock solution (2 mM) as shown in Table A2. H_2PtCI_6 standard curve was generated by reading the absorbance of these different concentrations at 285 nm (Figure 2). For the test sample, 200 µl of sample was the absorbance read at 285 nm.

Table A2: Preparation of H_2PtCI_6 standard curve

H_2PtCI_6 Stock solution (20 mM) (µl)	ddH_2O (µl)	H_2PtCI_6 Concentration (mM)
0	200	0
2	198	0.2
4	196	0.4
6	194	0.6
8	192	0.8
10	190	1.0
12	188	1.2
14	186	1.4
16	184	1.6
18	182	1.8
20	180	2.0

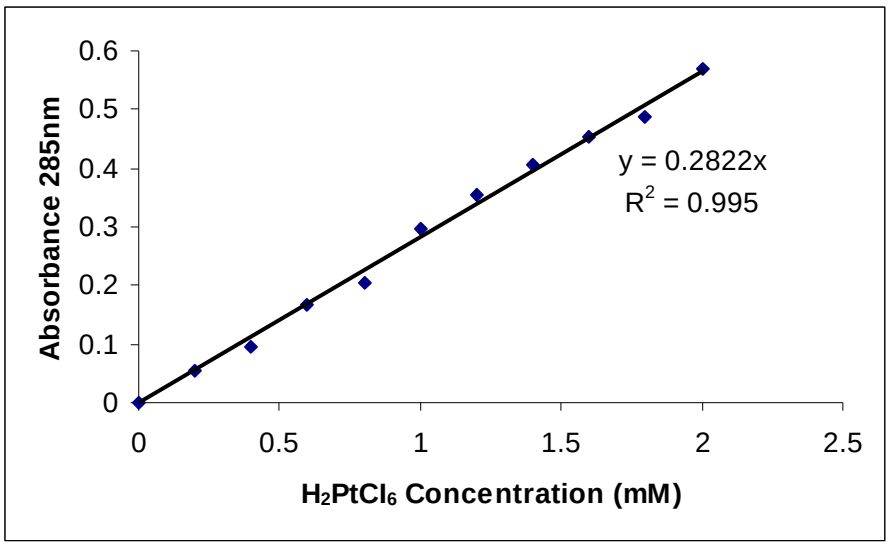

Figure II: H_2PtCI_6 standard curve (0-2 mM)

A4: Platinum (II) chloride stock solution

Dissolve 3.85 g of platinum (II) chloride ($PtCI_2$) in 100 ml hydrochloric acid (32 %).

A5: $PtCI_2$ standard curve (0-20 mM)

Various $PtCI_2$ concentrations were prepared from the $PtCI_2$ stock solution as shown in Table A3. A $PtCI_2$ standard curve was generated by reading the absorbance of these different concentrations at 290 nm (Figure 3). For the test sample, 200 µl of sample was the absorbance read at 290 nm.

Table A3: Preparation of $PtCI_2$ standard curve (0-20 mM)

$PtCI_2$ Stock solution (20 mM) (µl)	ddH_2O (µl)	H_2PtCI_6 Concentration (mM)
0	200	0
20	180	2
40	160	4
60	140	6
80	120	8
100	100	10
120	80	12
140	60	14
160	40	16
180	20	18
200	0	20

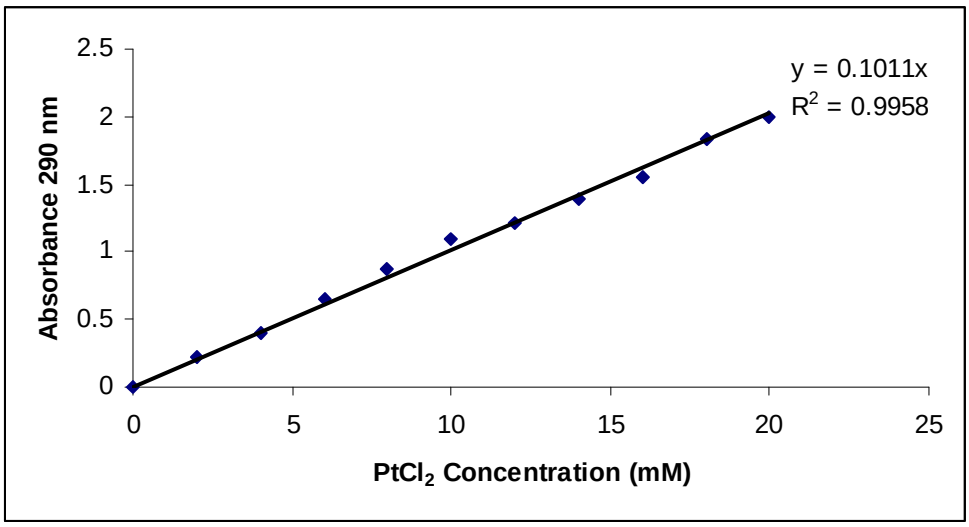

Figure III: $PtCI_2$ standard curve (0-20 mM)

A6: $PtCI_2$ standard curve (0-2 mM)

Various $PtCI_2$ concentrations were prepared from the $PtCI_2$ stock solution as shown in Table A4. A $PtCI_2$ standard curve was generated by reading the absorbance of these different concentrations at 290 nm (Figure 4). For the test sample, 200 µl of sample was the absorbance read at 290 nm.

Table A4: Preparation of $PtCI_2$ standard curve (0-2 mM)

$PtCI_2$ Stock solution (20 mM) (µl)	ddH_2O (µl)	H_2PtCI_6 Concentration (mM)
0	200	0
2	198	0.2
4	196	0.4
6	194	0.6
8	192	0.8
10	190	1.0
12	188	1.2
14	186	1.4
16	184	1.6
18	182	1.8
20	180	2.0

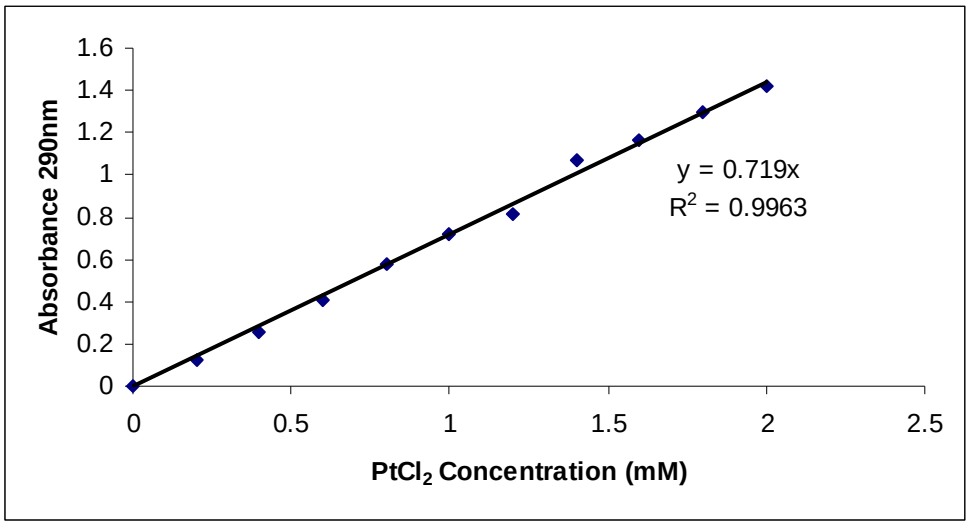

Figure III: $PtCI_2$ standard curve (0-2 mM)

Appendix B: Method of protein determination – Bradford assay (Bradford, 1976)

B1: Protein stock solution

Dissolve 0.02 g of Bovine serum albumin (BSA) in 10 ml ddH_2O

B2: Protein standard curve

Different protein concentrations were prepared from the BSA stock solution (2 $mgml^{-1}$) as shown in Table B1. A protein standard curve was generated by reading the absorbance of these different concentrations at 595 nm (Figure II). For the test sample, 250 µl Bradford reagent was added to 5 µl diluted sample and the absorbance was read at 595 nm.

Table B1: Preparation of protein standard curve

BSA Stock solution (2 $mgml^{-1}$) (µl)	ddH_2O (µl)	Bradford Reagent (µl)	Protein Concentration ($mgml^{-1}$)
0	5	245	0
0.31	4.69	245	0.1
0.63	4.37	245	0.2
1.25	3.75	245	0.4
1.88	3.12	245	0.6
2.50	2.50	245	0.8
3.13	1.87	245	1.0
4.38	0.62	245	1.4
5	0	245	1.6

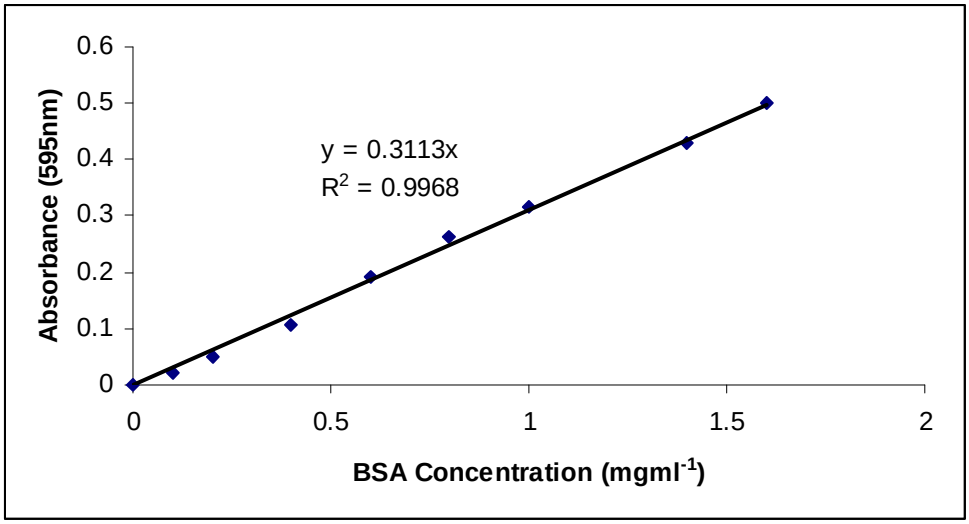

Figure II: Protein standard curve

Appendix C: Methods used for purification and partial characterization of the hydrogenase produced by *F.oxysporum*

C1 SDS-PAGE

Solution A: Acryl amide stock solution (30% acryl amide, 0.8% bis-acryl amide) – weigh 29.2g acryl amide and 0.8g bis-acryl amide, and then dissolve in 100ml de-ionised water and stir until acryl amide powder is completely dissolved. Store in the dark at 4 °C (30 days maximum).

Solution B: 4x Separating Gel buffer – add 75ml of 2M Tris-HCl buffer (pH 8.8) and 4ml of 10%SDS and then make up the volume to 100ml with deionised water.

Solution C: 4X Stacking Gel buffer – add 50ml of 1M Tris-HCl buffer (pH 6.8) and 4ml 10% SDS, and make up the volume to 100ml with deionised water.

Solution D: 10% Ammonium per sulphate solution (APS)-dissolve 0.5g ammonium persulfate in 5ml deionised water.

Solution E: Electrophoresis buffer – add together 3g Tris base, 14.4g glycine and 1g SDS. Dissolve all three in 1 litre of deionised water.

Solution F: 5× Sample buffer – add together 0.6ml 1M Tris-HCl buffer (pH 6.8), 5ml 50% glycerol, 2ml 10% SDS, 0.5ml 2-mercaptoethanol, 1ml 1% bromophenol blue, and make up the volume to 10ml with deionised water.

Solution G: Coomasie blue staining solution – stained with Brilliant blue R concentrate electrophoresis reagent

Solution H: Coomasie Gel Destain solution – add together 100ml methanol, 100 ml glacial acetic acid and 800 ml deionised water.

Table C1: Recipe for Resolving Gel

	Volume (µl)
Solution A	4170
Solution B	2500
Deionised water	3330
10% Ammonium per Sulphate	50
TEMED	5

Table C2: Recipe for stacking gel

	Volume (µl)
Solution A	670
Solution C	1000
Deionised water	2300
10% Ammonium per Sulphate	30
TEMED	5

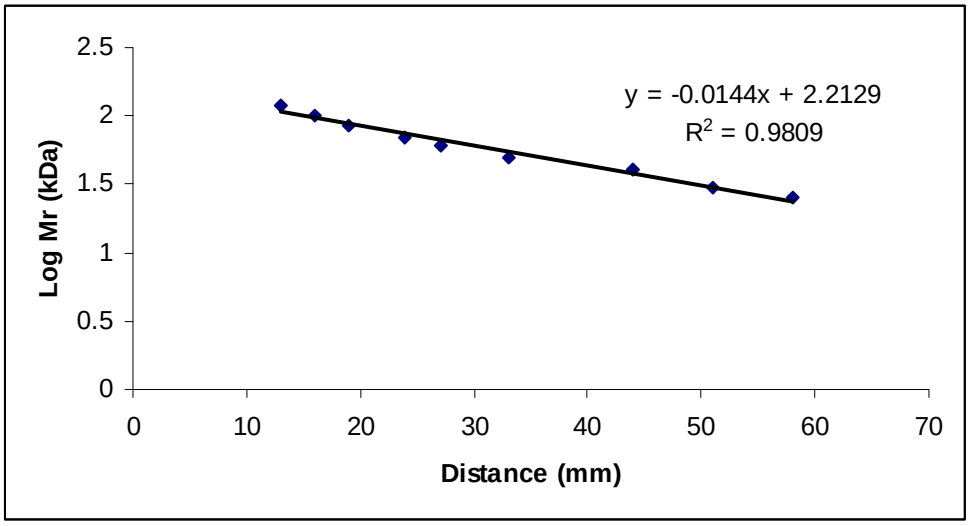

Figure III Calibration curve of the log molecular weight (Mr) markers. The molecular weight markers used consisted of nine precisely sized recombinant proteins of 25 000, 30 000, 40 000, 50 000, 60 000, 70 000, 85 000, 100 000 and 120 000 dalton (PeqGOLD Protein Marker II, 10 – 200 kDa, Optima Scientific, South Africa)